10 JANUARY, 1992

THE MIRAMICHI DUMP SITE B SEABED STABILITY SURVEY - NOVEMBER 1991

by

Carl L. Amos and Harold A. Christian
Geological Survey of Canada
Bedford Institute of Oceanography
Dartmouth, N.S., B2Y 4A2

a field report prepared for

Public Works Canada
Atmospheric and Environment Service
P.O. Box 7350, Saint John,
E2L 4J4

unpublished report

THE MIRAMICHI DUMP SITE B SEABED STABILITY SURVEY - NOVEMBER 1991

by

Carl L. Amos and Harold A. Christian
Geological Survey of Canada
Bedford Institute of Oceanography
Dartmouth, N.S., B2Y 4A2

SEA CAROUSEL

System Configuration - Sea Carousel

Sea Carousel, named after the carousels of Postma (1967) and Hydraulic Research Limited (Burt, 1984), is a benthic annular flume designed for field use in intertidal and subtidal settings. The carousel is 1.0 m in radius with an annulus 0.15 m wide and 0.30 m high (Figure 1). It weighs approximately 150 kg in air and 40 kg in water and is made entirely of aluminium. Flow in the annulus is induced by rotating a movable lid that is driven by a 0.35 hp DC motor powered from the surface. Eight small paddles, spaced equidistantly beneath the lid, induce a flow of water in the annulus. The width of the annulus (D) was made 0.15 m to give a relative roughness (e/D) $\approx$ 0.004 (where the wall roughness, e $\approx$ 0.0006 m; after Shames, 1962). The water depth in the annulus was minimized to 0.25 m to ensure conditions for Nikuradse's "rough-pipe zone of flow" wherein changes in wall friction factor with changes in Reynolds number are at a minimum (Shames, 1962).

A schematic diagram of the Sea Carousel configuration is shown in Figure 2. It is equipped with three optical backscatter sensors (OBS's; Downing, 1983). Two of these are located non-intrusively on the inner wall of the annulus at heights of 0.03 and 0.18 m above the skirt (the skirt is a horizontal flange situated around the outer wall of the annulus 0.04 m above the base; it was designed to standardize penetration of the flume into the seabed; see Figure 1). The third OBS detects ambient particle concentration outside the annulus, or it may be used to detect internal sediment concentration at a height between the other two. The OBS sensors give linear responses to particle concentration (of a constant size) for both mud and sand over a concentration range of 0.1 to 50 g/L (Downing and Beach, 1989). They are unaffected by flows below 1.5 m/s and are stable through time. A sampling port is situated in the outer wall of the annulus at a height of 0.2 m above the skirt through which water samples can be drawn to calibrate the three sensors under well mixed conditions.

A Marsh/McBirney current meter (model 511) is located on the centreline of the annulus at a height of 0.16 m above the skirt. It was used to detect the instantaneous azimuthal and vertical components of flow within the annulus (U_y and U_w respectively). Mean tangential lid rotational speed ($\bar{U}_r$) is detected through a shaft end-coder that runs on the lid. Controller boards for each sensor and the necessary power (12 VDC) are derived from an underwater pod located above the annulus. Output voltages from all sensors are digitized and transformed to scientific units on a Campbell Scientific CR10 data logger and stored on a Campbell Scientific SM192 storage module (storage capacity of 96,000 data values), also located in the underwater pod. The data logger is interrogated and programmed from the surface using a microcomputer linked to the data logger through an RS232 interface. Maximum sampling rate of all channels is approximately 2 Hz, whereas U_y and U_w may be logged at rates up to 10.66 Hz. All channels may be monitored and

displayed on the surface computer allowing the operator to control the experiment interactively. Bed shear stress is varied in time by varying the power supplied to the underwater motor up to 350 watts via a surface power supply. The data stored from each deployment may be downloaded remotely through the RS232 cable at the end of each experiment and the storage module re-initialized.

A window is located in the inner flume wall for purposes of observing and recording the mechanics of bed failure. A perspex wedge at the base of the window sections the sediment upon deployment. Thus the upper 20 mm of sediment and the lower 10 cm of the water column can be viewed in section. Visual observations are made using an Osprey underwater SIT black and white camera, displayed using a monitor. Light is provided by two 100 watt underwater lights powered from the surface. The housing has a lens that corrects for underwater geometric distortions and so is suitable for accurate image scaling. The camera lens is located approximately 20 mm from the window. Horizontal and vertical scale lines are present on the window and situated within the field of view. The camera images 30 frames/s. A co-axial cable connects the camera to a surface monitor for real-time detection. Video records are stored on a standard VHS video cassette recorder also at the surface. Sequential video images are digitized for particle trajectories at varying heights above the bed. From these, velocity profiles are constructed.

The root-mean-square value of the time and width averaged friction velocity ($\bar{U}_*rms$) is correlated with $\bar{U}_y$. The relationship of $\bar{U}_*rms$ and $\bar{U}_y$ is good, and takes the form:

$$\bar{U}_*rms = 0.0167 + 0.097\bar{U}_y \text{ (m/s; } r^2 = 0.96) \quad (1)$$

Thus $\bar{U}_*rms$ is used as the standard hydrodynamic measure in this study.By manipulation of the quadratic stress law a drag coefficient (C_d) relating $\bar{U}_y$ and $\bar{U}_*$ is derived:

$$\bar{U}_*rms = \sqrt{\tau/\rho} \quad (2)$$

$$\text{and } \tau = C_d\rho\bar{U}_y^2 \quad (3)$$

$$\text{thus } C_d = \tau/\rho\bar{U}_y^2 = \bar{U}_*rms^{\,2}/\bar{U}_y^2 \quad (4)$$

This results in a value of $C_d = 4.0 \times 10^{-2}$ and a corresponding C_{d100} of 1.3×10^{-3}. The latter coefficient falls within the range of values detected over flat bed in the field observations of Sternberg (1972).

Water samples were pumped at intervals from a port located in the side of Sea Carousel at a height of approximately 20 cm above the bed. These water samples were then filtered for total suspended particulate matter in order to calibrate the OBS sensors and to provide sample material of suspended material. A detailed description of the system is given in Amos *et al.* (in press) and results measured in the Bay of Fundy are presented in Amos *et al.* (in review).

System Configuration - SOBS

SOBS (Submersible Observatory of Benthic Stability) is a benthic tripod equipped with six Optical Backscatter Sensors (OBS's) that detect sediments in suspension (Figure 3). The sensors are arranged in a logarithmic progression from a height of 10 cm above the bed to 200 cm (item 6). Sensor 1 (10 cm) looks downwards and is designed to detect ripple mobilization and bedload transport. From it we can obtain the onset of bed motion. Sensors 2 - 6 are arranged to monitor in the horizontal at heights above the bed of 11 cm, 38 cm, 82 cm, 136 cm, and 200 cm respectively.

Data from each sensor are logged on an underwater Tattletale at a rate of 1 Hz (item 5). At this rate, the instrument can collect data for 19.3 days before saturating memory. An underwater video camera (Sony V101, item 1) and Amphibico flood lights (item 2) are also located on the tripod. The camera can burst sample the bed at programmable intervals and durations. This is controlled by the underwater Tattletail. A scale is located in the field of view for reference (item 7). Finally, an InterOcean S4 current meter (item 3) is mounted on a independent frame to provide data on wave height, and mean currents. The current meter is programmed independently of the SOBS system. Power is provided by a submersible 12 v battery pack (item 4). The whole system is weighted at the feet for stability (items 8 and 9).

The SOBS is normally deployed with a 50 m ground line, and is marked with a header float (Figure 4). The current meter frame is usually located at the end of the ground line, and is also marked with a header float.

System configuration - Lancelot

Lancelot is a tethered or remotely-operated piezometric sensor system that is used to investigate a number of difficult geological environments used to measure sediment pore water pressure *insitu*. The tool can assess liquefaction conditions caused by dynamic build-up of pore water pressure, consolidation rates by evaluation of the penetration pressure decay curves, and the *insitu* steady-state pore pressure which governs the state of effective stress (Christian and Heffler, in prep.). Similar tools have been developed for deep-sea applications (Davis et al, 1991; Schultheiss, 1990a, 1990b; and Bennett et al, 1989, 1990).

Figure 5 illustrates the various components of the tool, consisting of an outer weight stand and cage containing the telescoping probe and electronics package. The outer weight stand is only used in deep-water deployments to assist penetration; a 2 m-wide base is substituted in shallow waters to provide resistance to overturning under storm conditions and to reduce vertical stress imposed on the seabed. The entire system in shallow-water mode only weighs 20 lbs submerged (vertical stress of 100 Pa, which is equivalent to a head of 1 cm of water). The device comprises a Tattletale 4 datalogger that can store data on differential and absolute pressure derived from transducers that sample at rates programmed by the operator. For example, it can store data at 4 samples per second continuously for 1.5 hours, or at varying rates in burst sample mode for more extended periods of time.

Christian et al. (in prep.) describe the device in detail in terms of its technical components. Lancelot measures vertical tilt in two directions (pitch and roll), vertical acceleration, absolute pressure (water depth), and differential pore pressure at the filter tip embedded beneath the seabed relative to the water column above. Electronic noise in the data acquisition package is extremely low being at the digital limit of 1 bit.

RESULTS

Sea Carousel

Sea Carousel was deployed successfully at 10 locations in the central Miramichi estuary. Four deployments were made on Dump site B; three on material dumped in 1990 (MIR7, MIR8, and MIR9), one on undisturbed material adjacent to the 1990 dump site (MIR11). Four deployments were made in the dredged navigation channel: 2 in the silty outer channel (near buoy 40; MIR13 and MIR14), and 2 in the clayey inner channel (near buoy 48; MIR18 and MIR19). Finally, 2 deployments were made on the control site north of the navigation channel (MIR15 and MIR16).

The locations of the Sea Carousel sites are listed in Table 1.

Table 1. The location of Sea Carousel sites occupied in this study.

STATION	LATITUDE	LONGITUDE
DUMP SITE B		
MIR7	47° 7' 12.8"	65° 11' 00.5"
MIR8	47° 7' 06.8"	65° 11' 07.5"
MIR9	47° 7' 07.1"	65° 11' 08.0"
PERIFERAL TO DUMP SITE B		
MIR11	47° 6' 59.4"	65° 11' 05.6"
OUTER CHANNEL		
MIR13	47° 7' 50.6"	65° 09' 57.5"
MIR14	47° 7' 55.2"	65° 10' 02.4"
INNER CHANNEL		
MIR18	47° 6' 41.6"	65° 15' 16.9"
MIR19	47° 6' 43.8"	65° 15' 10.6"
CONTROL SITE		
MIR15	47° 8' 21.5"	65° 09' 20.2"
MIR16	47° 8' 22.3"	65° 09' 19.1"

Approximately eight water samples were pumped during the course of each deployment. The times of pumping and the total suspended sediment concentration (dry weight) is given in Table 2. Suspended mass measured on the filtered samples were regressed against the OBS voltage readings to derive total suspended mass in the flume. Plots of the regression analysis for the dump site, the navigation channel, and the control site are shown respectively in Figures 6, 7, and 8.

Table 2. The analyses of water samples pumped from the Sea Carousel during the course of the 10 deployments.

TIME(AST)	SSC (mg/L)	TIME (AST)	SSC (mg/L)	TIME (AST)	SSC (mg/L)
MIR7		MIR8		MIR9	
1203	16.5	1313	24.7	1527	24.4
1209	76.7	1323	82.0	1544	264.6
1219	90.9	1336	145.5	1600	388.8
1224	109.6	1338	152.0	1616	305.1
1233	138.8	1344	216.0	1625	246.9
1236	314.3	1354	111.4	1633	316.0

TIME(AST)	SSC (mg/L)	TIME (AST)	SSC (mg/L)	TIME (AST)	SSC (mg/L)
1247	168.6			1644	609.7
MIR11		MIR13		MIR14	
1749	63.5	1350	21.3	1439	53.5
1802	351.5	1352	478.5	1441	1444
1822	388.6	1355	590	1447	1967
1832	433.7	1358	1564	1452	2059
1840	637.1	1358B	1901	1458	2959
1854	1065.1	1403	2572	1503	2893
1903	1276.6	1403B	2920	1511	3376
1912	1285.1	1413	3044	1516	3320
				1522	3160
MIR15		MIR16		MIR18	
1627	40.0	1745	24.6	1111	11.3
1632	402.8	1747	17.7	1131	684.5
1637	378.0	1759	361.0	1135	1861
1639	927.5	1808	840.9	1146	4127
1644	1069	1814	926.9	1153	5269
1649	1414	1818	1003	1204	4413
1654	1760	1824	1130	1213	3559
1659	1411	1829	1019	1224	1982
1705	1251	1834	1225		
MIR19					
1242	753.5				
1253	3156				
1257	4564				
1302	5002				

TIME(AST)	SSC (mg/L)	TIME (AST)	SSC (mg/L)	TIME (AST)	SSC (mg/L)
1305	9192				
1316	3944				

The calibration functions so derived were as follows:

DUMP SITE SSC(1) = 4.01(OBS1 voltage) - 60; r = 0.95 (5)
DUMP SITE SSC(3) = 2.92(OBS3 voltage) - 60; r = 0.93 (5a)

CHANNEL SSC(1) = $2.56(OBS1) + 0.0008(OBS1)^2 - 4.5e\text{-}7(OBS1)^3$; r = 0.95 (6)
CHANNEL SSC(3) = $3.14(OBS3) - 0.0009(OBS3)^2 + 1.8e\text{-}7(OBS3)^3$; r = 0.87 (6a)

CONTROL SITE SSC(1) = $1.88(OBS1) + 0.0023(OBS1)^2$; r = 0.97 (7)
CONTROL SITE SSC(3) = $1.17(OBS3) + 0.0016(OBS3)^2$; r = 0.95 (7a)

SSC(1) and SSC(3) refer to the suspended sediment concentration inside the annulus recorded by the upper and lower sensors respectively. OBS sensor 2 was situated outside the annulus and gave a measure of the ambient bottom water suspended concentration. Only one ambient water sample was collected during the course of each experiment.

The results of the Sea Carousel deployments provide information on

1. the presence or absence of a fluid mud layer at the time of deployment (as seen on the video camera)

2. cohesion (or resistance to erosion) of the existing surface of the seabed

3. the resistance of the seabed to scour to depths of approximately 5 cm below the seabed, and

4. the density of the bed (through the internal friction angle) i.e. consolidated, unconsolidated, or gel states.

The stresses imposed on the bed are artificial, however the bed responses are real and representative. We emphasise that to put these results into a long-term context specific to Miramichi we need to now the return interval of each imposed bed stress. This can only be derived from long-term measures of the wave and current conditions.

Three illustrations for each deployment site are given in the Appendix A. These are:

1. (A) the time series of azimuthal and vertical current speed induced in the flume (m/s); (B) the raw and cumulative suspended sediment concentration from the 3 OBS's (mg/L); and (C) the erosion rate (differential in sediment concentration in $kg/m^2/s$).

2. Results of the deployment shown on a Mohr-Coulomb plot (applied bed stress (Pa) versus effective stress (Pa)). The effective stress is proportional to depth in the sediment. The solid lines in the figures trace the failure envelope of the sediment with depth (i.e. increase in sediment shear strength). The slope of the line is the friction angle of the

sediment and is a direct indicator of sediment density, and

3. The relationship of erosion rate to applied bed shear stress. This relationship is important to the prediction of bed stability.

Summary

The main parameters derived from this study are: cohesion or surface shear strength, also known as the critical shear stress for erosion; internal friction angle; density profile with depth; and erosion rate as a function of applied bed stress. Table 3 summarizes the results derived from the 10 deployments of Sea Carousel:

Table 3. A summary of results from the 10 Sea Carousel sites reported in this study.

STATION	COHESION (Pa)	EROSION RATE ($kg/m^2/s$)	APPARENT FRICTION ANGLE (degrees)
DUMP SITE B (90)			
MIR7	1.5	3.5×10^{-4}	60
MIR8	0.8	$2 - 3 \times 10^{-4}$	55
MIR9	0.7	1×10^{-3}	44(26)[1]
PERIFERAL TO DUMP SITE B (90)			
MIR11	0.4	1×10^{-3}	4 (NEAR FLUIDIZED BED)
OUTER CHANNEL			
MIR13	0.5	2×10^{-3}	0 (FLUIDIZED BED)
MIR14	0.0	$2\text{-}4 \times 10^{-3}$	0 (FLUIDIZED BED)
INNER CHANNEL			
MIR18	0.0	$2\text{-}3 \times 10^{-3}$	0 (FLUIDIZED BED)
MIR19	0.0	$3\text{-}5 \times 10^{-3}$	0 (FLUIDIZED BED)
CONTROL SITE			
MIR15	1.0	1×10^{-3}	3.6(22)
MIR16	0.0	1×10^{-3}	14

Good results were obtained from the 10 Sea Carousel deployment sites. Our tentative results show that the sediments at all sites were mobilized during the deployment of the Sea Carousel. The most stable sediments were found at dump site B (90). This is illustrated by the high friction angle (suggesting they are the most densified sediments measured), the highest critical shear stress for erosion, and the lowest erosion rates. We found no evidence at this site for the presence of a fluid mud layer.

[1] The bracketed value in the friction angle column indicates a change in friction angle with depth in the sediment.

Site Results - Dump Site B (90)

Deployments MIR7, 8, and 9 were located on the 1990 dump site within dump site B. We found no evidence on the video for the existence of a fluid mud layer at these sites at the time of deployment. In all tests we detected a measurable cohesion of the seabed (0.7 - 1.5 Pa). Erosion rates were less than 1 x 10^{-3} kg/m^2/s and typically 2 - 3 x 10^{-4} kg/m^2/s. The friction angle was high in all cases and showed a linear increase with depth in sediment shear strength. This suggests the sediment was consolidated and was not in a fluidized state. Erosion took place in Type II fashion (chronic erosion). That is, once failure occurred the erosion process continued as long as the applied stress continued. The highest erosion rates were associated with removal of the very surface layer. Beyond this, erosion rate showed a high degree of scatter when plotted against applied stress. An "eyeball" fit through the scatter suggests that erosion rate was independent of absolute applied bed stress. Further study to plot erosion as a function of excess bed shear stress (the incremental increase of the stress only) yielded no better fits.

MIR11 was located on the perifery of the 1990 dump site. It showed the lowest cohesion (0.4 Pa), and the highest erosion rates (2 - 4 x 10^{-3} kg/m^2/s) in this region. The erosion character was of Type II. The site was, therefore, the least stable seabed monitored in this region and would be subject to chronic erosion. The internal friction angle of 4° was very close to a fluidized state, and suggested that this bed had not consolidated to the extent of the 1990 dump site material. Erosion rate versus bed shear stress showed a high degree of scatter and no relationship to applied bed stress.

Site Results - Navigation Channel

The outer channel was surveyed during deployments MIR13 and 14. No evidence of a fluid mud layer was detected at either site on the video. Cohesion was virtually absent. That is, erosion began even at the lowest applied stresses. Erosion exibited both Type I and Type II characteristics. Peaks in the erosion rate were up to 4 x 10^{-3} kg/m^2/s. These are amongst the highest measured in the entire survey. Failure took place by aggregate release from the bed rather than as discrete particles. These aggregates moved as saltation load along the bed whereupon corrasion disaggregated them. The disaggregated material thereafter moved in suspension. This impacts the choice of settling velocity that one uses in numerical prediction. Clearly a higher settling rate is required than is predicted by Stoke's settling of disaggregated particles. The Mohr-Coulomb plots indicated a friction angle of zero. That is the weight of the sediment was supported by the pore pressure and the bed was fluidized. Video observations showed, however, that the bed was not behaving as a viscous fluid (as might be supposed) but was exhibiting behaviour diagnostic of a gel. This gel appeared to be held together by organic fibres within the sediment.

The inner channel was surveyed during deployments MIR18 and 19. No evidence for a fluid mud layer was detected on the video at either of these sites. The seabed possessed no cohesion (resistance to erosion at low stresses), although the same gel-like qualities (as seen in the outer channel) of the bed were observed. The bed was characterised principally by Type II erosion. The greatest erosion rates were associated with the very surface sediments (0.1 kg/m^2/s). Beneath this layer erosion rate decreased to 2 - 5 x 10^{-3} kg/m^2/s. The erosion rate was independent of the applied bed shear stress. Again, the erosion process took place by releases of aggregates that moved in saltation along the bed without the development of a fluid mud layer.

Site Results - Control Site

MIR15 and 16 were undertaken within the area of the control site. It was chosen to be representative of a natural seabed within the Miramichi estuary. No evidence for a fluid mud

layer was detected at either site. A high degree of variability in cohesion (up to 1.0 Pa) was measured which in both cases was lower than that measured at dump site B (90). The erosion rate, also showed a high degree of variability with depth and with applied stress. It appeared to increase with depth to a local maximum of 0.01 $kg/m^2/s$ and thereafter decreased to a constant value of 1 x 10^{-3} $kg/m^2/s$; this latter value was independent of applied bed shear stress. The friction angle was intermediate between those of the channel and those of the dump site, and reached a maximum value of 26°. Changes in friction angle with depth and between the two sites illustrated a complex bed microfabric and a complex depositional history for the area.

Site Results - SOBS - Control Site

Deployed: 1135 AST, 5 November, 1991

Recovered: 1015 AST, 7 November, 1991

The video camera was set up to record for 10 seconds every 5 minutes. The OBS sensors were logged continuously at 1Hz. The S4 current meter logged two horizontal components of flow and water depth every 2 seconds at a height of 50 cm above the seabed.

The tripod and current meter were pulled over during the deployment of the system. Consequently, no meaningful data were recovered at this site. The camera system worked well but was pointing upwards and showed only the water column. The current meter experienced interference, presumably because some if its electrodes were in the sediment.

Site Results - SOBS - Dump Site 90

Deployed: 1235 AST, 7 November, 1991

Recovered: 1630 AST, 8 November, 1991

The video camera was set up to record for 10 seconds every 5 minutes. The OBS sensors were logged continuously at 1Hz. The S4 current meter logged two horizontal components of flow and water depth every 2 seconds at a height of 50 cm above the seabed.

Data from the SOBS system are still being analysed. The video camera unfortunately did not work. The current meter gave good results and the time series of the currents and water depth are shown in Appendix A. This Figure shows current speed, current direction, and water depth for the 28 hour deployment. Notice that the currents rarely exceed 0.2 m/s. Compare this to the erosion at Sea Carousel site MIR9. Notice that there is virtually no erosion at this velocity suggesting that under normal tidal conditions the dump site is stable. The peaks in current speed and the rotation of the current direction is not strongly linked to tidal elevation. Clearly, the currents in Miramichi bay are complex and not driven purely by the tides.

Results - Lancelot

Lancelot calibration graphs are given in Appendix B; penetration records are also shown in Appendix B. Table 4 summarizes key deployment data for all Lancelot stations. Table 5 summarizes the interpretation of sediment type based upon the penetration pore pressure data. The general finding was that the seabed ranged from a fine sandy silt to silt with a trace of clay; several deployments indicated a bottom density ranging from very loose to medium-dense. Cobbles damaged the filter tip during several deployments, significantly altering penetration response but not the longer-term measurements.

Table 4. A summary of the deployments of Lancelot in this study.

STATION	START TIME	END TIME	SCANS/SECOND
LAN1	Nov. 5 11:58:02	Nov. 6 10:12:42	4
LAN7	Nov. 6 11:24:56	Nov. 6 13:49:37	2
LAN9	Nov. 6 15:14:53	Nov. 6 17:10:52	2
LAN10	Nov. 6 17:25:31	Nov. 7 11:07:24	4
LAN13	Nov. 7 13:28:00	Nov. 7 14:40:21	4
LAN15	Nov. 7 16:07:42	Nov. 7 17:36:00	2
LAN17	Nov. 7 19:38:17	Nov. 8 14:07:10	4
LAN20	Nov. 8 14:59:13	Nov. 8 16:47:02	2

Table 5. A summary of inferred sediment types based upon the Lancelot data.

STATION	SEDIMENT TYPE (inferred)	SEABED DENSITY (inferred)	EXCESS PORE PRESSURE
CONTROL SITE			
LAN1	Silt	Medium Dense	1 cm
LAN15	Silt, some Clay	Very Loose	3 cm
DUMP SITE B			
LAN7	Silty Sand	Loose	0
LAN9	Silty Sand, some Clay	Loose	2 cm
LAN10	Silty Sand, with Clay	Loose	2 cm
OUTER CHANNEL			
LAN13	Fine Sand, some Silt	Medium Dense	0
INNER CHANNEL			
LAN17	Silt	Very Loose	1 cm
LAN20	Silt	Medium Dense	1 cm

Negative differential pore pressure spikes develop in dense (dilatant) coarse-grained sediments subjected to rapidly-applied shearing stress. This was found to occur in the early stages of all Miramichi Lancelot deployments, indicating that the seabed is generally composed of incompressible material with a low clay content.

The height of an initial positive differential pore pressure spike in loose (contractant) coarse-grained or soft fine-grained (cohesive) sediment is indicative of a threshold for liquefaction; note

that this then corresponds to an undrained failure around the probe. Subsequently, the bed reconsolidates and differential pore pressure drops to the stable value, which may be in excess of the hydrostatic reference if the seabed is underconsolidated. The zero excess pore pressures recorded at sites LAN7 and LAN 13 indicate the sediments to be in equilibrium over the long-term.

Table 6 summarizes the magnitude of the penetration pore pressure spike (du) and the inferred *insitu* undrained shear strength (S_u) at 50 cm below seabed (where applicable). S_u can be estimated from the height of the initial pore pressure spike according to Vesic (1972); also Bennett al. (1985) and Esrig (1977):

$$S_u = F\ du \qquad (8)$$

where F is a coefficient varying between 3 and 6, depending on plasticity. For the silty sediments encountered in this study, a mean value of 4.5 was adopted. For almost the entire study, surface wave activity was minimal to non-existent. Stresses and pressures are therefore expressed in this report as equivalent heads of water for comparison to surface wave height as follows:

$$du_{eq} = 100\ du\ /\ 9.81 \qquad (9)$$

where du is a pressure in kPa and du_{eq} is the same pressure expressed in cm of head. So equation (8) becomes

$$S_u = 0.44145\ du \qquad (10)$$

Skempton (1970) observed that undrained shear strength in a fully consolidated soil deposit was governed by the effective stress (P') where

$$P' = 4\ S_u \qquad (11)$$

Insitu effective vertical stress is also calculated directly from the saturated bulk density (ρ_s), the density of seawater (ρ_{sw}), the gravitational constant (g) and the burial depth (Z) according to Terzaghi and Peck (1967) where

$$P_v' = (\rho_s - \rho_{sw})\ g\ Z - u_e \qquad (12)$$

where u_e is the excess pore pressure, which is zero for an equilibrium condition. Then, by rearranging equation (12)

$$\rho_s = (P_v' + u_e)\ /\ (g\ Z) + \rho_{sw} \qquad (13)$$

Equation (11) can be used to estimate the vertical effective stress from the penetration record of Lancelot, which can then be compared to the fully consolidated estimate produced from bulk density measurements, or alternatively, equation (13) can be used to predict the *insitu* density, which can then be compared to measured density data.

Table 6. Estimates of undrained strength based upon Lancelot data recorded in this study.

STATION	TIDAL STAGE	du cm	S_u kPa	P_v' kPa
LAN1	flood/ebb	-	NA	NA
LAN7	flood	3.6	1.59	6.36
LAN9	Turning	-	NA	NA
LAN10	ebb	5.0	2.21	8.84
LAN13	flood	-	NA	NA
LAN15	Unknown	9.6	4.24	16.96
LAN17	ebb/flood	5.0	2.21	8.84
LAN20	flood	-	NA	NA

Note that LAN1, LAN10 and LAN 17 were overnight deployments and were sampled in burst mode. The effective stress was calculated from equation (12), ranging between 0.5 and 3 kPa for a point 50 cm below the mudline and densities varying from 1.1 to 1.6 g/cm^3. Effective stress estimates calculated using equation (11) are listed in Table 6 along with the Lancelot shear strength and pore pressure data used. P_v' is overestimated by this approach by about a factor of 4, probably indicating that penetration was not entirely undrained, hence the empirical correlation developed for clays (equation 8) is not directly applicable for the silty sediments encountered in the Miramichi. For this reason, estimates of bulk density using equation (13) are unreliable for these sediments.

Wave Loading and Liquefaction

Lancelot has the capability of resolving excess or differential pore pressure within the seabed to within 1 mm of head over a total range of 4 m. The capability to measure surface wave height on the absolute pressure transducer is not as high, being 2.2 cm over a total range of 25 m.

Small surface waves overnight at the LAN10 site did not register on the absolute pressure channel, therefore they were attenuated, and therefore very small. However, a differential pore pressure within the seabed was set up that oscillated about the long-term value of 2 cm (from 1 to 3 cm). Wave period was about 2.5 seconds, which is in the right range for small surface waves. This oscillation would eventually lead to liquefaction if it were to reach a critical value wherein the pore pressure momentarily supported the bouyant weight of the sediment column above the point of measurement (-50 cm), in the manner described by Clukey et al (1985). The point of liquefaction can be assumed to be roughly equivalent to du, which was 5 cm for LAN10. The inference from this observation is that the bed was nearly liquefied by a small surface wave. One could imagine the effect that large waves would have, as often develop during storms. The net result would be widespread liquefaction during the storm event.

LAN17 produced a dataset that was also remarkable in that the liquefaction threshold was about 3.5 cm, with a very rapid dissipation stage after penetration. This indicated a very loose deposit, probably composed of silt (at 50 cm burial). Long-period seiche waves (again less than 2 cm in surface amplitude) or infra-gravity waves developed during the overnight burst sampling, perhaps in response to the incoming tide. The internal wave amplitude was very low, about 4 mm with a period of 1.7 minutes. The long-term differential pore pressure du was negative, indicating that the seabed was dilating (expanding) in response to a shearing stress, much in the same way as it does when it is dense and incompressible yet must deform around a penetrating probe. The

seabed in essence "stiffened" during this loading event.

Discussion

The direction and magnitude of the pore pressure differential spike upon insertion gave information on the "state" of the seabed over the depth of penetration. The data for the Miramichi Harbour indicated that in general, sediments were very loose to loose; several locations were more dense. Density plays an important role in determining how a sedimentary deposit will behave under cyclic loading; dense sediments dilate or expand, creating negative pore pressures which increase the effective stress; hence they become stronger until the loss of interlocking (failure) strength. Loose deposits contract during shear, resulting in residual excess pore pressure which needs time to dissipate; these deposits therefore experience a reduction in effective stress and become weaker during loading.

Accurate measurements of density are extremely difficult in coarse-grained sediments, which unfortunately remould very easily when sampled, even using the best-available techniques. Indirect penetration techniques minimize sampling disturbance by sensing the response of the sediment ahead of and around a probe as it goes into the undisturbed deposit. Efforts are ongoing to correlate penetration data with sediment density and grain size.

With soft cohesive or loose cohesionless deposits it is possible to estimate the undrained shear strength at failure as previously discussed, and therefore place a limit on the threshold for liquefaction. Cyclic loading of the seabed by waves can lead to liquefaction and loss of integrity if the sediment is unable to dissipate excess pore pressures rapidly enough. Lancelot is useful in detecting the threshold for liquefaction, as well as monitoring the buildup of excess pore pressures during various loading events. The rate of decay of penetration pore pressure can used in a quantitative way to calculate the time-rate of consolidation which can then be used to determine the capacity to dissipate pore pressures developed under cyclic loading.

The long-term differential pore pressure allows an interpretation of the time-dependent state of consolidation of a sediment deposit, wherein a fully consolidated package will be at equilibrium; an underconsolidated deposit will show some residual pore pressure still to be dissipated.

Post-liquefied sediment shearing resistance is governed by residual parameters since particle interlocking has been removed; mobility is greatly enhanced and flowslides will occur at slope angles in excess of the residual friction angle. Detailed laboratory analyses can provide this type of information, but are beyond the scope of this study at present.

RECOMMENDATIONS

1. This study of dump site B (90) was undertaken 2 years after dumping took place. Consolidation of this material has clearly taken place. In order to put our results into context a laboratory study of consolidation rates of dump material is necessary.

2. We measured the stability of dump site B, but only the 1990 dumped material. In view of the complexity of dumping and the variety of dumped material it would be wise to monitor other dumps within dump site B.

3. Variability of the natural seabed was high. Unfortunately, we base this on only two stations. Tentatively, the natural bed appears less stable than does the dump site. Approximately 5 - 10 more stations would be valuable to define more conclusively the natural bed stability, and to show more clearly the relative stability between dumped and natural material.

4. We could not find any evidence of fluid muds anywhere in the estuary. The fluid state may well occur under severe storms, under dredging of channel material, or during the passage of a ship. We recommend the deployment of SOBS near the channel for up to 1 month and possibly to coincide with dredging, in order to evaluate the potential for fluid mud generation. Even when fluidized, the bed does not behave as a viscous fluid, but possesses elastic properties that supress the resuspension process. Are these properties typical of all parts of the channel, what causes it, and what bed stresses overcome it if any ?

5. We recommend both SOBS and Sea Carousel deployments during a period of dumping of dredged material in order to detect the level of suspended solids in the water column. Do fluid muds develop during the dumping process, and if so, how persistent are they ?

6. In order to put our results into a long-term context percentage exceedence plots of wave climate and current speed should be compiled. From these percentage exceedence plots of long-term bed stability can be defined.

7. Lancelot has been used in shallow-water mode to successfully monitor cyclic loading events in the Miramichi estuary; preliminary findings are that the seabed is easily liquefied. Penetration pore pressure responses suggest a very loose, variable silty seabed at depth. Undrained strengths are very low, estimated at less than 5 kPa at 50 cm depth. No natural liquefaction events were detected during the study period, but substantial differential pore pressures developed during two deployments due to minor wave loading events. Surface wave activity was overall small to non-existent. Future studies should involve longer-term deployments of Lancelot to capture the seabed response under transient loading generated by storms and ship passage, particularly adjacent to the channel. This will require upgrading of the memory capacity to 20 mbytes, but will allow for 28-day deployments with continuous sampling at a rate of 2 scans per second.

8. Stability analyses of the seabed adjacent to the ship channel should be carried out as part of a future study to assess the potential for chronic failure under larger wave loading events.

REFERENCES

Amos, C.L., Daborn, G.R. H.A. Christian, A. Atkinson, and A. Robertson. in review. *Insitu* erosion measurements on fine-grained sediments from the Bay of Fundy. Marine Geology.

Amos, C.L. Grant, J, Daborn, G.R. and Black, K. in press. Sea Carousel - a benthic annular flume. Estuarine Coastal and Shelf Sciences.

Bennett, R.H., Burns, J.T., Li, H., Walter, D., Valent, P.J., Percival, C.M. and Lipkin, J. 1990. Subseabed Disposal Project Experiment: Piezometer probe measurement technology. Geotechnical Engineering of Ocean Waste Disposal, ASTM Special Technical Publication 1087, K.R. Demars and R.C. Chaney, Eds., American Society for Testing and Materials, Philadelphia: 175-189.

Bennett, R.H., Li, H., Burns, J.T., Percival, C.M. and Lipkin, J. 1989. Application of piezometer probes to determine engineering properties and geological processes in marine sediments. Applied Clay Science, 4, Elsevier Science Publishers B.V., Amsterdam: 337-355.

Bennett, R.H., Li, H., Valent, P.J., Lipkin, J. and Esrig, M.I. 1985. In-situ undrained shear strengths and permeabilities derived from piezometer measurements. Strength Testing of Marine Sediments, Laboratory and In-Situ Measurements, ASTM Special Technical Publication 883, R.C. Chaney and K.R. Demars, Eds., American Society for Testing and Materials, Philadelphia, pp. 83-100.

Burt, T.N. 1984. The Carousel: commissioning of a circular flume for sediment transport research. Hydraulic Research Limited Report SR 33.

Christian, H.A. and Gillespie, D.G. (in prep.) Permeability from a piezometric penetrometer deployed in deep-sea clays at the Bermuda Rise. Marine Geotechnology.

Christian, H.A. and Heffler, D. (in prep.) LANCELOT - A seabed piezometer for geotechnical studies. Current Research, Geological Survey of Canada.

Christian, H.A., Heffler, D. and Davis, E.E. (in prep.) LANCELOT - An in-situ piezometer for soft marine sediments. Deep-Sea Research.

Clukey, E.C., Kulhawy, F.H. and Liu, P. L.-F. 1985. Response of silts to wave loads: experimental study. Strength Testing of Marine Sediments, Laboratory and In-Situ Measurements, ASTM Special Technical Publication 883, R.C. Chaney and K.R. Demars, Eds., American Society for Testing and Materials, Philadelphia: 381-396.

Davis, E.E., Horel, G.C., MacDonald, R.D., Villinger, H., Bennett, R.H. and Li, H. 1991. Pore pressures and permeabilities measured in marine sediments with a tethered probe. Journal of Geophysical Research, 96: 5975-5984.

Downing, J.P. 1983. An optical instrument for monitoring suspended particulates in ocean and laboratory. in Proceedings of Oceans'83: 199-202.

Downing, J.P. and Beach, R.A. 1989. Laboratory apparatus for calibrating optical suspended solids sensors. Marine Geology 86: 243 - 249.

Esrig, M.I., Kirby, R.C. and Bea, R.G. 1977. Initial development of a general effective stress method for the prediction of axial pile capacity for driven piles in clay. 9_{th} Annual Offshore Technology Conference, OTC 2943, Houston, TX, May 2-5: 495-501.

Postma, H. 1967. Sediment transport and sedimentation in the estuarine environment. in Lauff, G.M. (ed), Estuaries. Publ. American Association for the Advancement of Science, No. 83: 158-179.

Shames, I. 1962. Mechanics of Fluids. Publ. McGraw-Hill Book Company,New York: 555p.

Schultheiss, P.J. 1990. In situ pore pressure measurements for a detailed geotechnical assessment of marine sediments: state of the art. Geotechnical Engineering of Ocean Waste Disposal, ASTM Special Technical Publication 1087, K.R. Demars and R.C. Chaney, Eds., American Society for Testing and Materials, Philadelphia: 190-205.

Schultheiss, P.J. 1990. Pore pressures in marine sediments: an overview of measurement techniques and some geological engineering applications. Marine Geophysical Researches, 12: 153-168.

Skempton, A.W. 1970. The consolidation of clays by gravitational compaction. Quarterly Journal of the Geological Society of London, 125: 373-411.

Sternberg, R.W. 1972. Predicting initial motion and bedload transport of sediment particles in the shallow marine environment. in D.J.P. Swift, D.B. Duane and O.H. Pilkey (eds) Shelf Sediment Transport, Processes and Pattern, Publ. Dowden, Hutchinson and Ross: 61-83.

Terzaghi, K. and Peck, R.B. 1967. Soil Mechanics in Engineering Practice. John Wiley & Sons, New York, 729 p.

Vesic, A.S. 1972. Expansion of cavities in infinite soil masses. Journal of the Soil Mechanics and Foundation Engineering Division, American Society for Civil Engineers, 98, SM3, pp. 265-290.

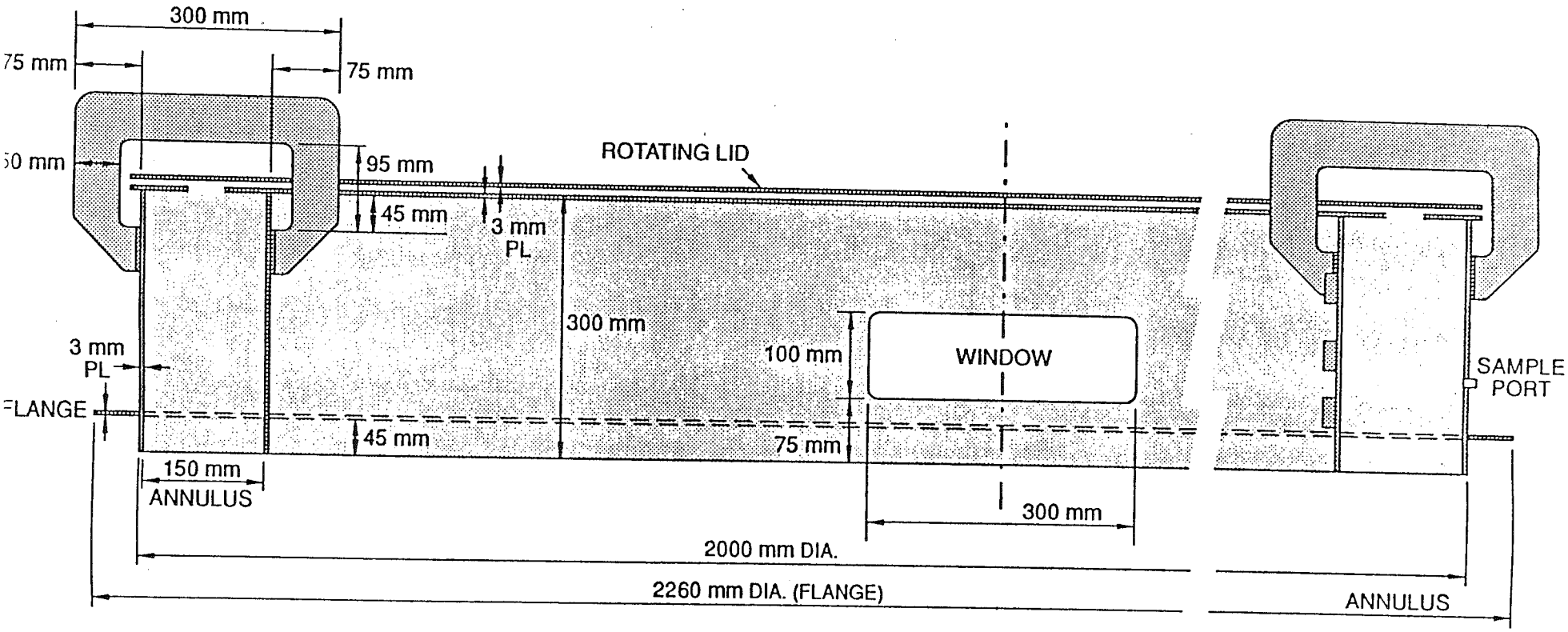
300 mm
75 mm
75 mm
50 mm
95 mm
45 mm
3 mm
PL
ROTATING LID
300 mm
3 mm
PL
100 mm
WINDOW
SAMPLE
PORT
FLANGE
45 mm
75 mm
150 mm
ANNULUS
300 mm
2000 mm DIA.
2260 mm DIA. (FLANGE)
ANNULUS

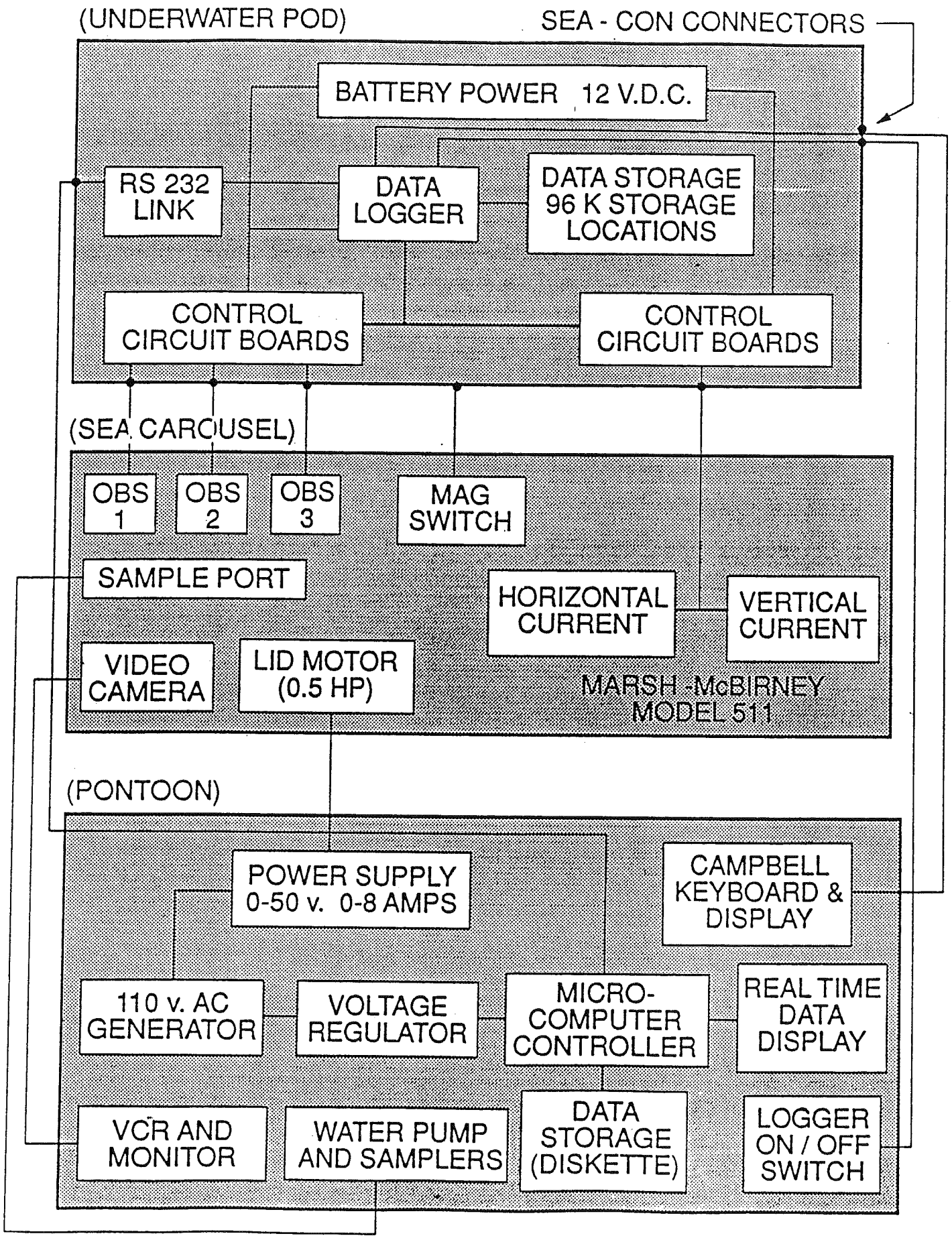
(UNDERWATER POD)
SEA - CON CONNECTORS
BATTERY POWER 12 V.D.C.
RS 232 LINK
DATA LOGGER
DATA STORAGE 96 K STORAGE LOCATIONS
CONTROL CIRCUIT BOARDS
CONTROL CIRCUIT BOARDS
(SEA CARCUSEL)
OBS 1
OBS 2
OBS 3
MAG SWITCH
SAMPLE PORT
HORIZONTAL CURRENT
VERTICAL CURRENT
VIDEO CAMERA
LID MOTOR (0.5 HP)
MARSH -McBIRNEY MODEL 511
(PONTOON)
POWER SUPPLY 0-50 v. 0-8 AMPS
CAMPBELL KEYBOARD & DISPLAY
110 v. AC GENERATOR
VOLTAGE REGULATOR
MICRO-COMPUTER CONTROLLER
REAL TIME DATA DISPLAY
VCR AND MONITOR
WATER PUMP AND SAMPLERS
DATA STORAGE (DISKETTE)
LOGGER ON / OFF SWITCH

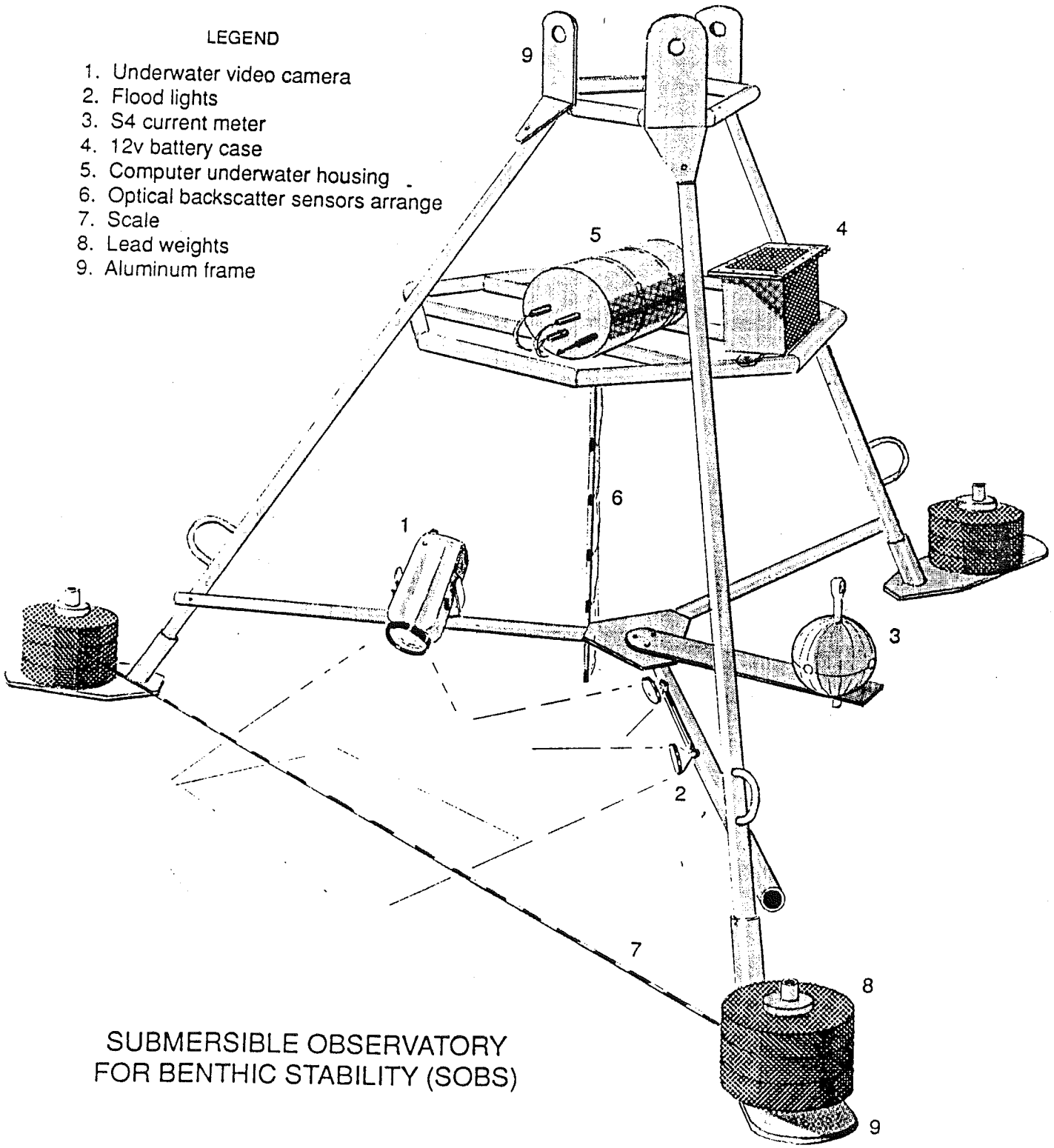
LEGEND
1. Underwater video camera
2. Flood lights
3. S4 current meter
4. 12v battery case
5. Computer underwater housing
6. Optical backscatter sensors arrange
7. Scale
8. Lead weights
9. Aluminum frame
SUBMERSIBLE OBSERVATORY
FOR BENTHIC STABILITY (SOBS)

FIGURE 3

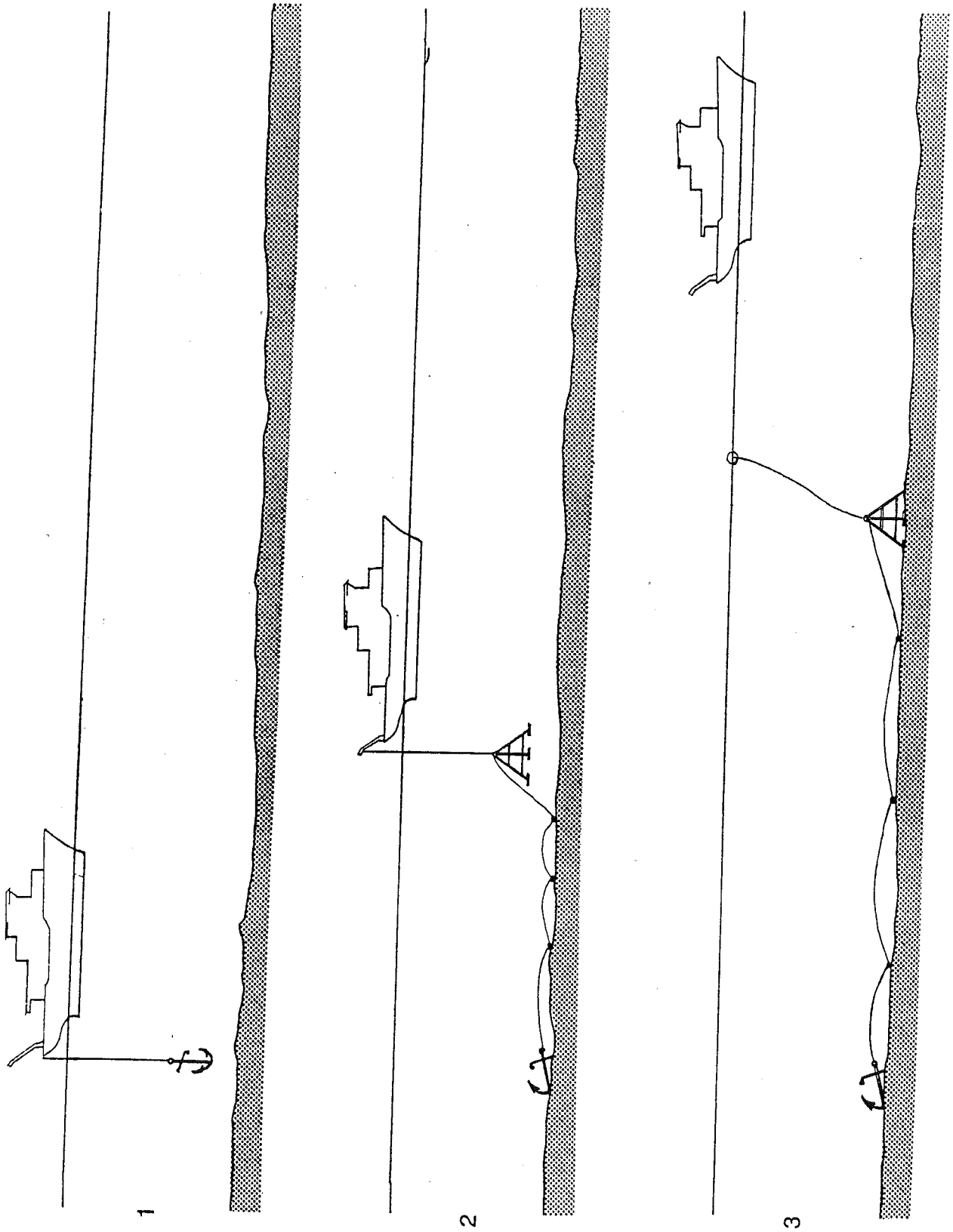

FIGURE 4

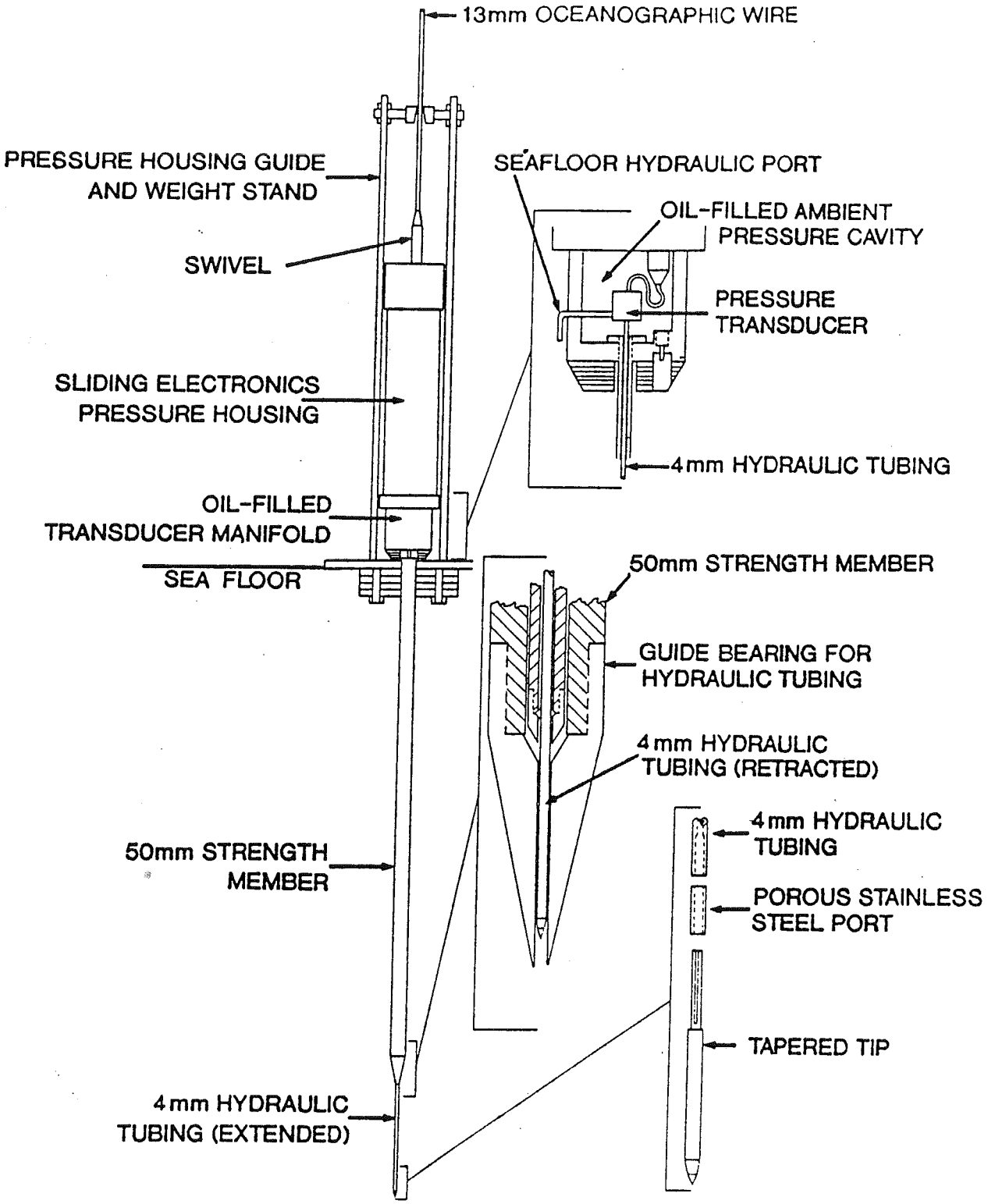
13mm OCEANOGRAPHIC WIRE
PRESSURE HOUSING GUIDE AND WEIGHT STAND
SWIVEL
SLIDING ELECTRONICS PRESSURE HOUSING
OIL-FILLED TRANSDUCER MANIFOLD
SEA FLOOR
50mm STRENGTH MEMBER
4mm HYDRAULIC TUBING (EXTENDED)
SEAFLOOR HYDRAULIC PORT
OIL-FILLED AMBIENT PRESSURE CAVITY
PRESSURE TRANSDUCER
4mm HYDRAULIC TUBING
50mm STRENGTH MEMBER
GUIDE BEARING FOR HYDRAULIC TUBING
4mm HYDRAULIC TUBING (RETRACTED)
4mm HYDRAULIC TUBING
POROUS STAINLESS STEEL PORT
TAPERED TIP

FIGURE 5

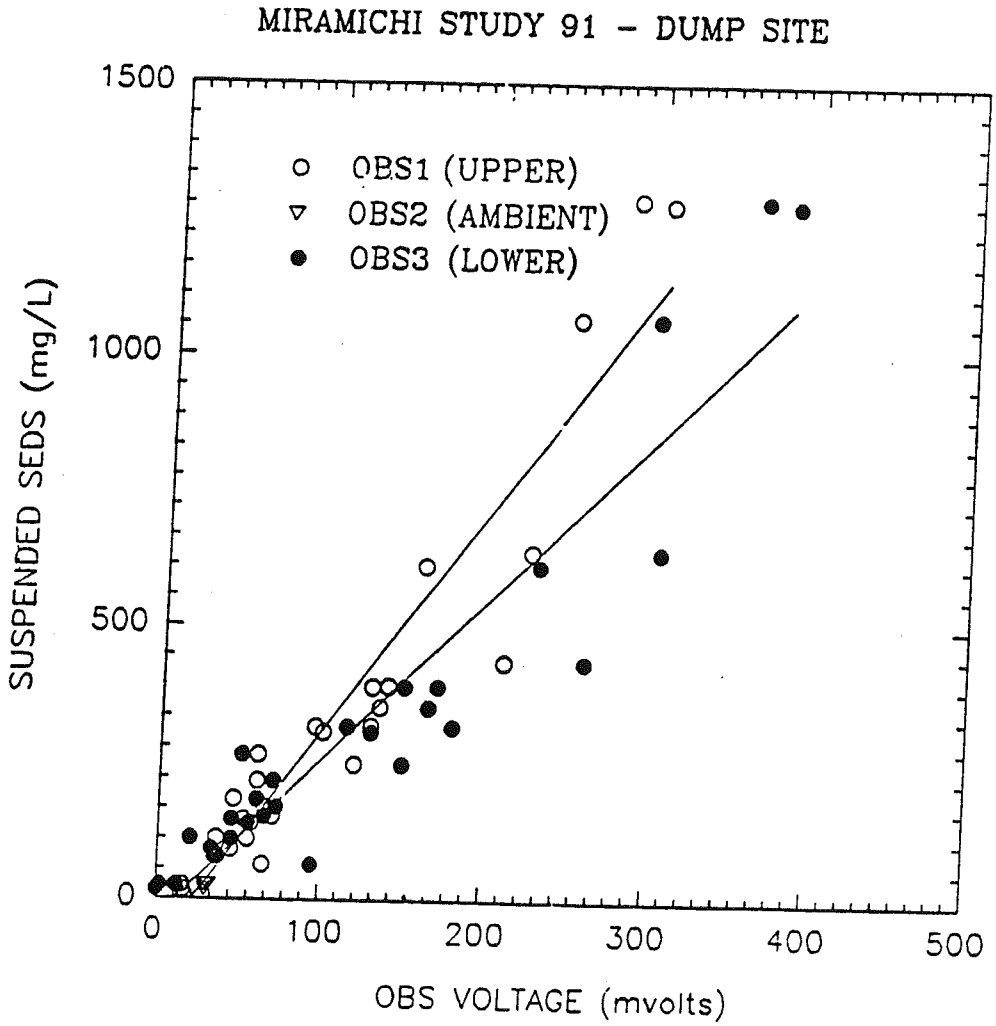
MIRAMICHI STUDY 91 - DUMP SITE
OBS1 (UPPER)
OBS2 (AMBIENT)
OBS3 (LOWER)
SUSPENDED SEDS (mg/L)
1500
1000
500
0
0
100
200
300
400
500
OBS VOLTAGE (mvolts)

FIGURE 6

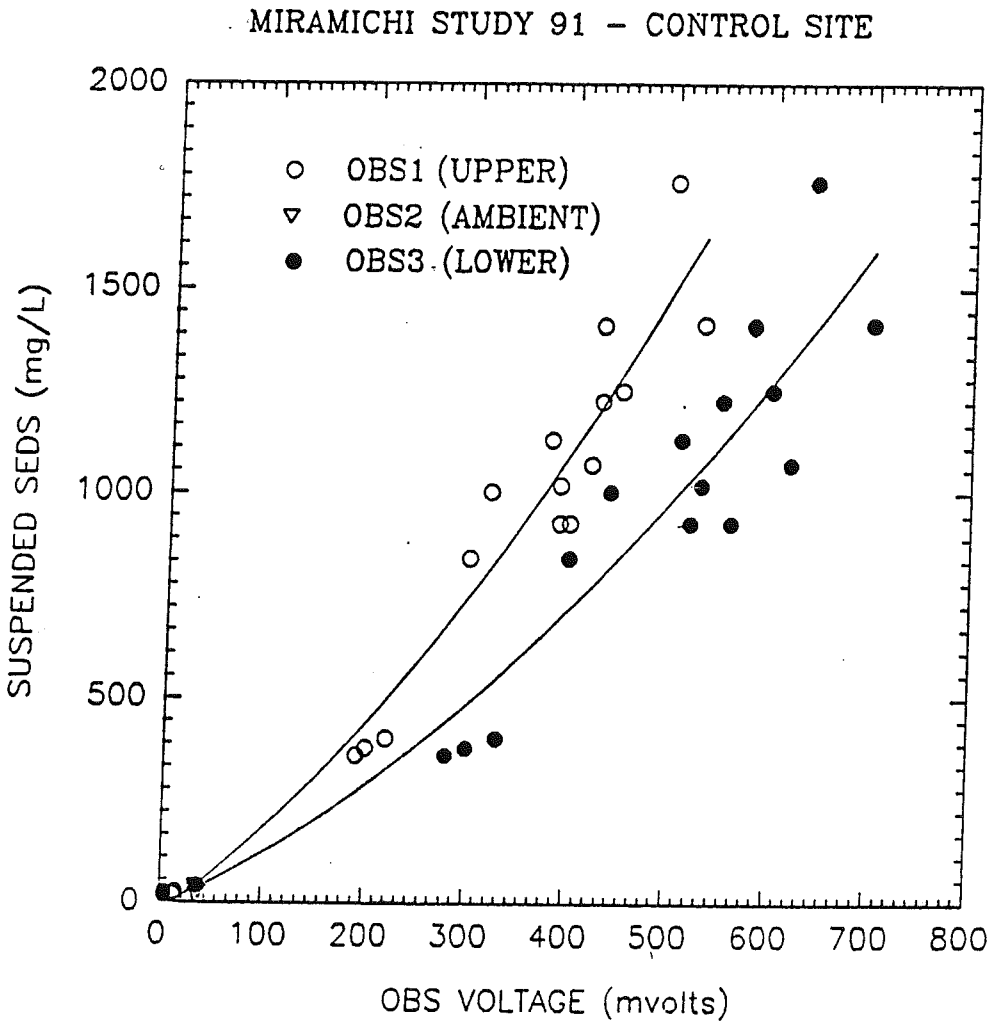
MIRAMICHI STUDY 91 – CONTROL SITE
OBS1 (UPPER)
OBS2 (AMBIENT)
OBS3 (LOWER)
SUSPENDED SEDS (mg/L)
2000
1500
1000
500
0
0
100
200
300
400
500
600
700
800
OBS VOLTAGE (mvolts)

FIGURE 7

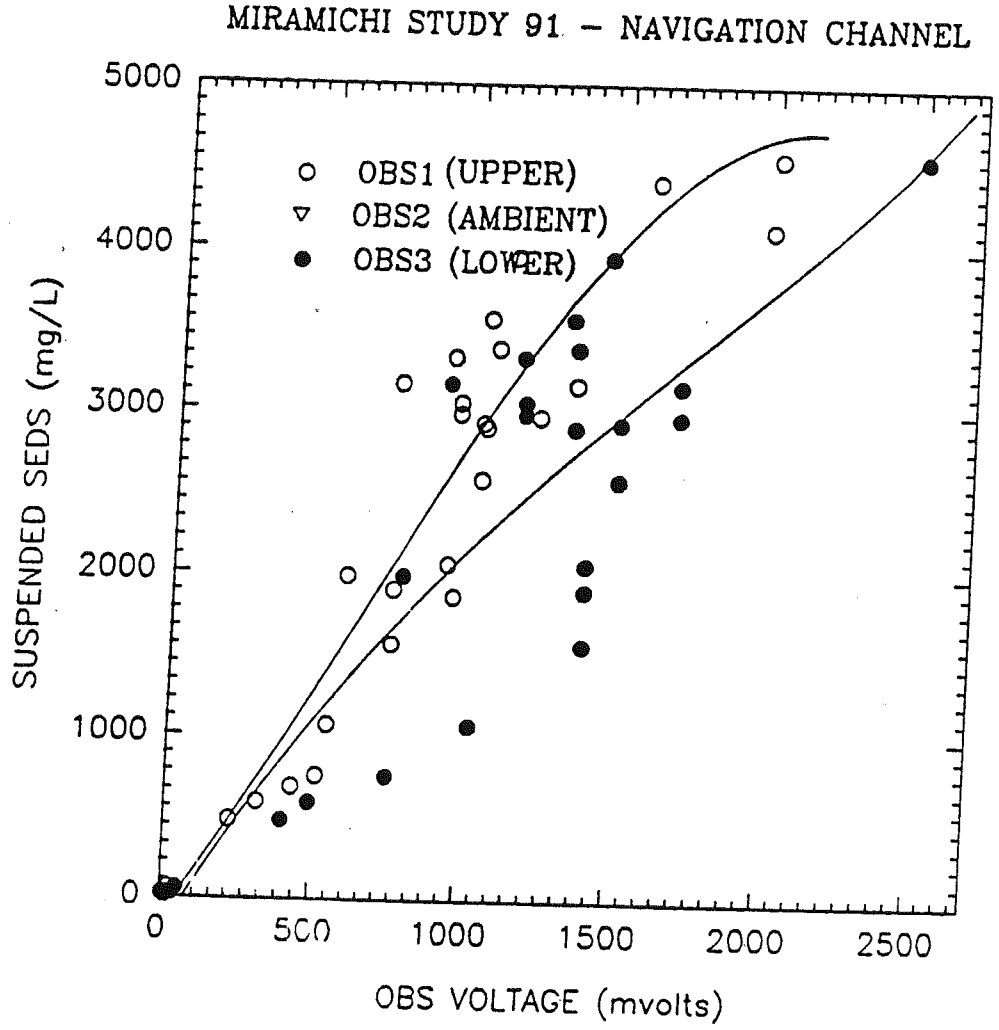
MIRAMICHI STUDY 91 – NAVIGATION CHANNEL
OBS1 (UPPER)
OBS2 (AMBIENT)
OBS3 (LOWER)
SUSPENDED SEDS (mg/L)
OBS VOLTAGE (mvolts)
0
1000
2000
3000
4000
5000
500
1500
2500

FIGURE 8

APPENDIX A

SEA CAROUSEL – MIRAMICHI DUMP SITE B (90)

STATION MIR7 – 6 Nov. 1991

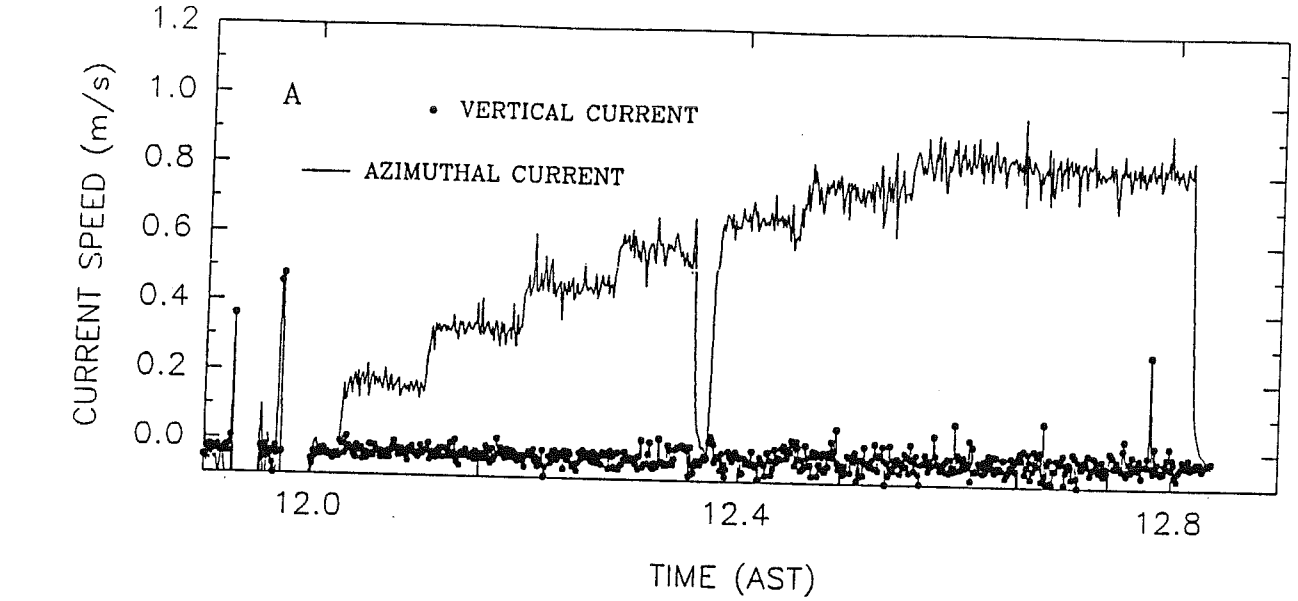

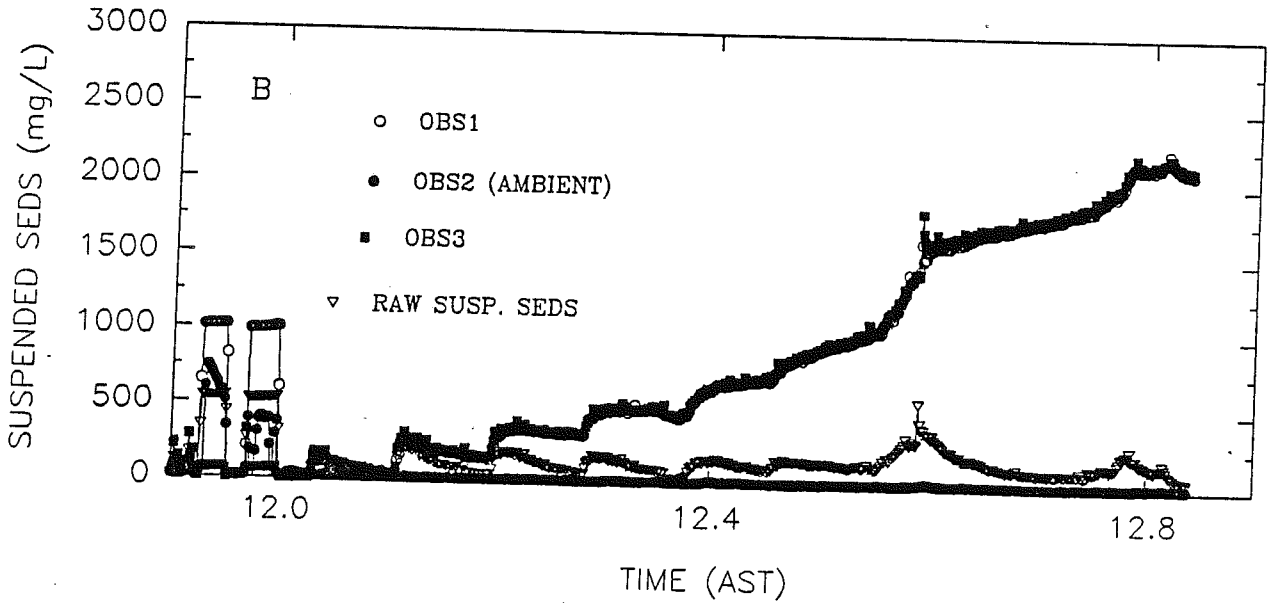

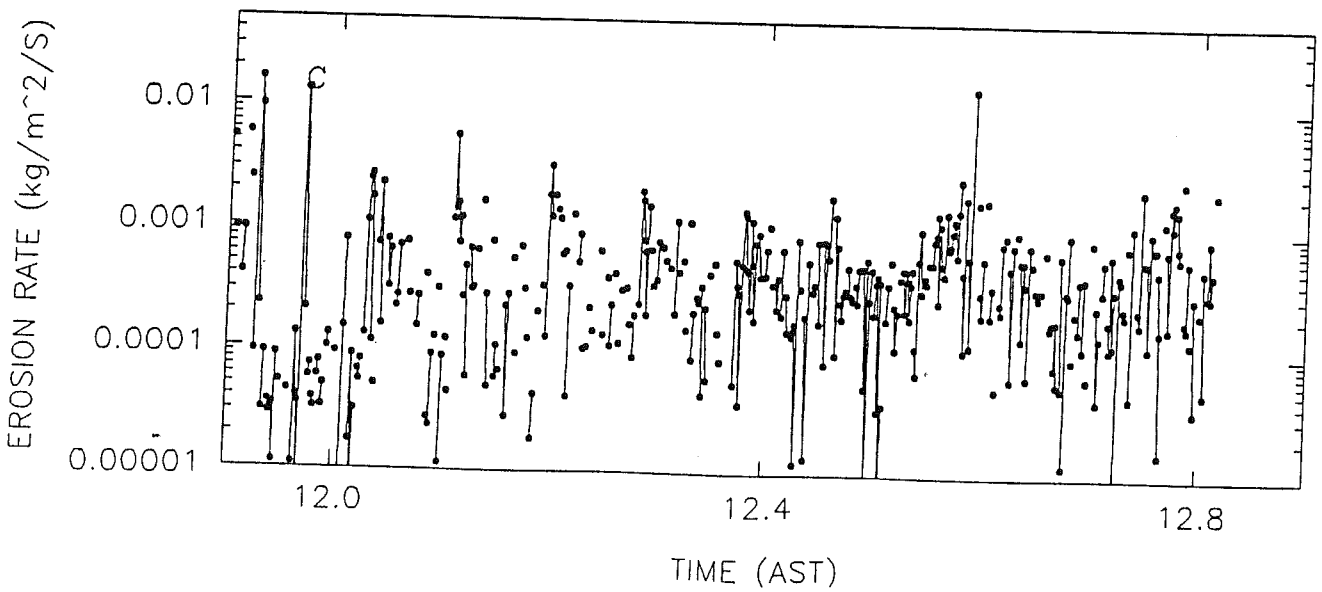

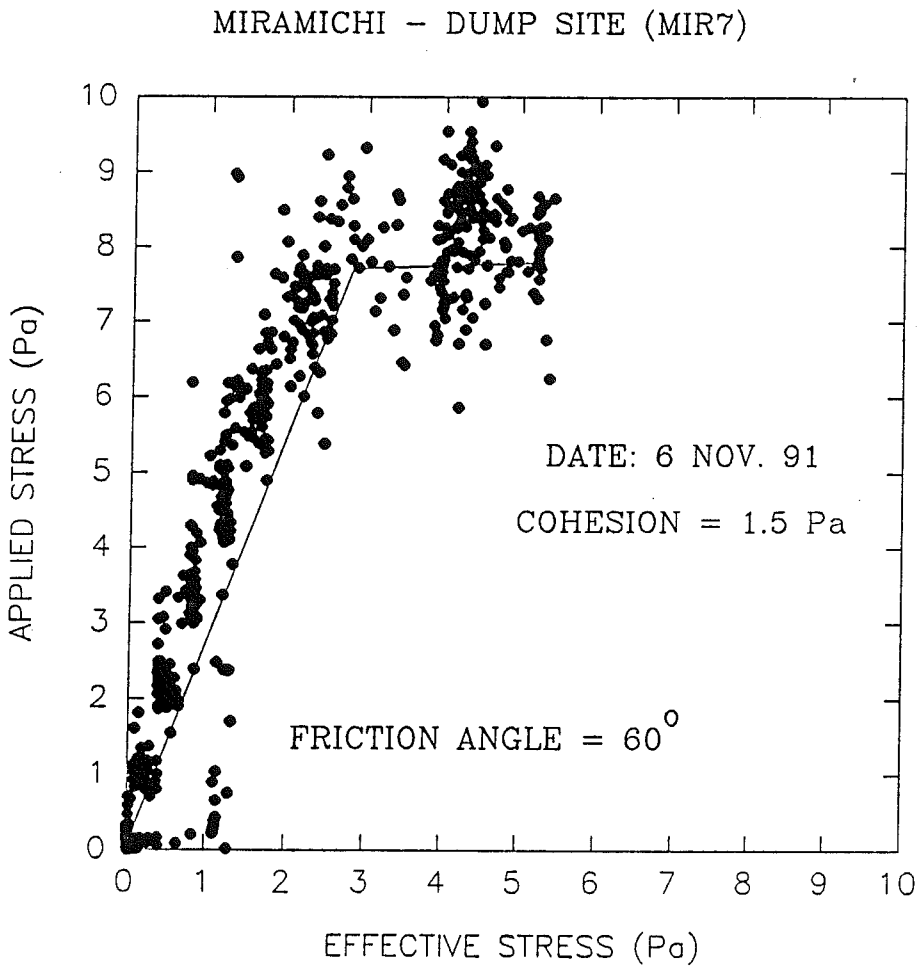
MIRAMICHI – DUMP SITE (MIR7)
APPLIED STRESS (Pa)
EFFECTIVE STRESS (Pa)
0
1
2
3
4
5
6
7
8
9
10
DATE: 6 NOV. 91
COHESION = 1.5 Pa
FRICTION ANGLE = 60°

SEA CAROUSEL – MIRAMICHI – DUMP SITE (90)

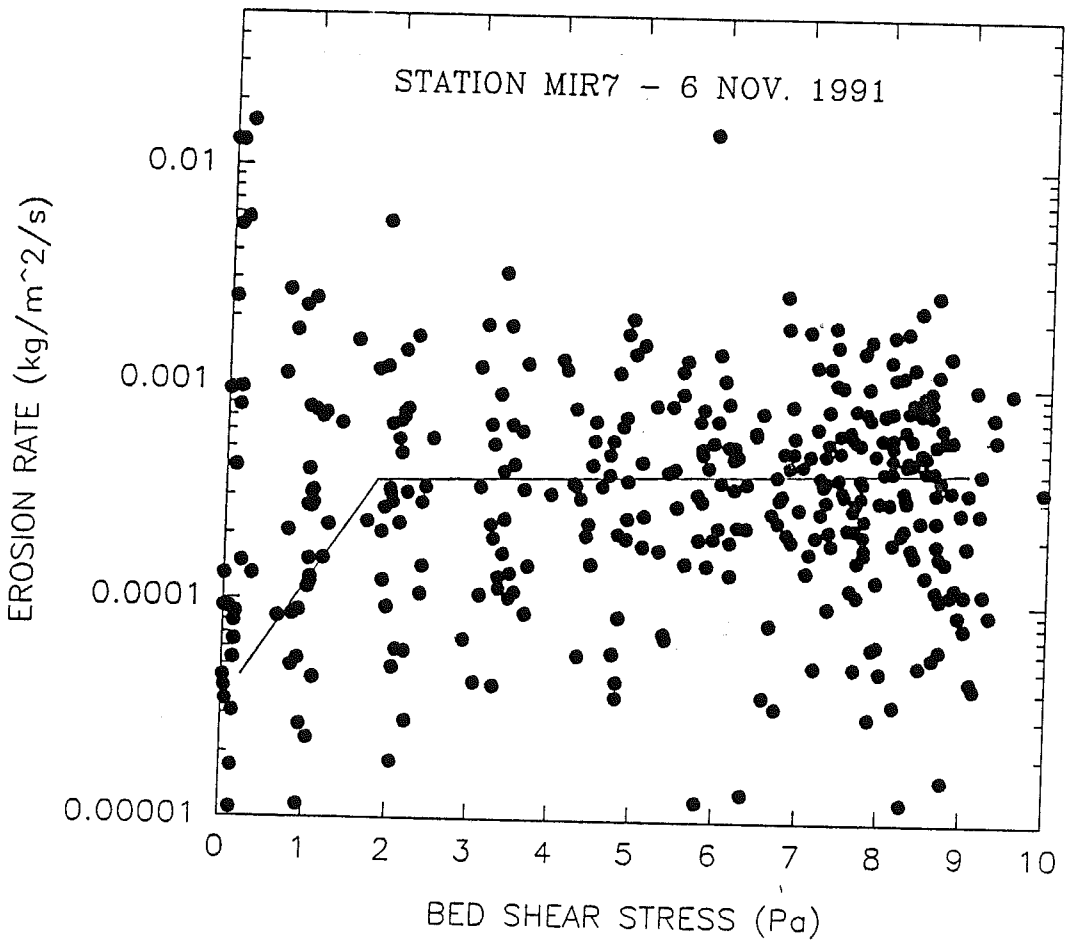

SEA CAROUSEL – MIRAMICHI DUMP SITE B (90)

STATION MIR8 – 6 Nov. 1991

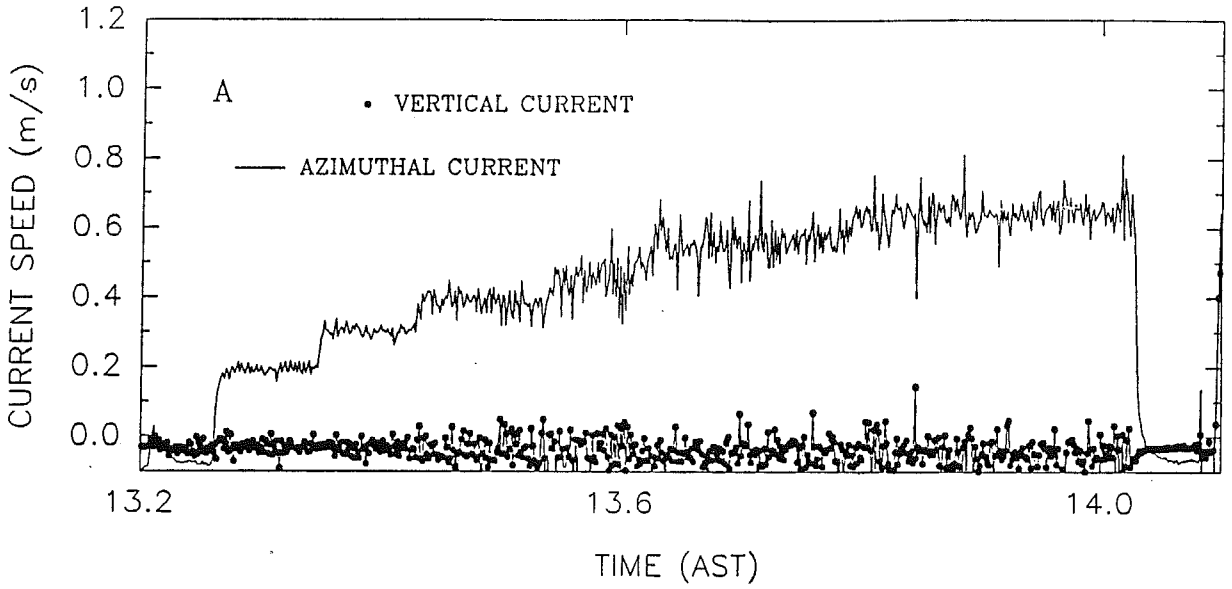

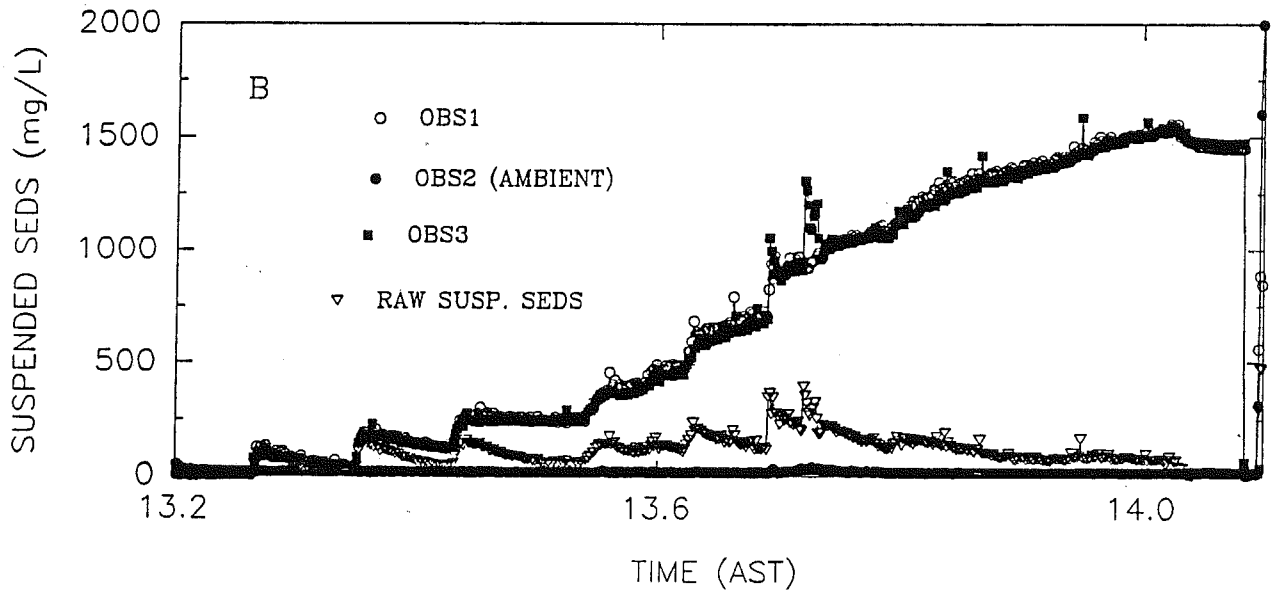

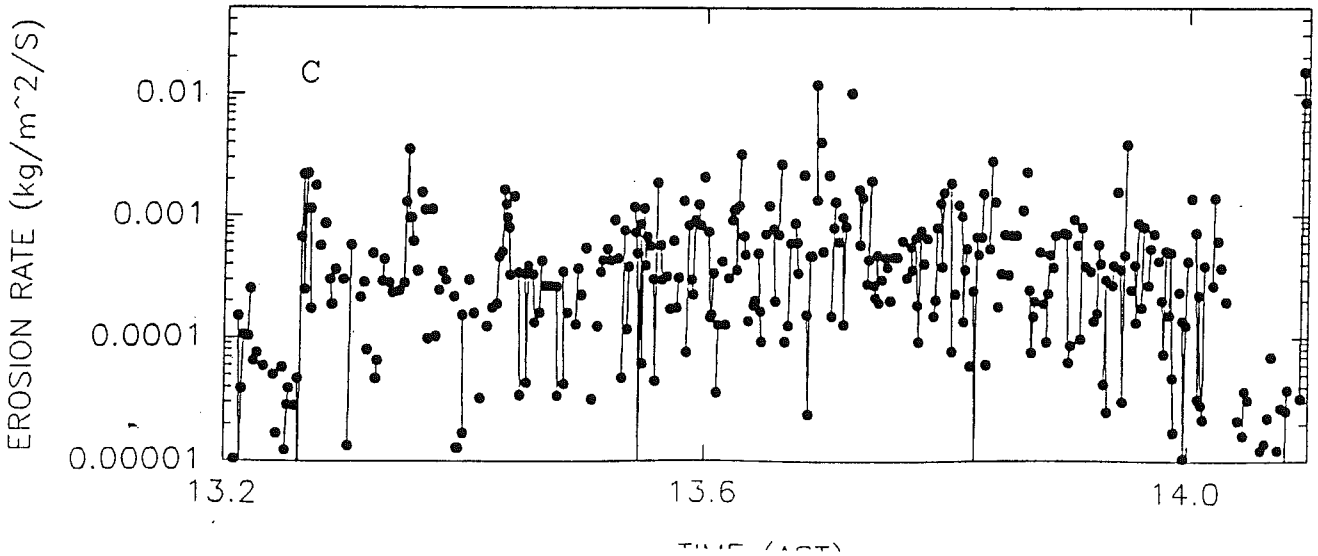

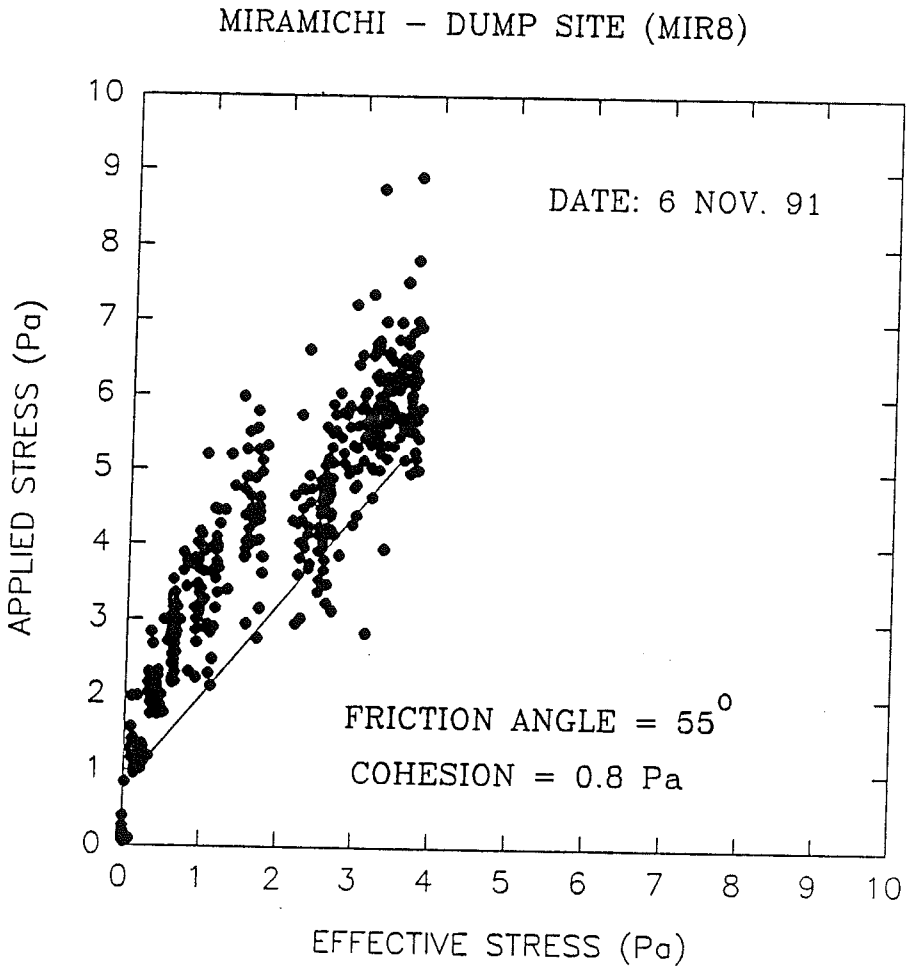
MIRAMICHI – DUMP SITE (MIR8)
DATE: 6 NOV. 91
FRICTION ANGLE = 55°
COHESION = 0.8 Pa
APPLIED STRESS (Pa)
EFFECTIVE STRESS (Pa)
0
1
2
3
4
5
6
7
8
9
10

SEA CAROUSEL – MIRAMICHI – DUMP SITE (90)

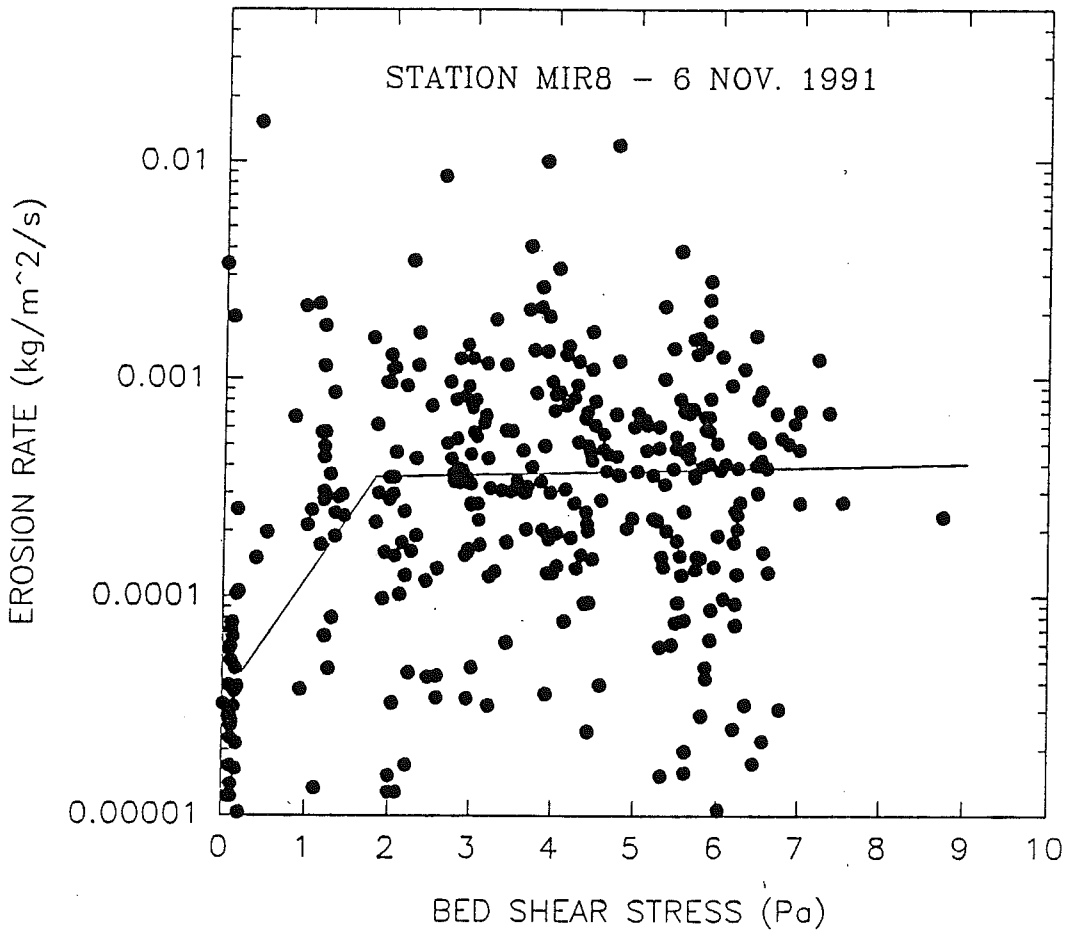

SEA CAROUSEL – MIRAMICHI DUMP SITE B (90)

STATION MIR9 – 6 Nov. 1991

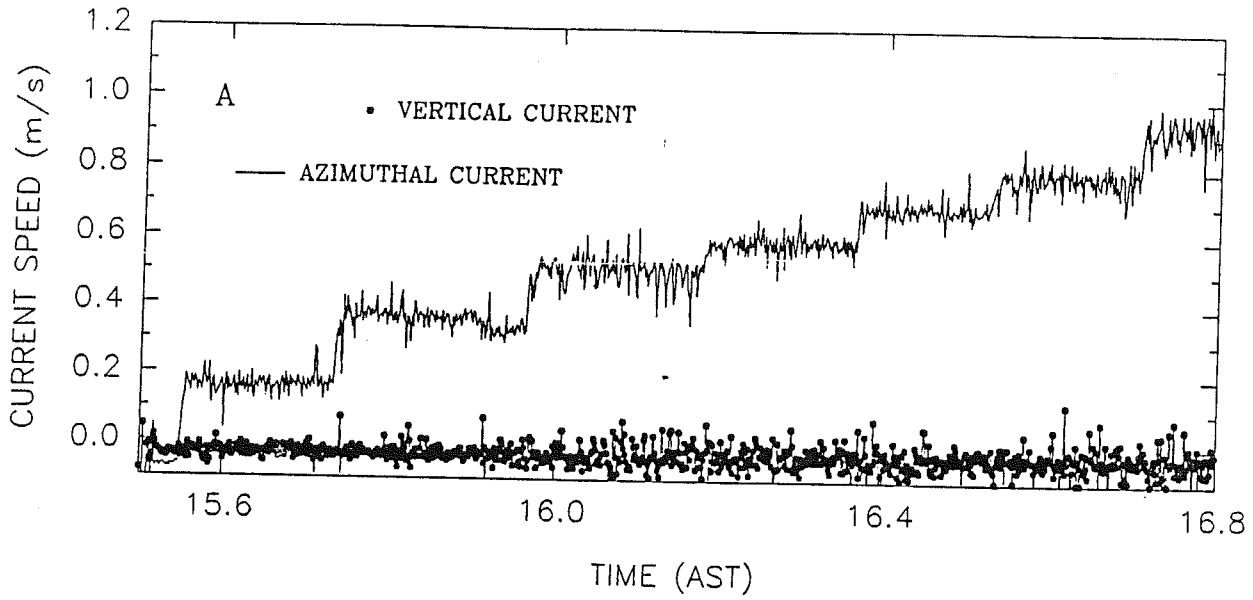

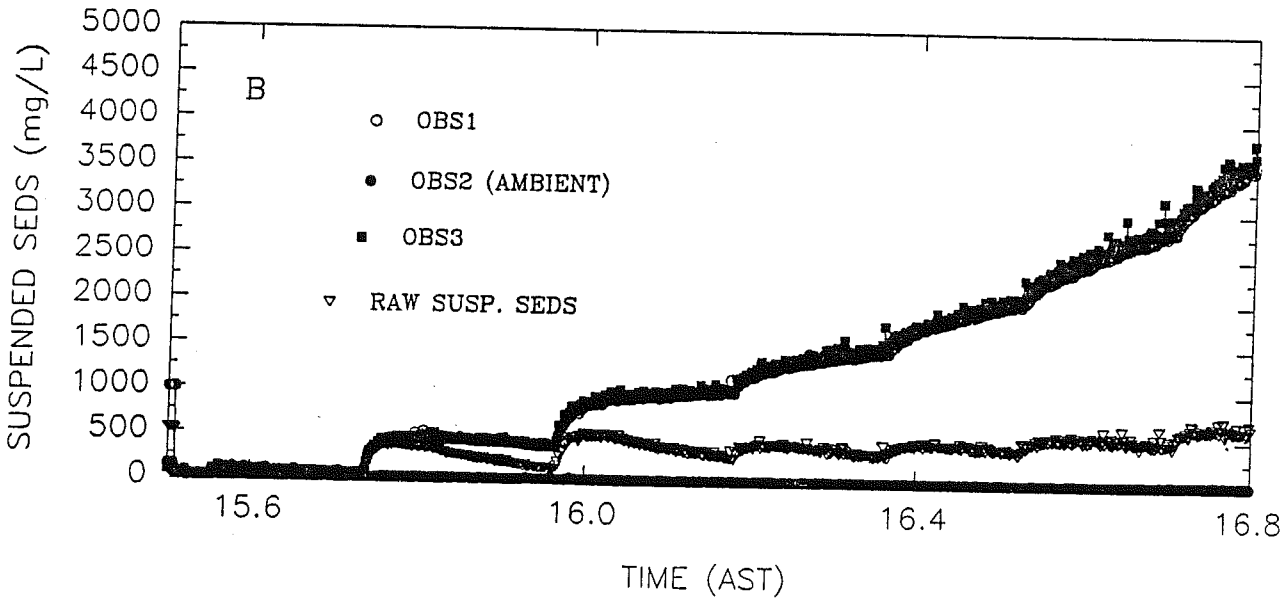

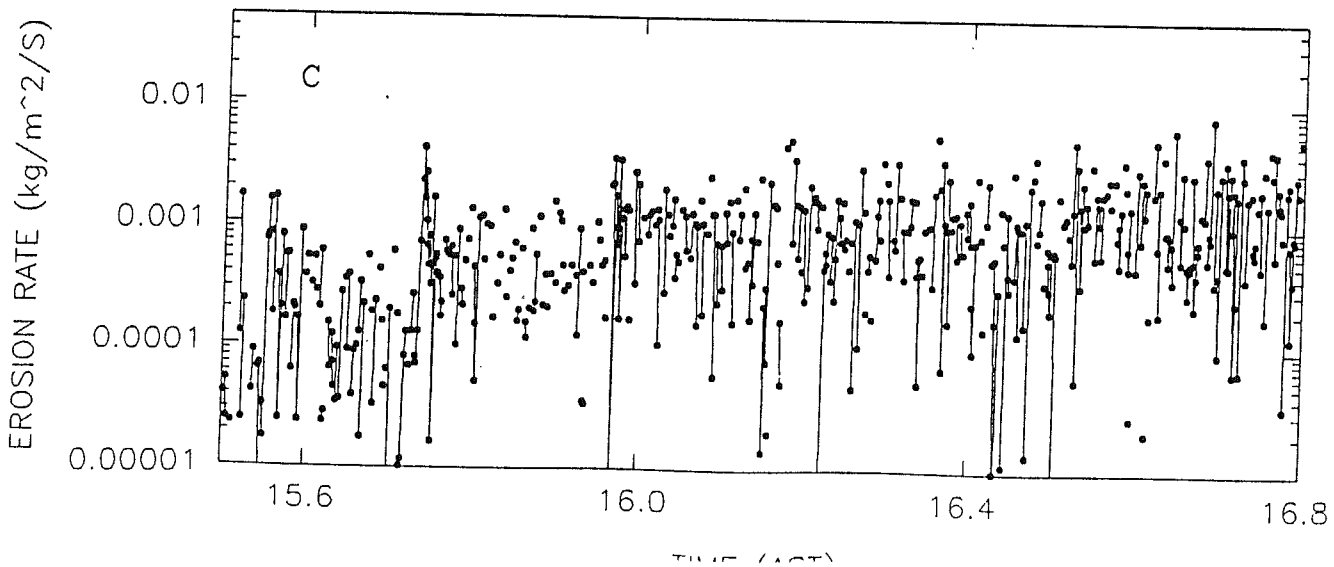

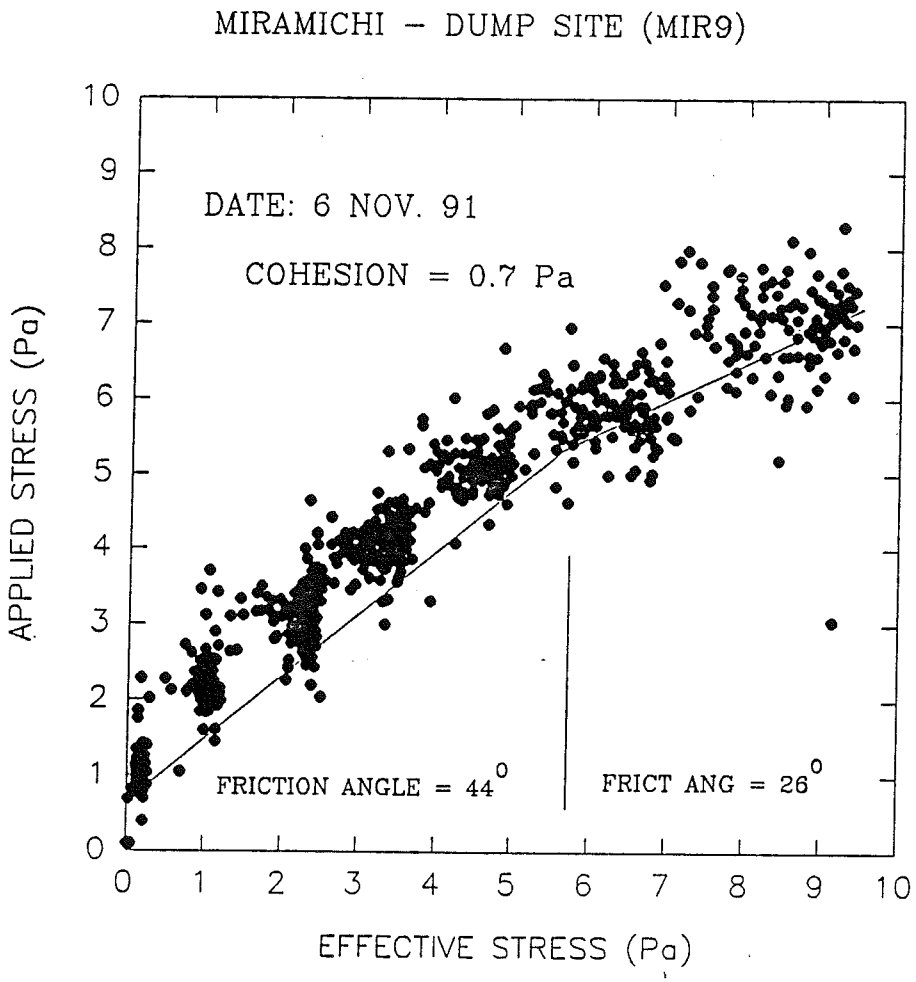
MIRAMICHI – DUMP SITE (MIR9)
DATE: 6 NOV. 91
COHESION = 0.7 Pa
FRICTION ANGLE = 44°
FRICT ANG = 26°
APPLIED STRESS (Pa)
EFFECTIVE STRESS (Pa)
0
1
2
3
4
5
6
7
8
9
10

SEA CAROUSEL – MIRAMICHI – DUMP SITE (90)

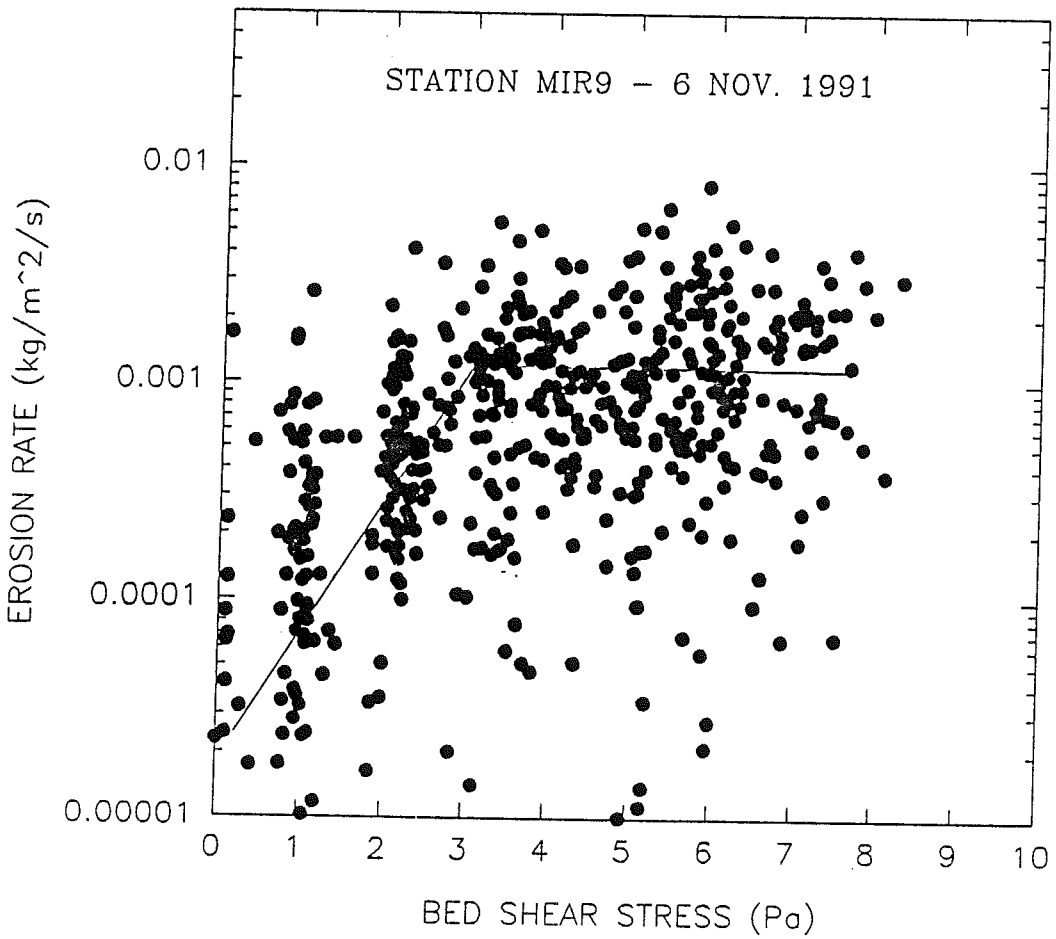

SEA CAROUSEL – MIRAMICHI DUMP SITE B (90)

STATION MIR11 – 6 Nov. 1991

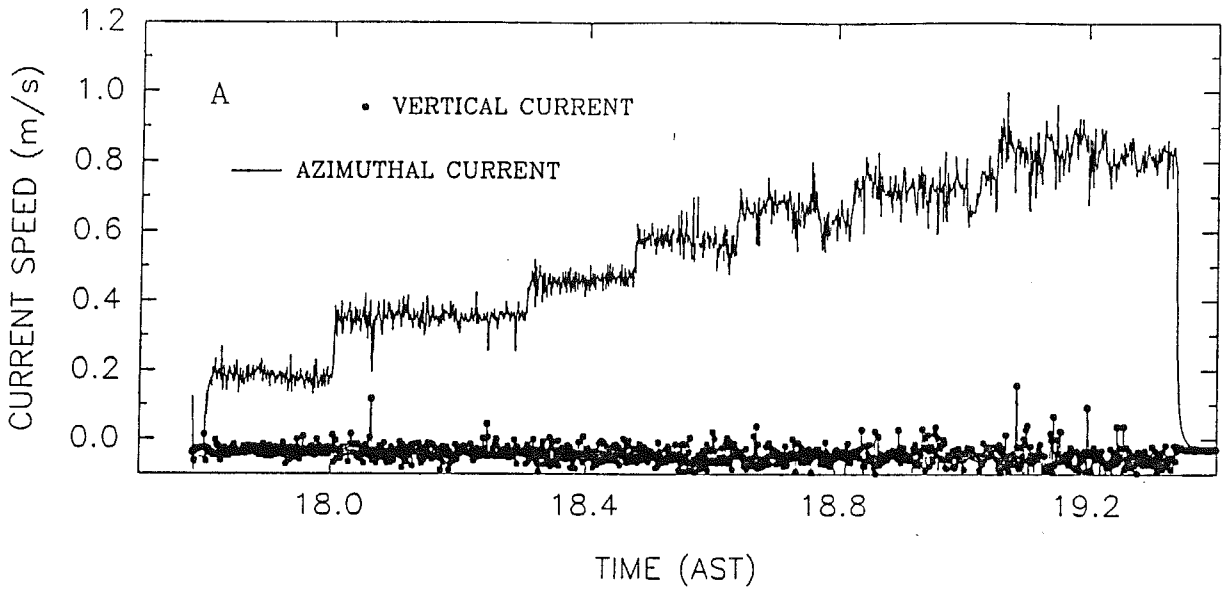

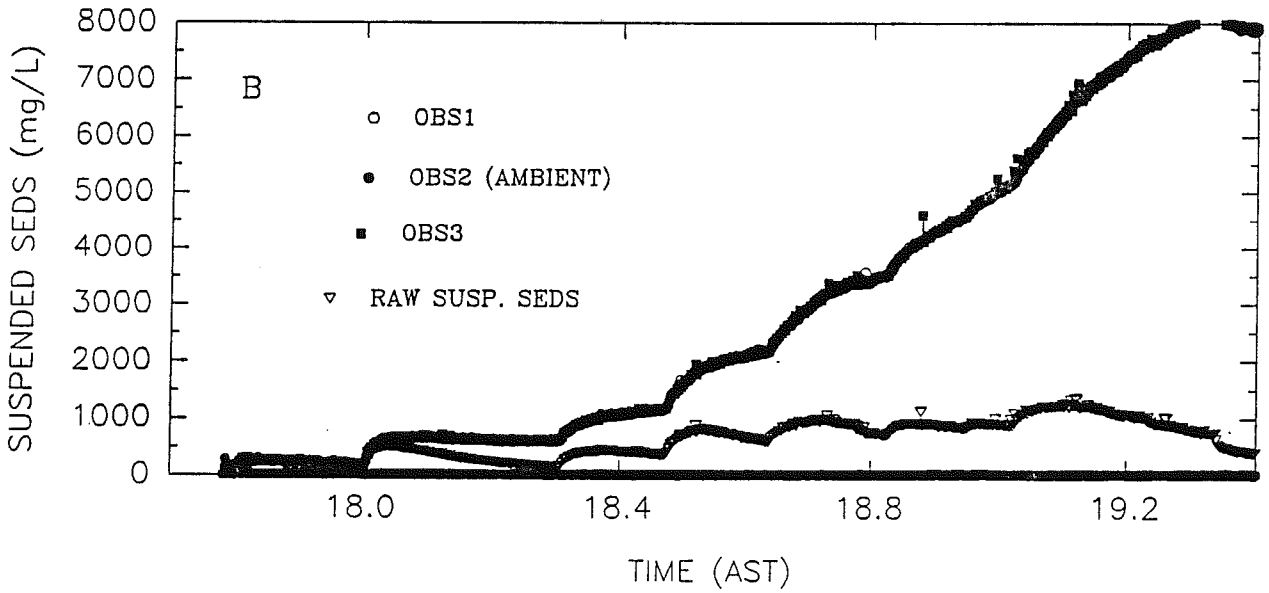

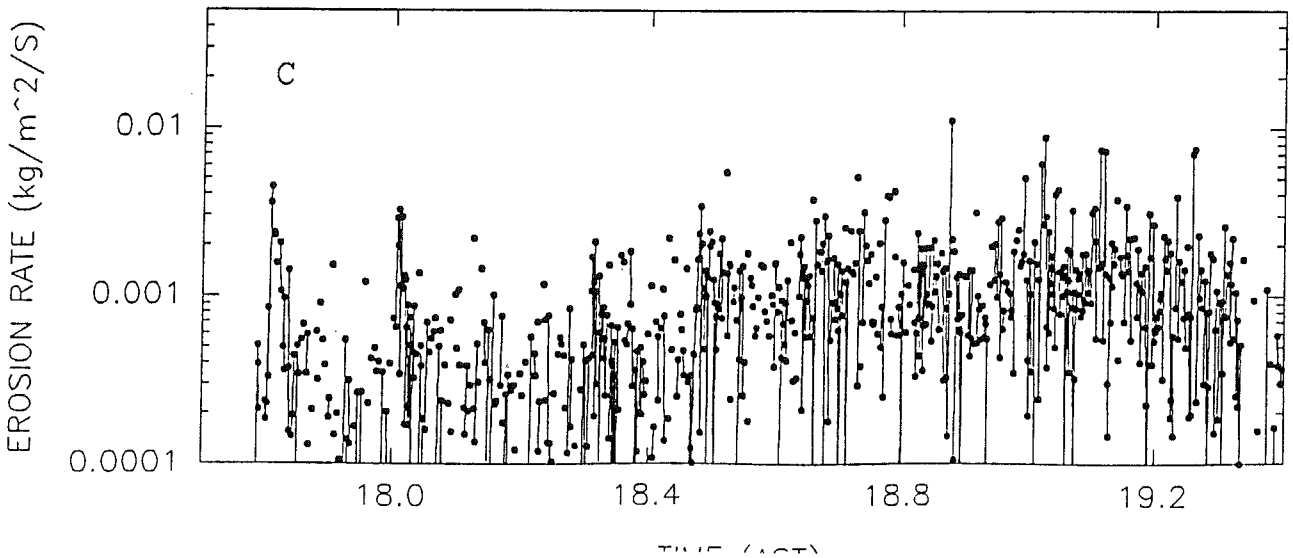

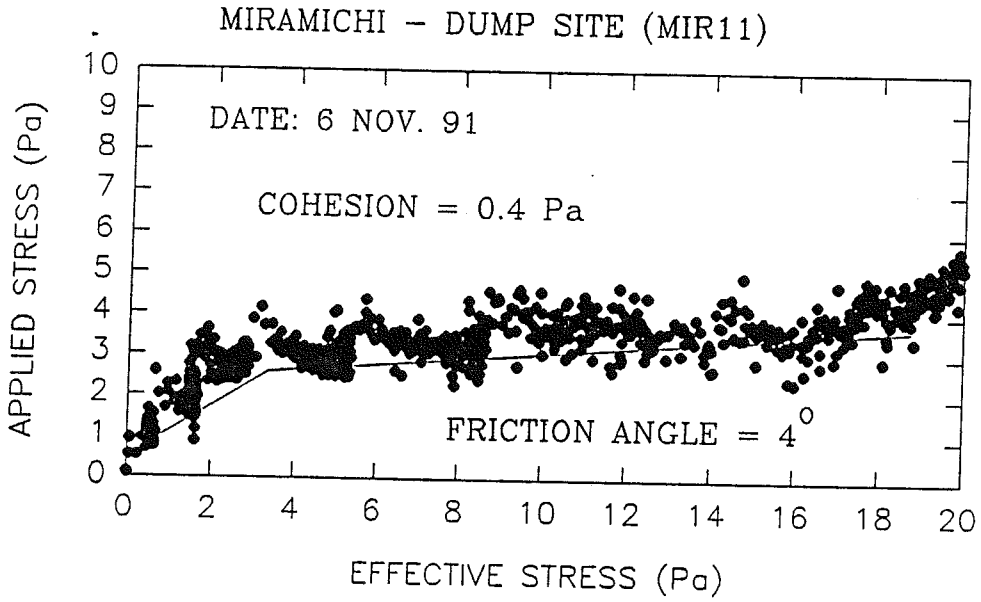
MIRAMICHI – DUMP SITE (MIR11)
DATE: 6 NOV. 91
COHESION = 0.4 Pa
FRICTION ANGLE = 4°
APPLIED STRESS (Pa)
EFFECTIVE STRESS (Pa)
0
1
2
3
4
5
6
7
8
9
10
0
2
4
6
8
10
12
14
16
18
20

SEA CAROUSEL – MIRAMICHI – DUMP SITE (90)

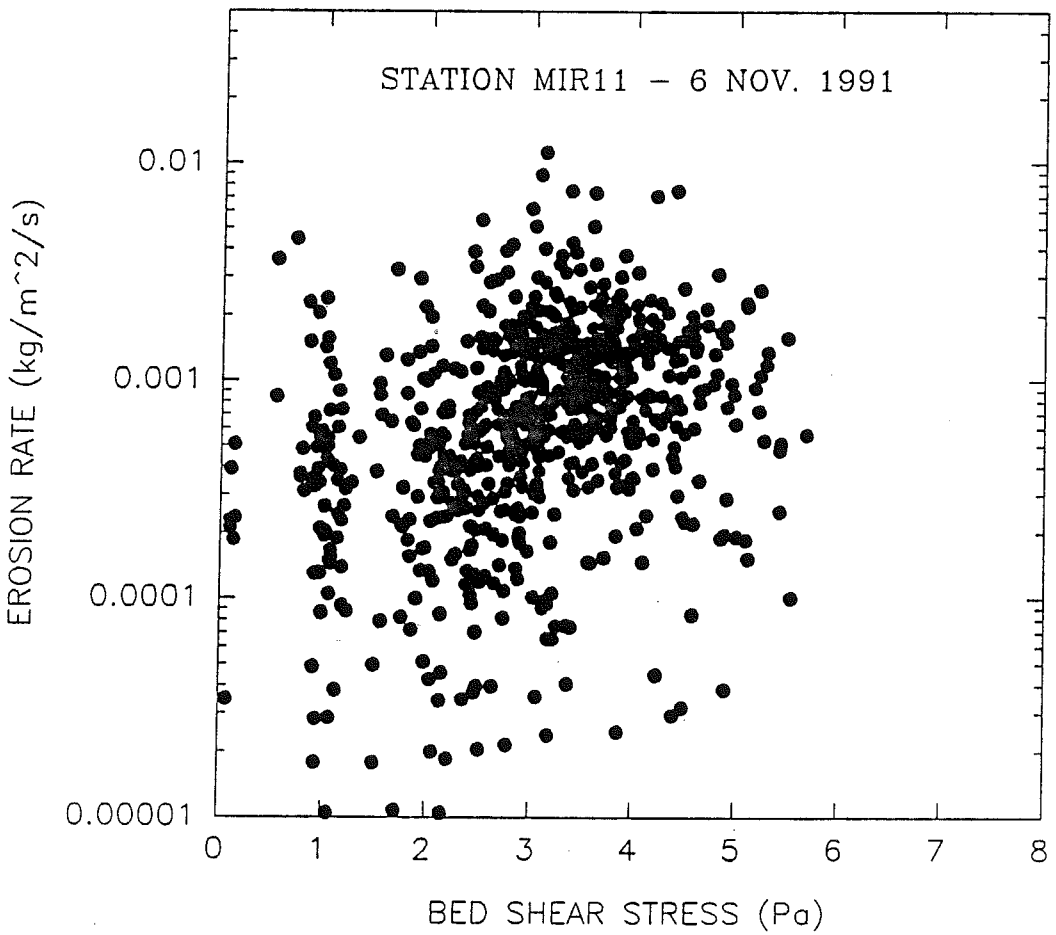

SEA CAROUSEL – MIRAMICHI CHANNEL

STATION MIR13 – 7 Nov. 1991

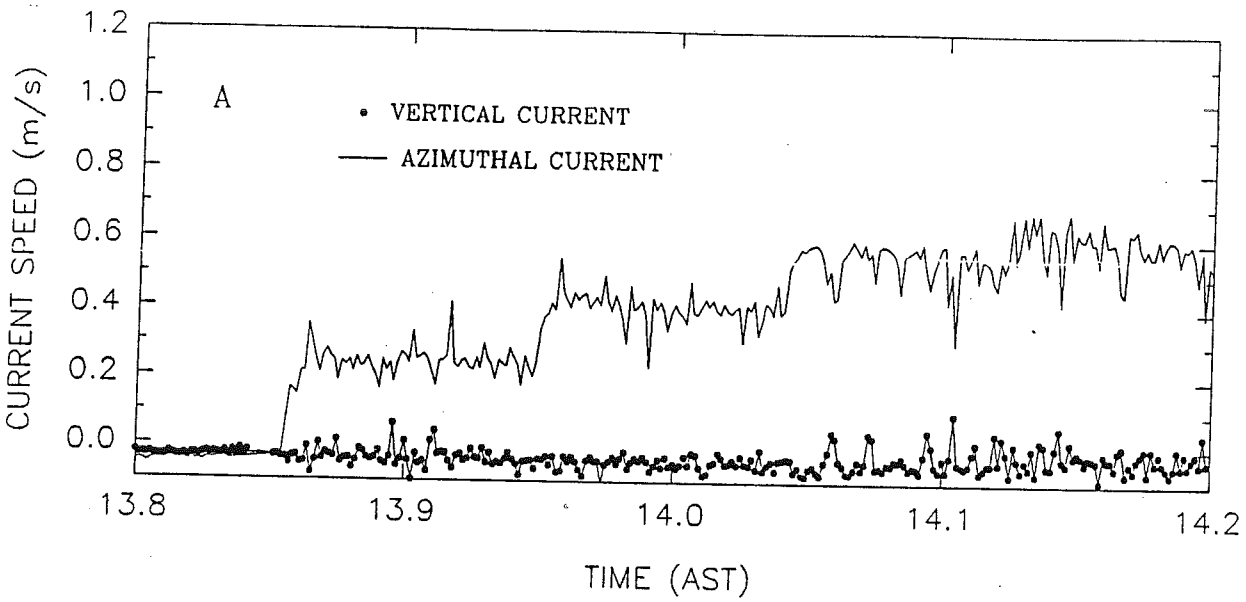

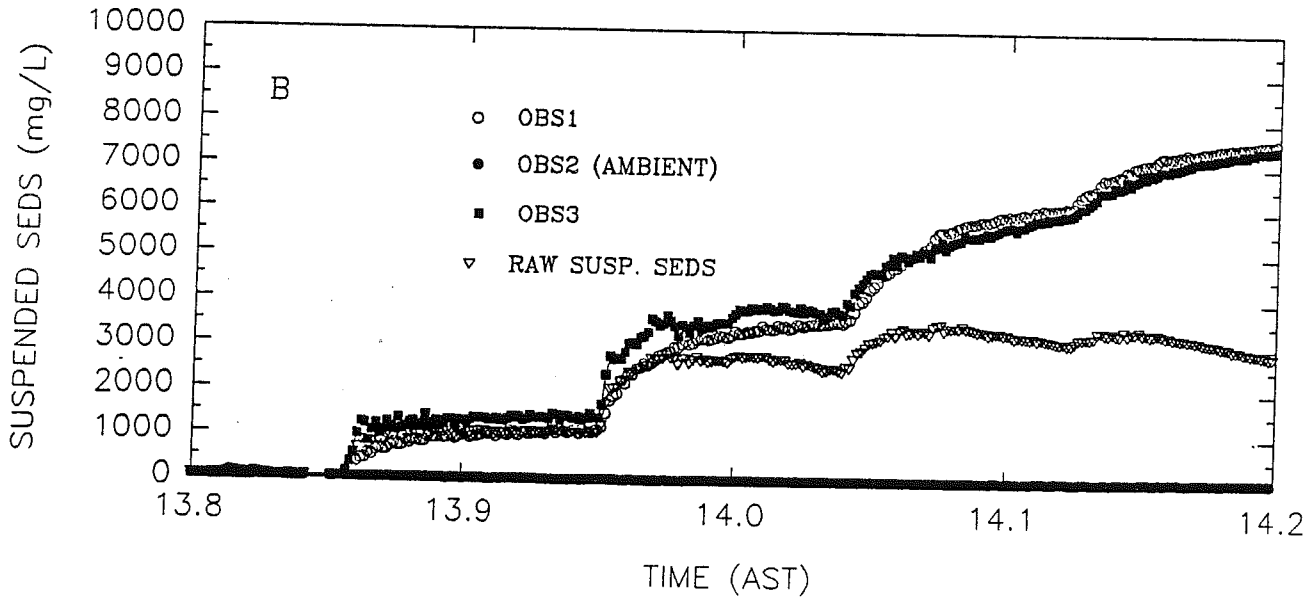

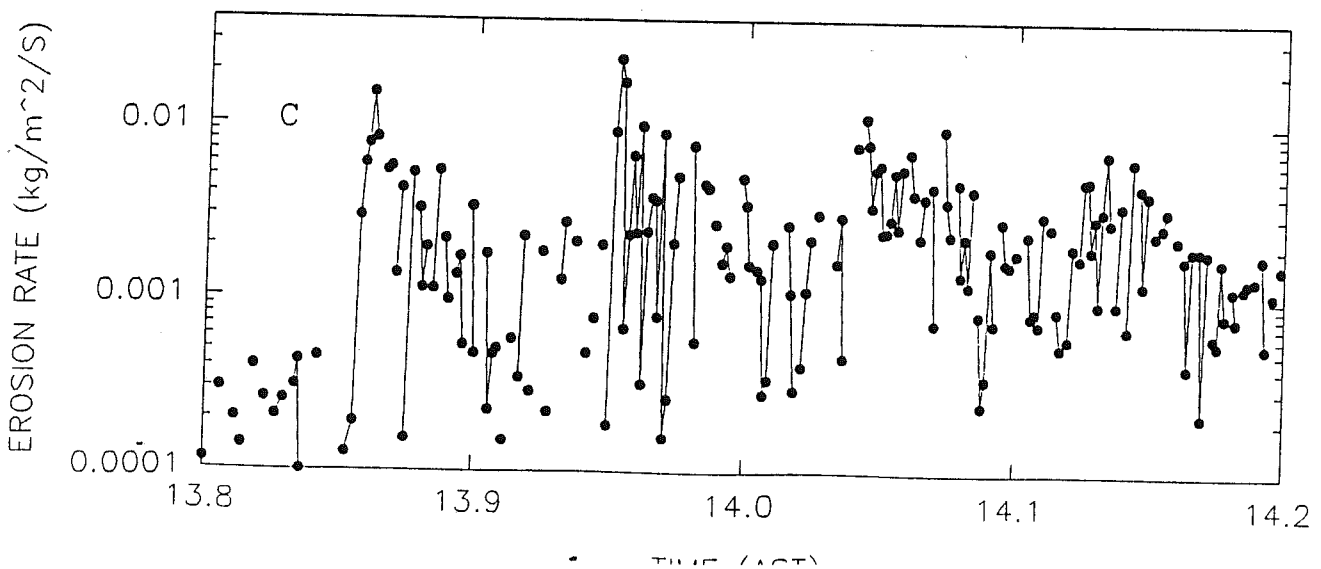

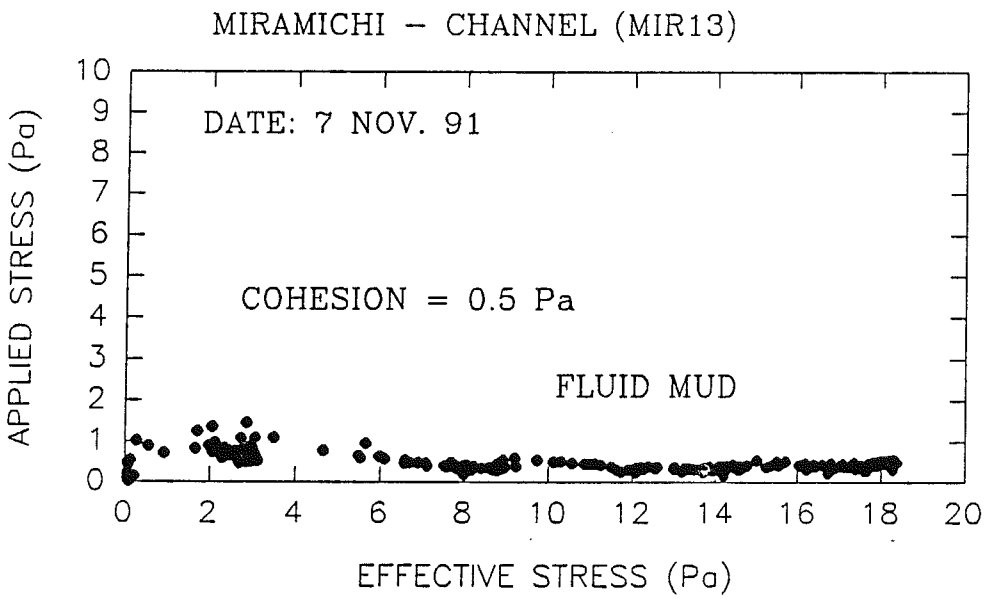
MIRAMICHI – CHANNEL (MIR13)
DATE: 7 NOV. 91
COHESION = 0.5 Pa
FLUID MUD
APPLIED STRESS (Pa)
EFFECTIVE STRESS (Pa)
0
1
2
3
4
5
6
7
8
9
10
0
2
4
6
8
10
12
14
16
18
20

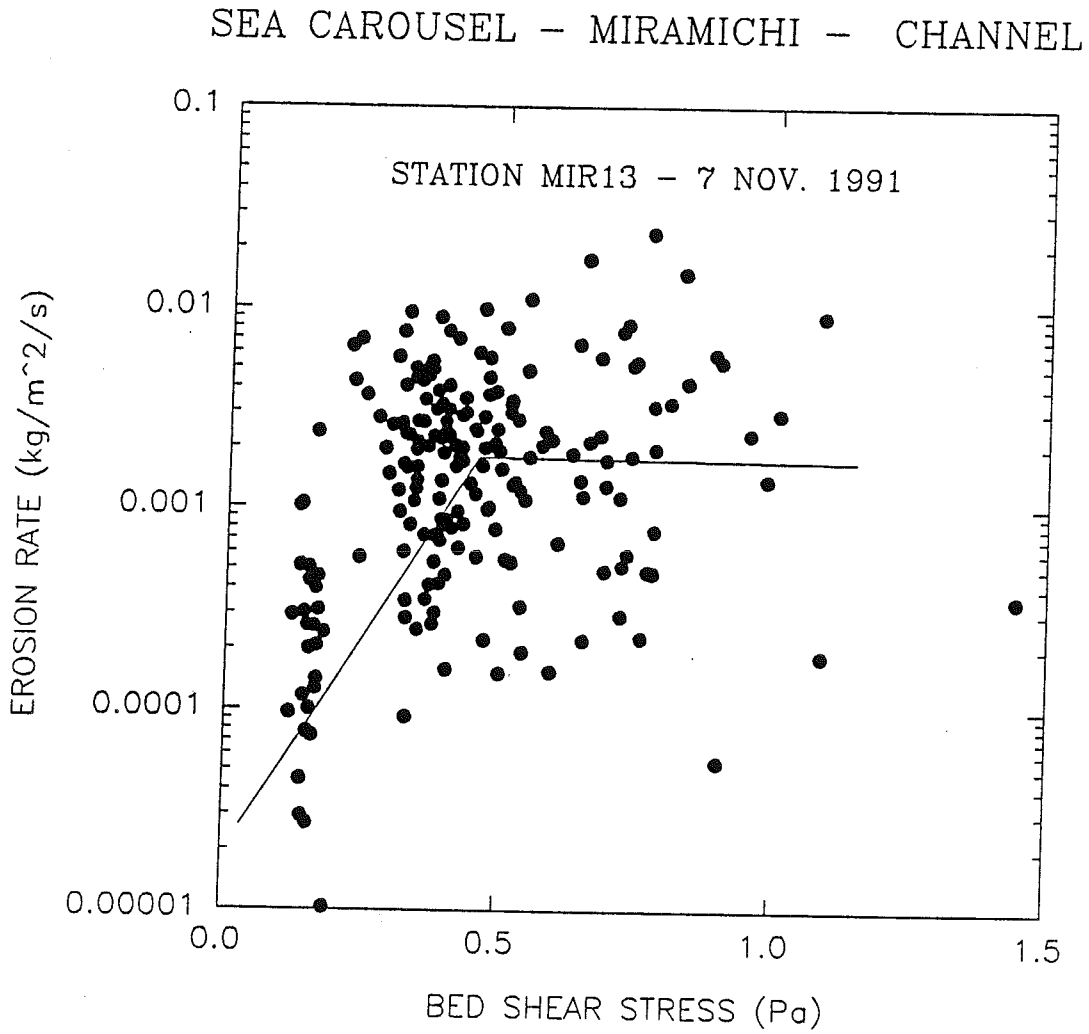
SEA CAROUSEL – MIRAMICHI – CHANNEL
STATION MIR13 – 7 NOV. 1991
EROSION RATE (kg/m^2/s)
0.1
0.01
0.001
0.0001
0.00001
0.0
0.5
1.0
1.5
BED SHEAR STRESS (Pa)

SEA CAROUSEL – MIRAMICHI NAVIGATION CHANNEL

STATION MIR14 – 7 Nov. 1991

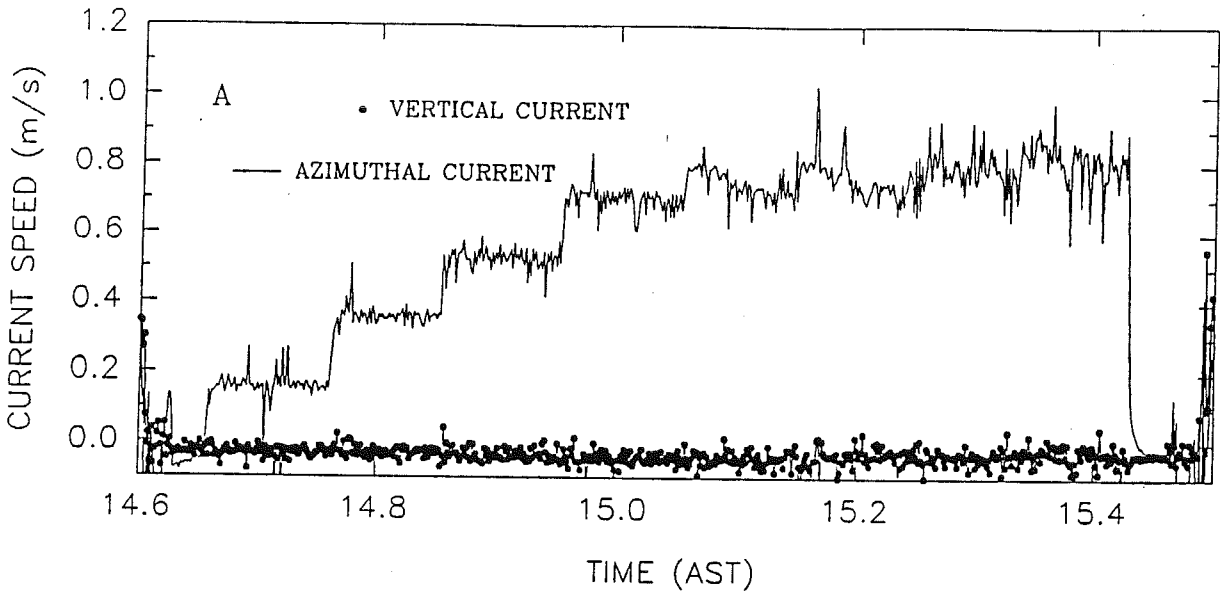

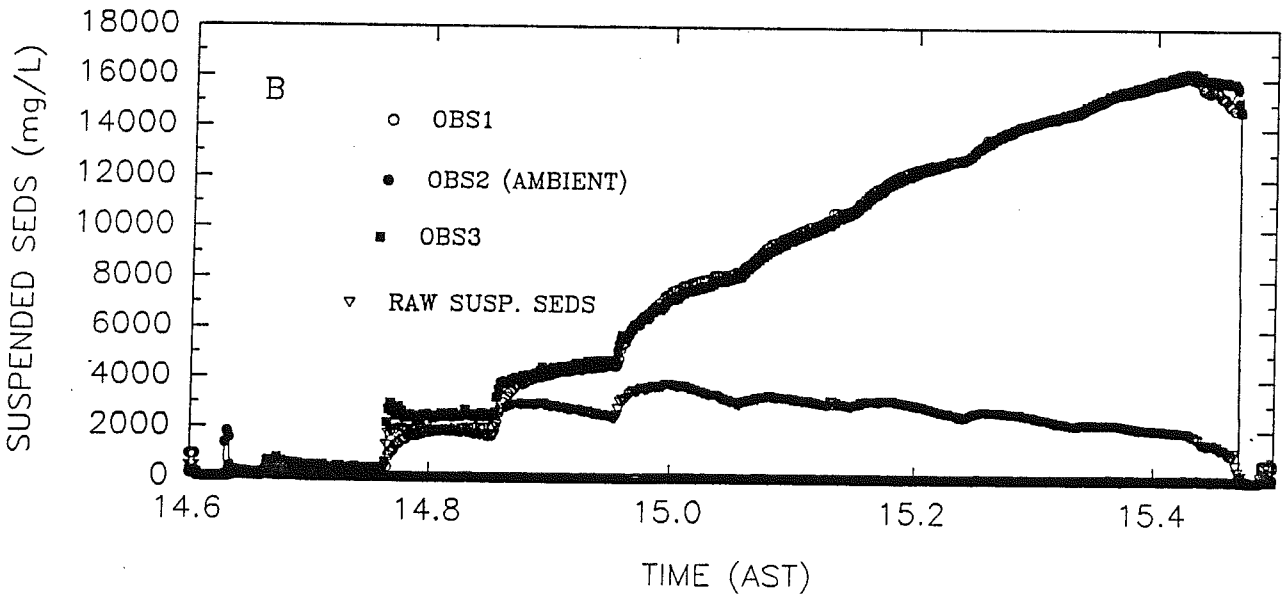

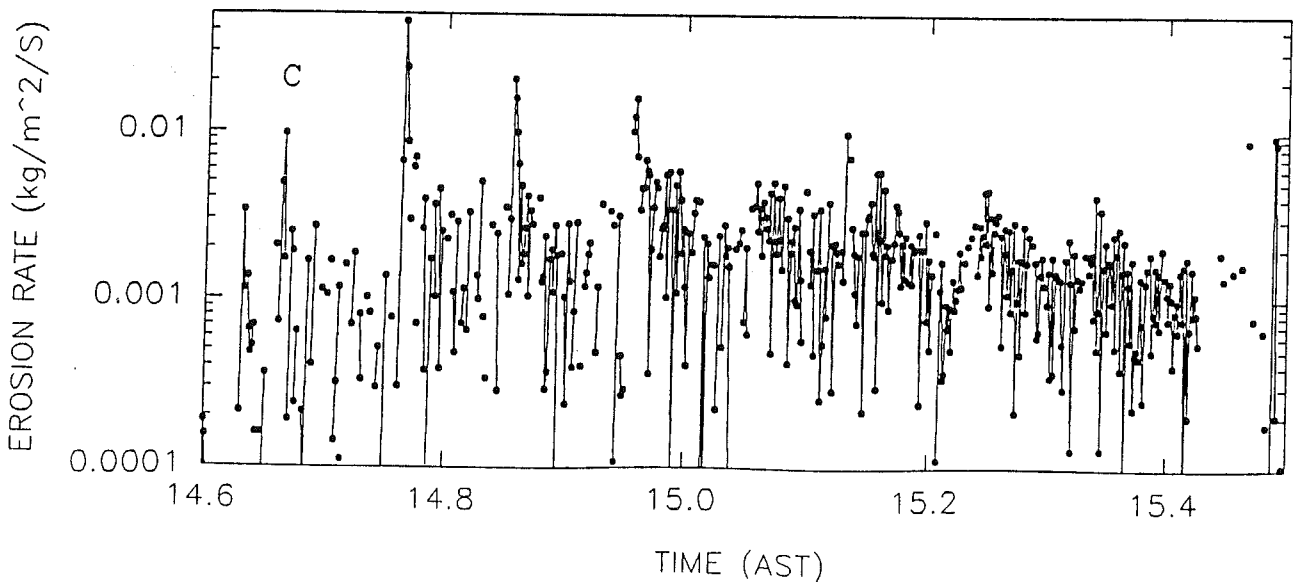

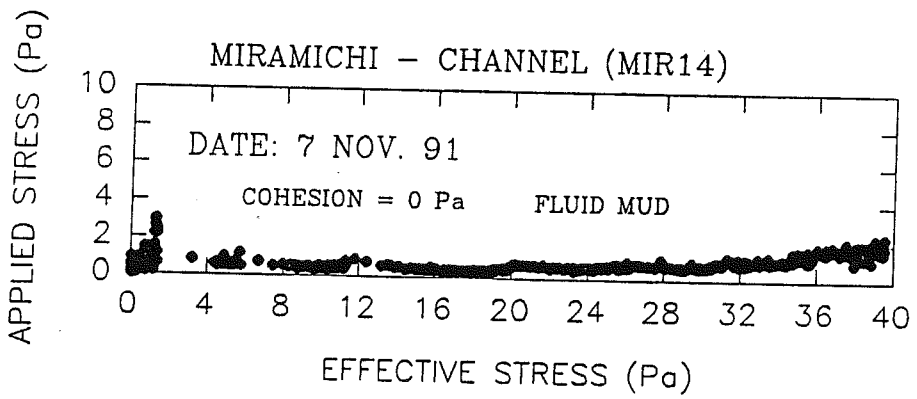
MIRAMICHI – CHANNEL (MIR14)
DATE: 7 NOV. 91
COHESION = 0 Pa
FLUID MUD
APPLIED STRESS (Pa)
EFFECTIVE STRESS (Pa)
0
2
4
6
8
10
0
4
8
12
16
20
24
28
32
36
40

SEA CAROUSEL – MIRAMICHI – CHANNEL

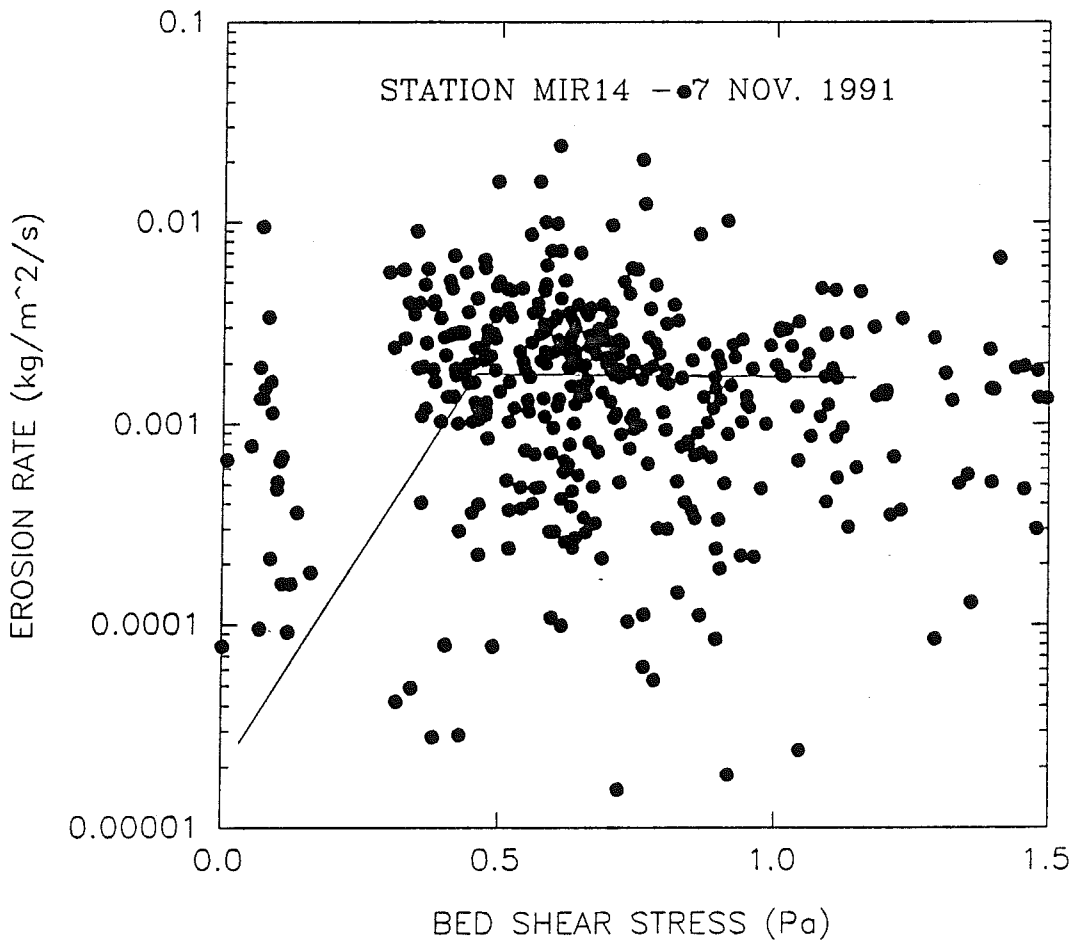

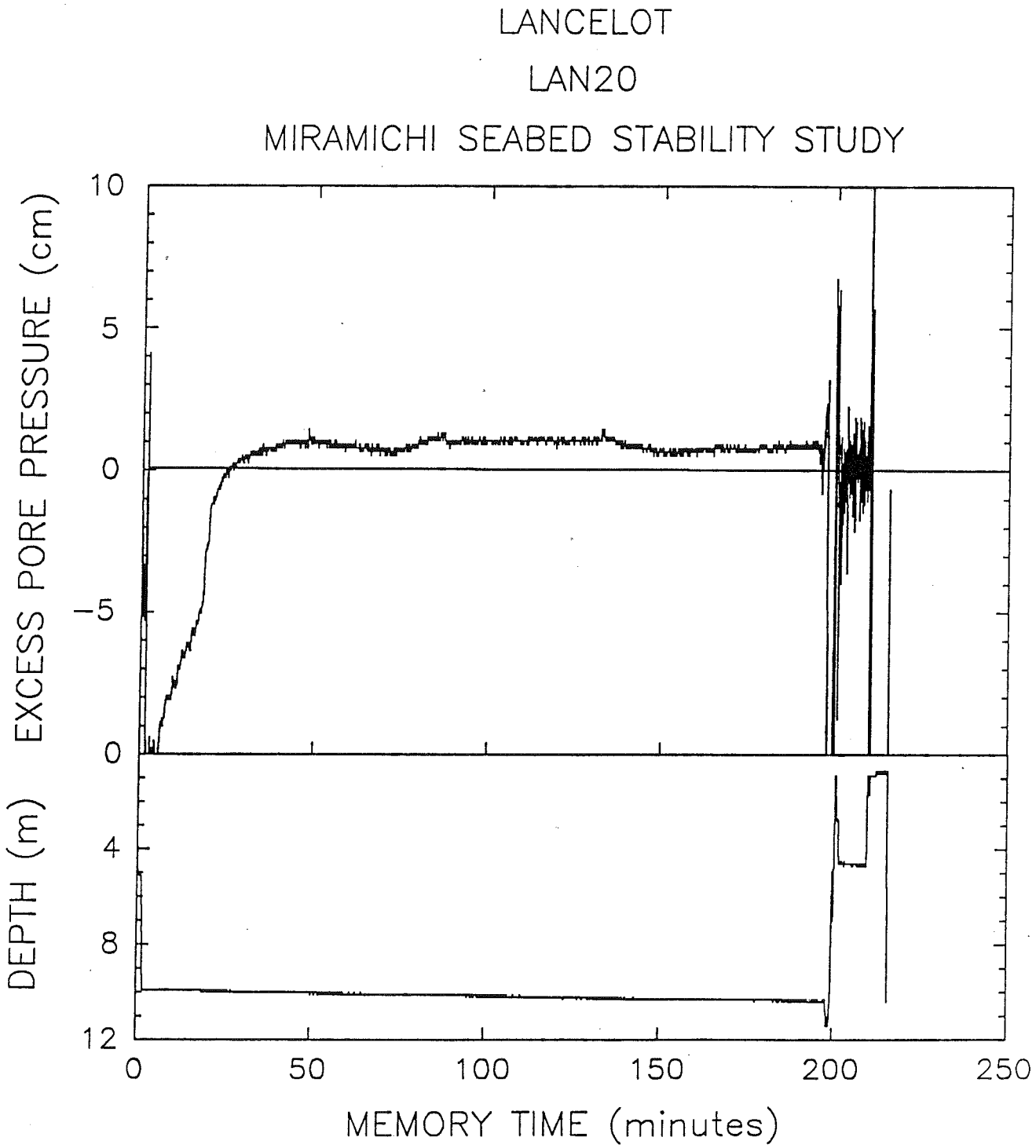
LANCELOT
LAN20
MIRAMICHI SEABED STABILITY STUDY
EXCESS PORE PRESSURE (cm)
10
5
0
−5
0
DEPTH (m)
4
8
12
0
50
100
150
200
250
MEMORY TIME (minutes)

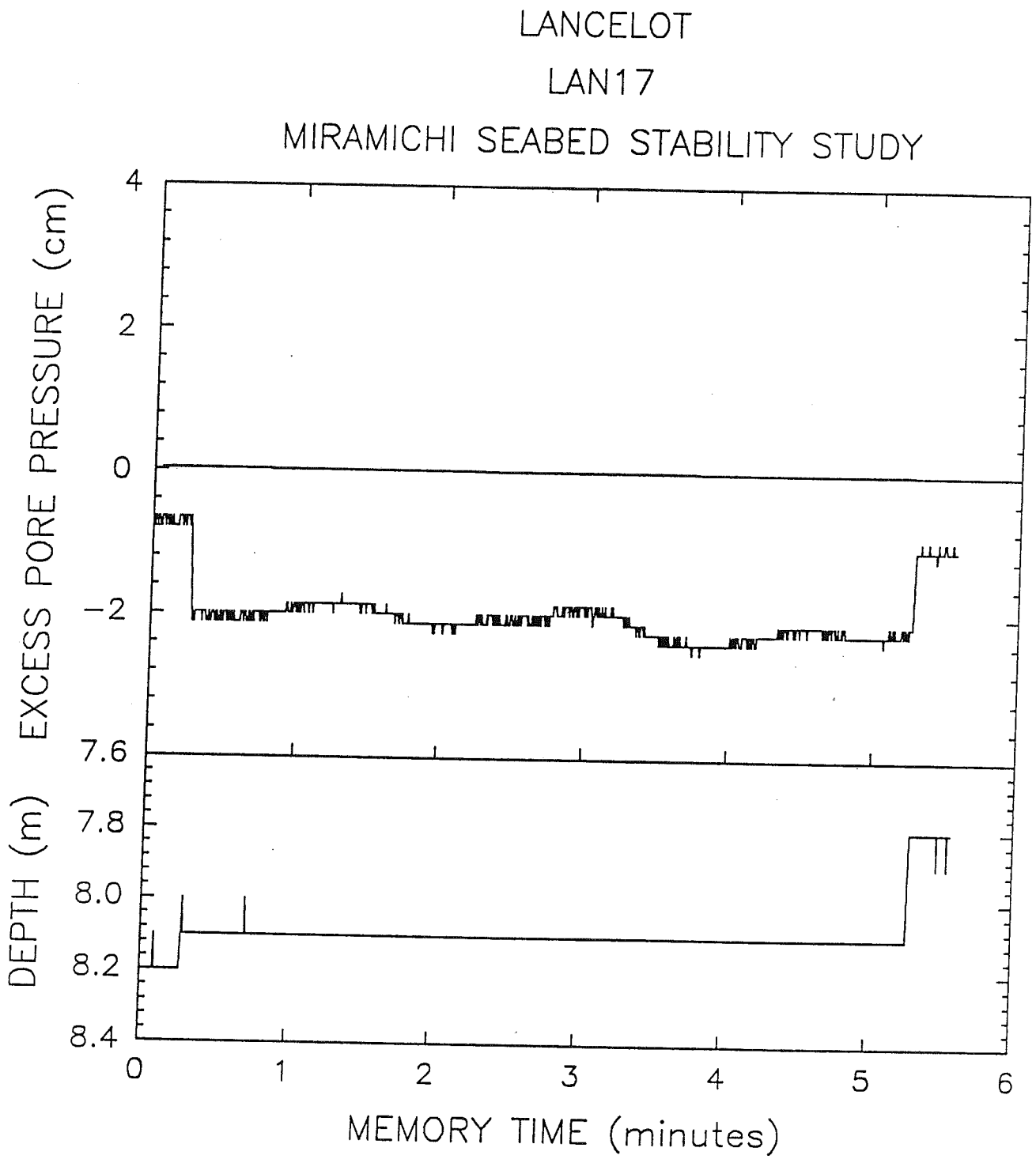
LANCELOT
LAN17
MIRAMICHI SEABED STABILITY STUDY
EXCESS PORE PRESSURE (cm)
4
2
0
−2
7.6
DEPTH (m)
7.8
8.0
8.2
8.4
0
1
2
3
4
5
6
MEMORY TIME (minutes)

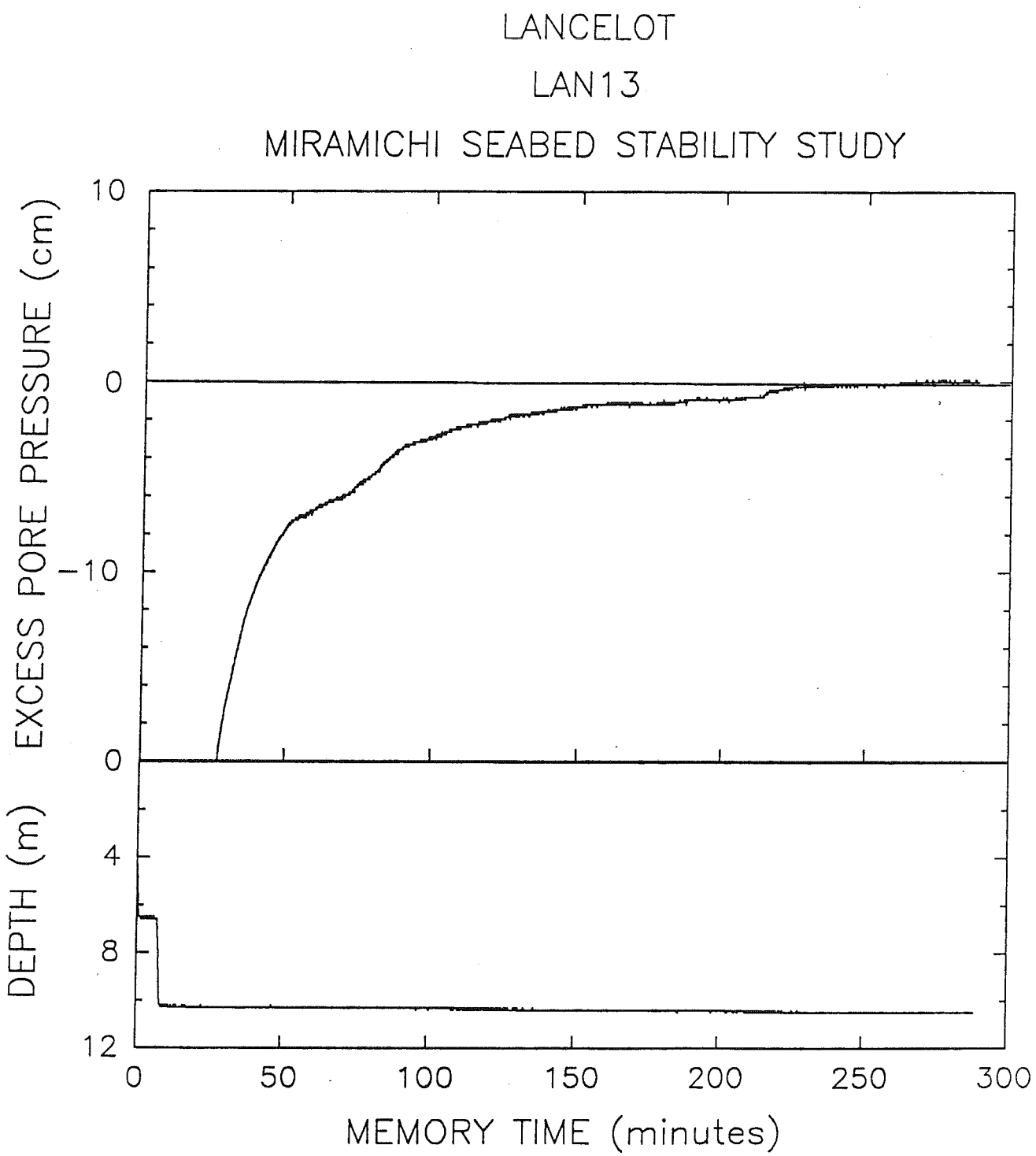
LANCELOT
LAN13
MIRAMICHI SEABED STABILITY STUDY
EXCESS PORE PRESSURE (cm)
10
0
-10
0
DEPTH (m)
4
8
12
0
50
100
150
200
250
300
MEMORY TIME (minutes)

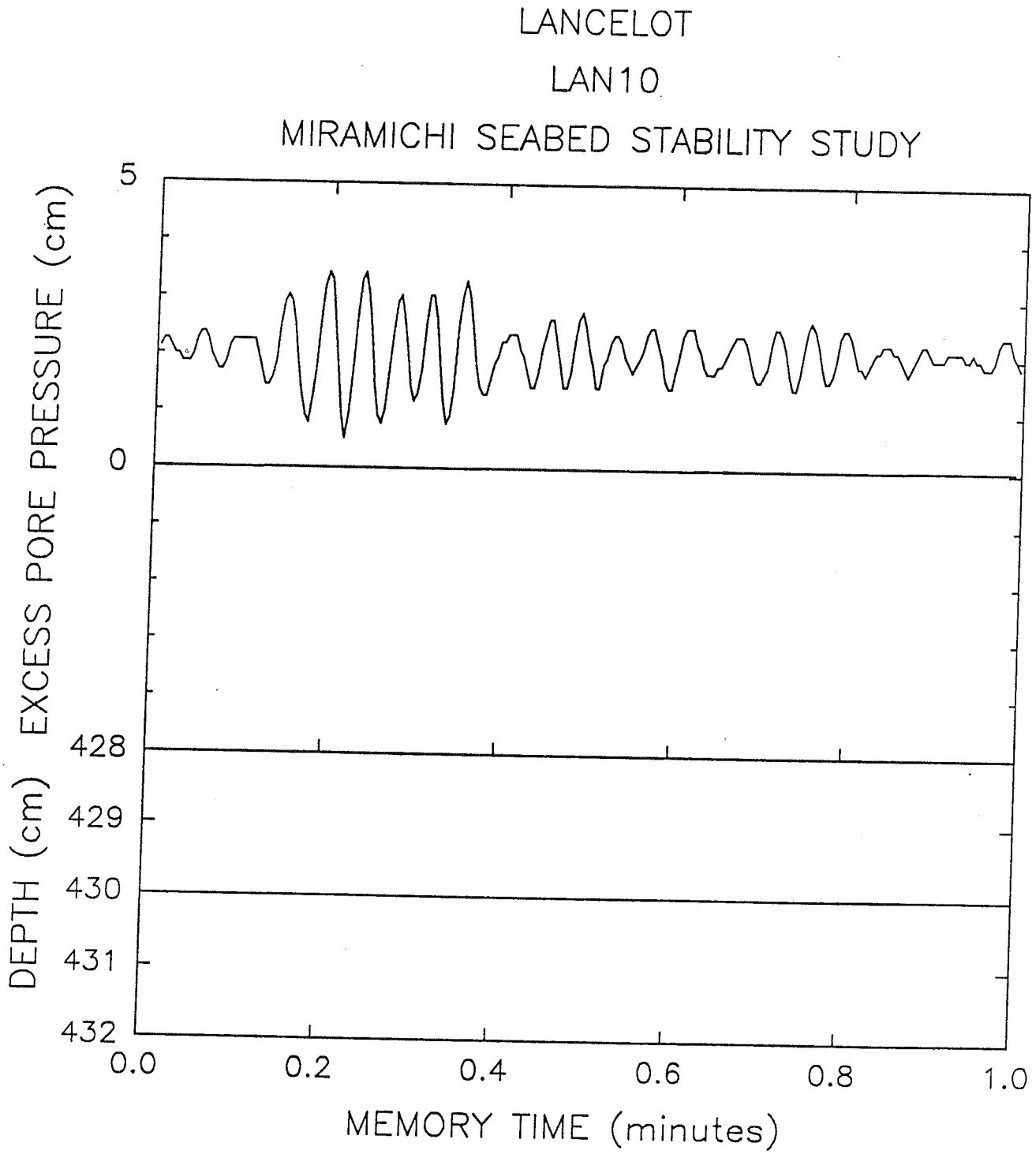
LANCELOT
LAN10
MIRAMICHI SEABED STABILITY STUDY
DEPTH (cm) EXCESS PORE PRESSURE (cm)
5
0
428
429
430
431
432
0.0
0.2
0.4
0.6
0.8
1.0
MEMORY TIME (minutes)

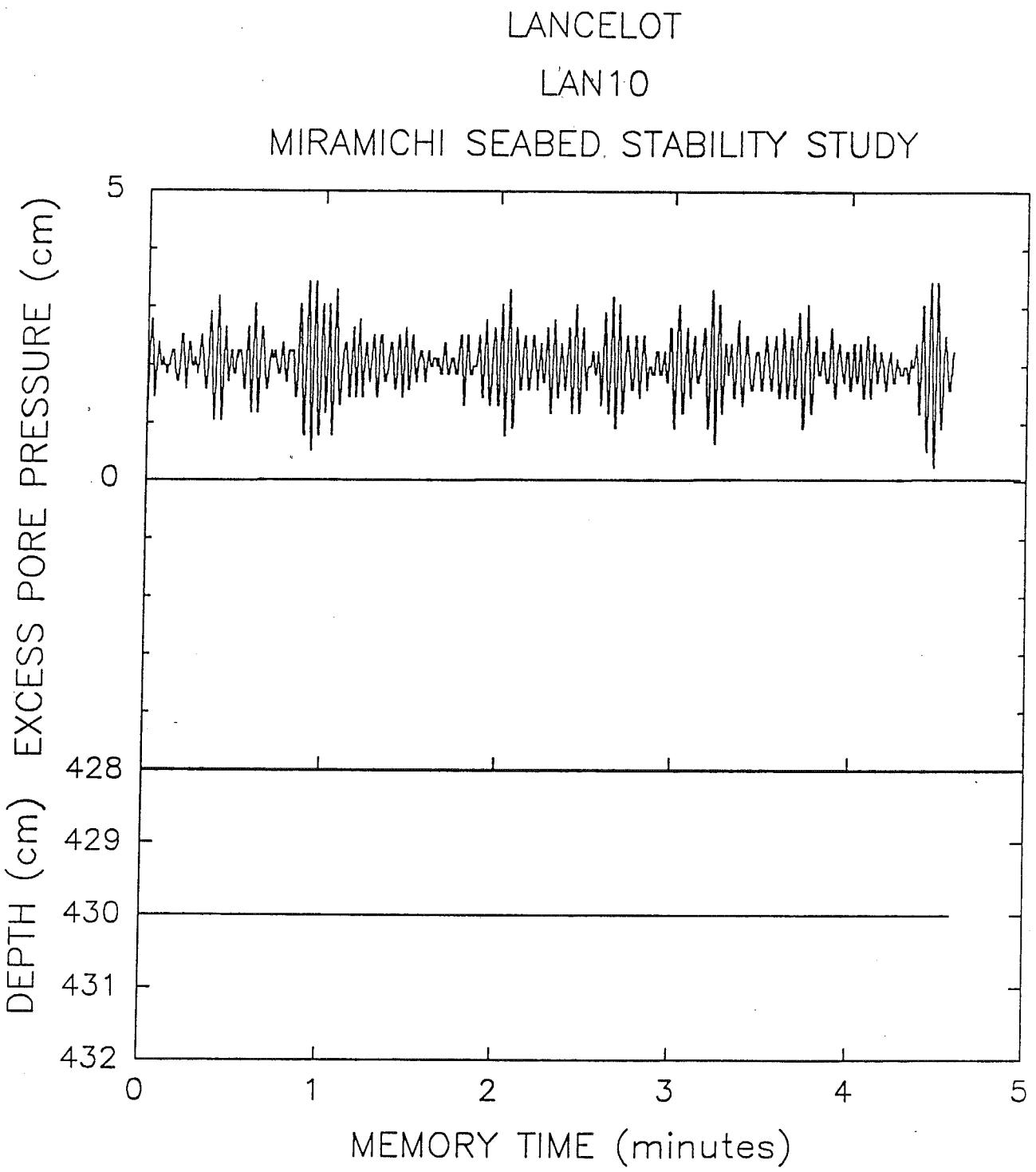
LANCELOT
LAN10
MIRAMICHI SEABED STABILITY STUDY
5
0
EXCESS PORE PRESSURE (cm)
428
429
430
431
432
DEPTH (cm)
0
1
2
3
4
5
MEMORY TIME (minutes)

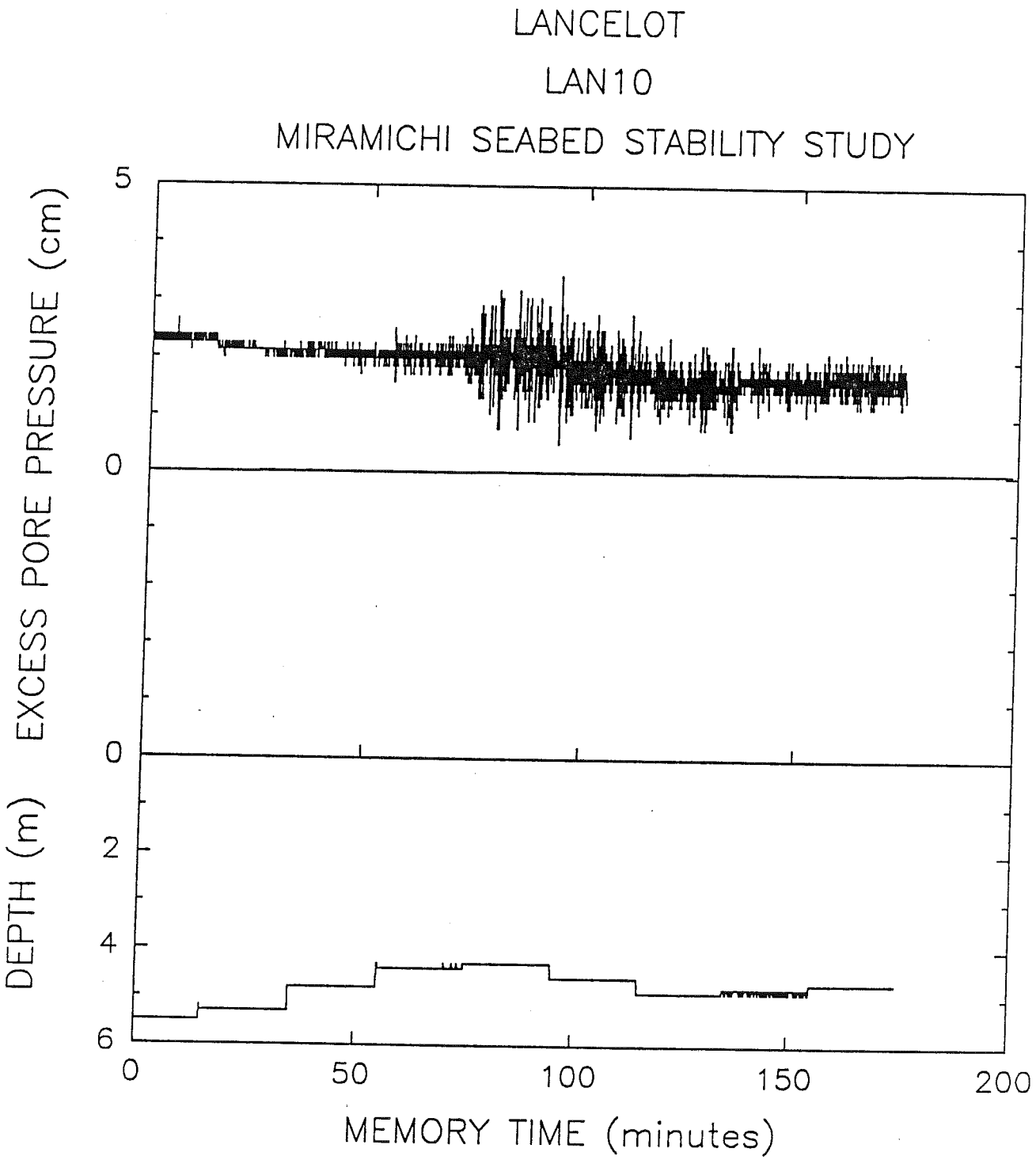
LANCELOT
LAN10
MIRAMICHI SEABED STABILITY STUDY
EXCESS PORE PRESSURE (cm)
5
0
0
DEPTH (m)
2
4
6
0
50
100
150
200
MEMORY TIME (minutes)

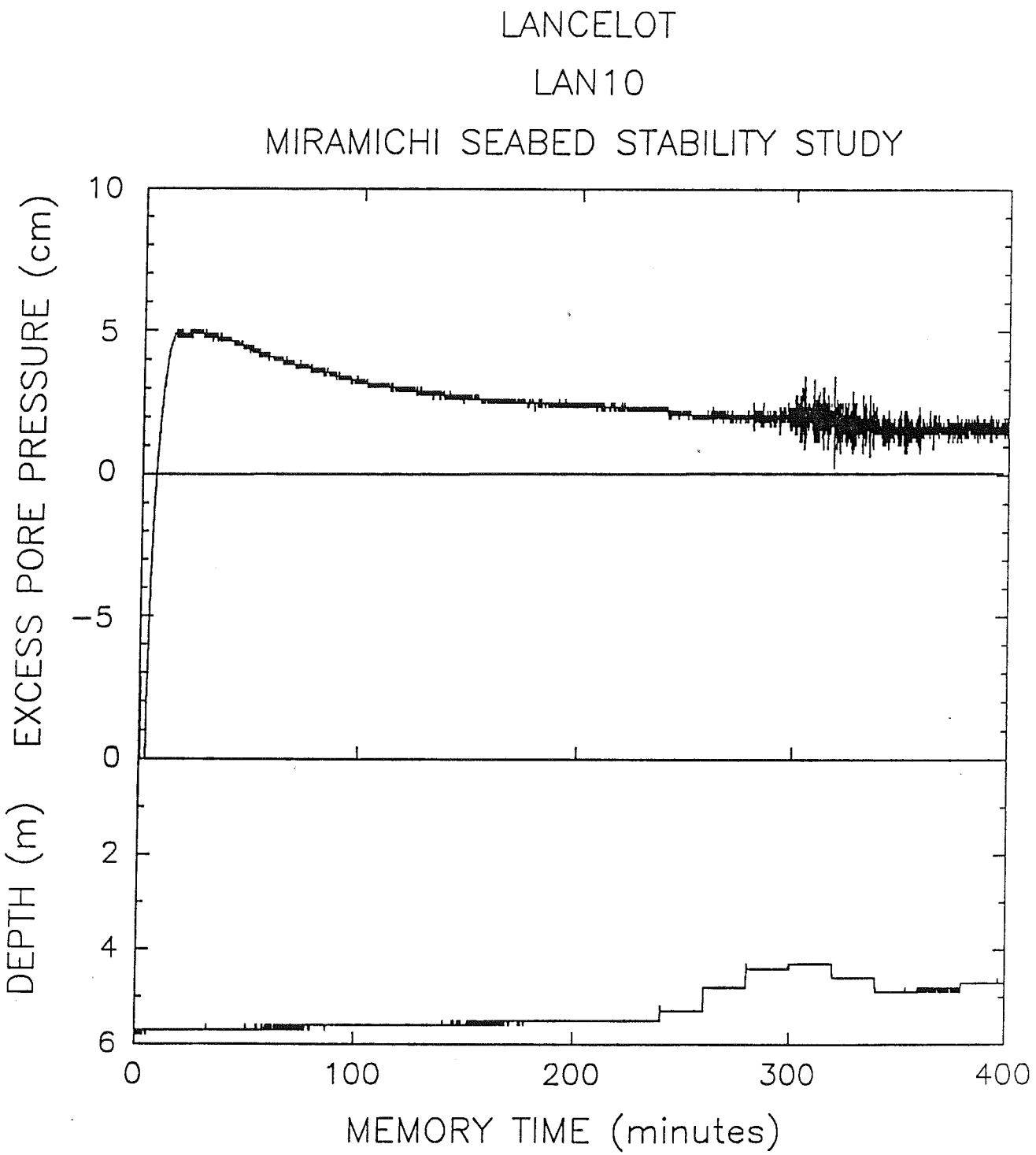
LANCELOT
LAN10
MIRAMICHI SEABED STABILITY STUDY
EXCESS PORE PRESSURE (cm)
10
5
0
-5
0
DEPTH (m)
2
4
6
0
100
200
300
400
MEMORY TIME (minutes)

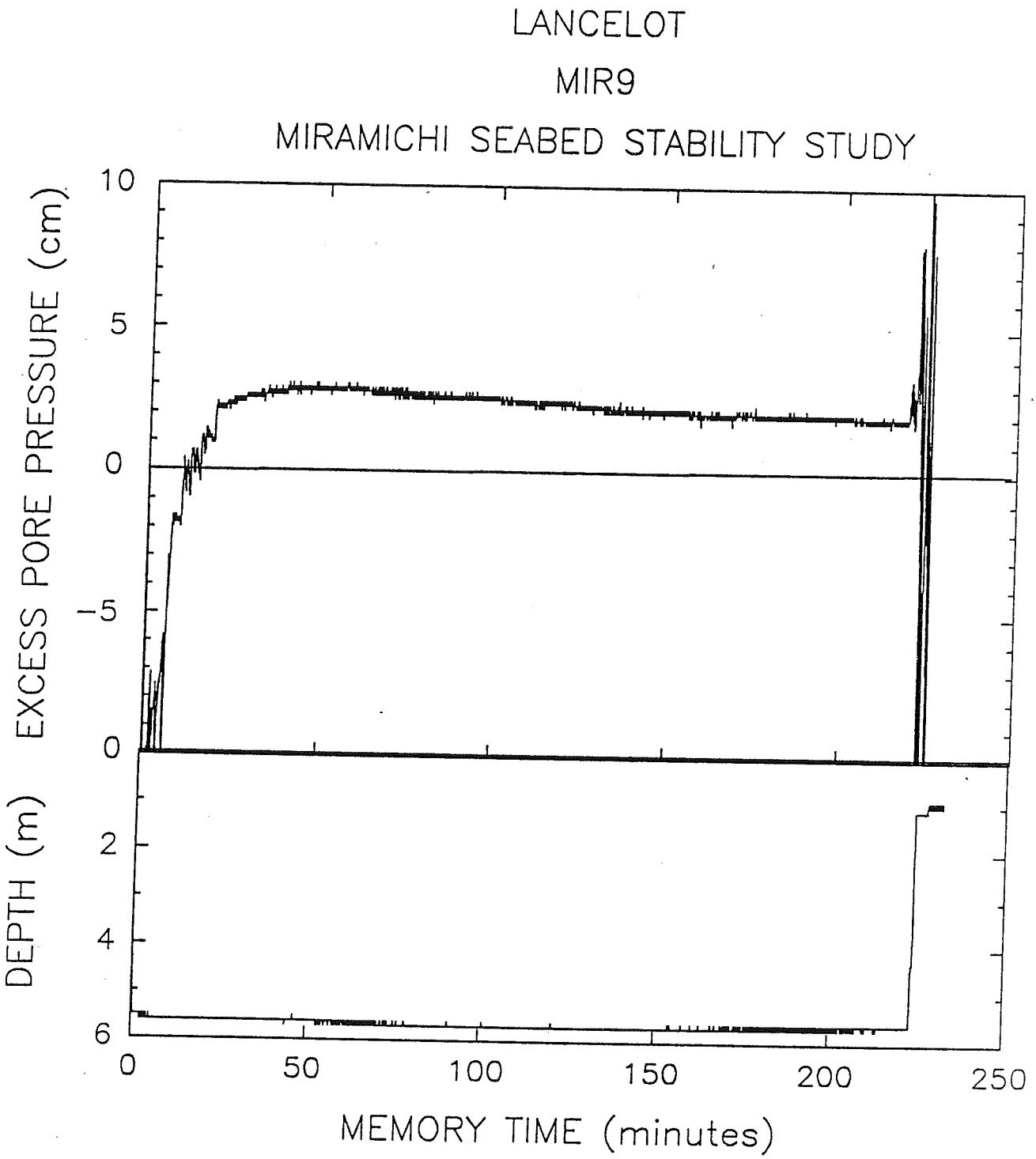
LANCELOT
MIR9
MIRAMICHI SEABED STABILITY STUDY
EXCESS PORE PRESSURE (cm)
10
5
0
-5
0
DEPTH (m)
2
4
6
0
50
100
150
200
250
MEMORY TIME (minutes)

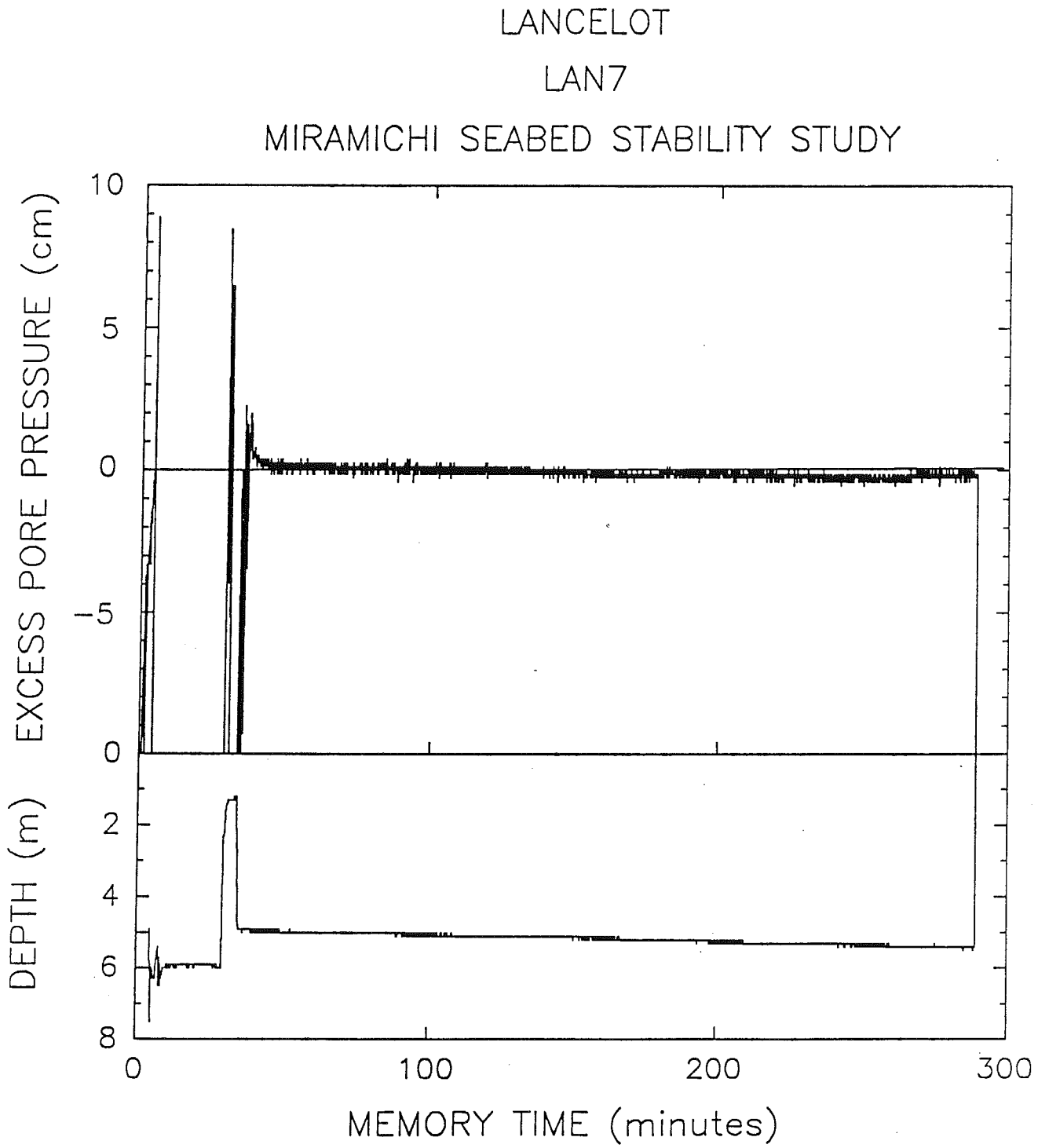
LANCELOT
LAN7
MIRAMICHI SEABED STABILITY STUDY
EXCESS PORE PRESSURE (cm)
10
5
0
−5
0
DEPTH (m)
2
4
6
8
0
100
200
300
MEMORY TIME (minutes)

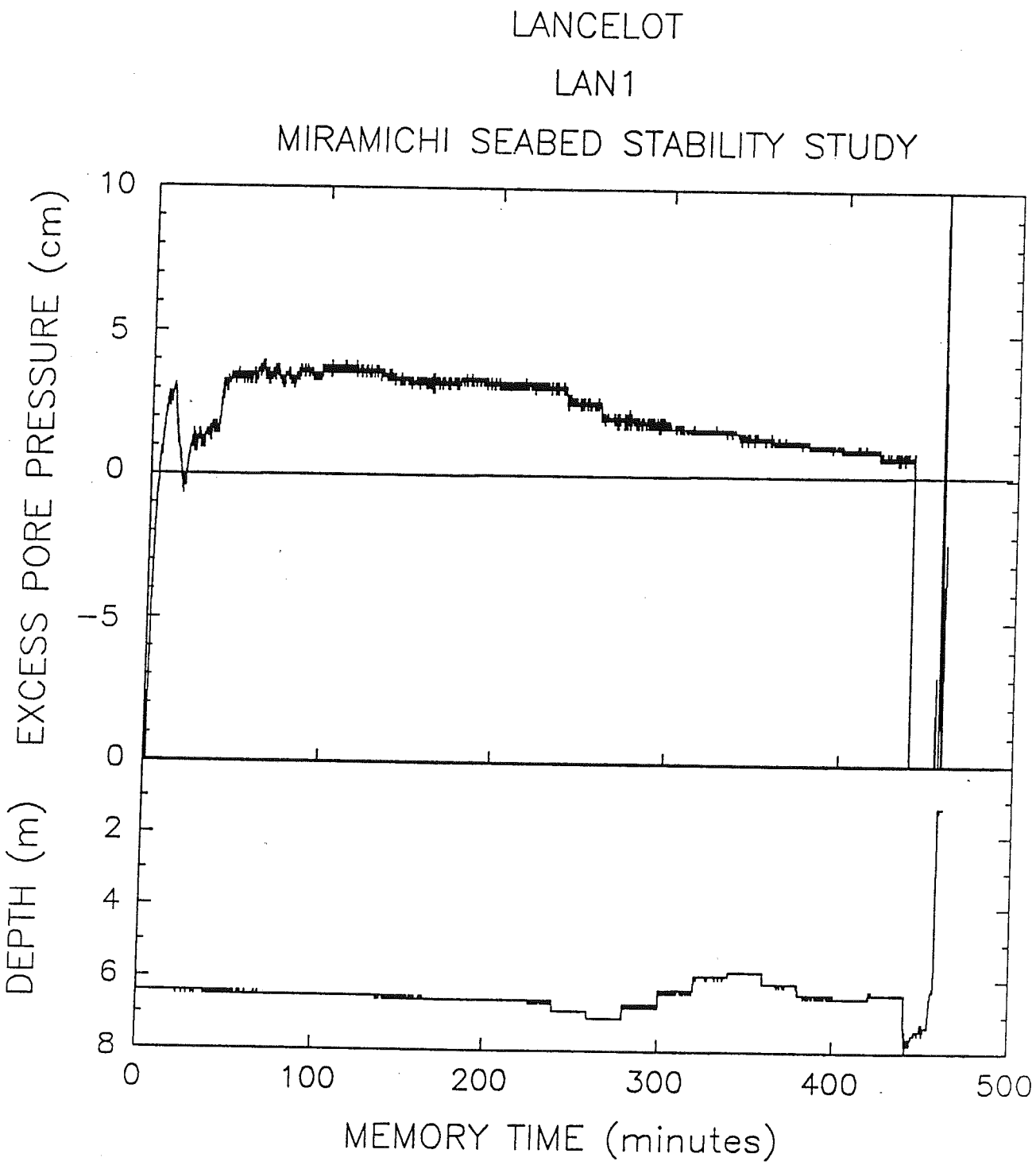
LANCELOT
LAN1
MIRAMICHI SEABED STABILITY STUDY
EXCESS PORE PRESSURE (cm)
10
5
0
−5
0
DEPTH (m)
2
4
6
8
0
100
200
300
400
500
MEMORY TIME (minutes)

APPENDIX B

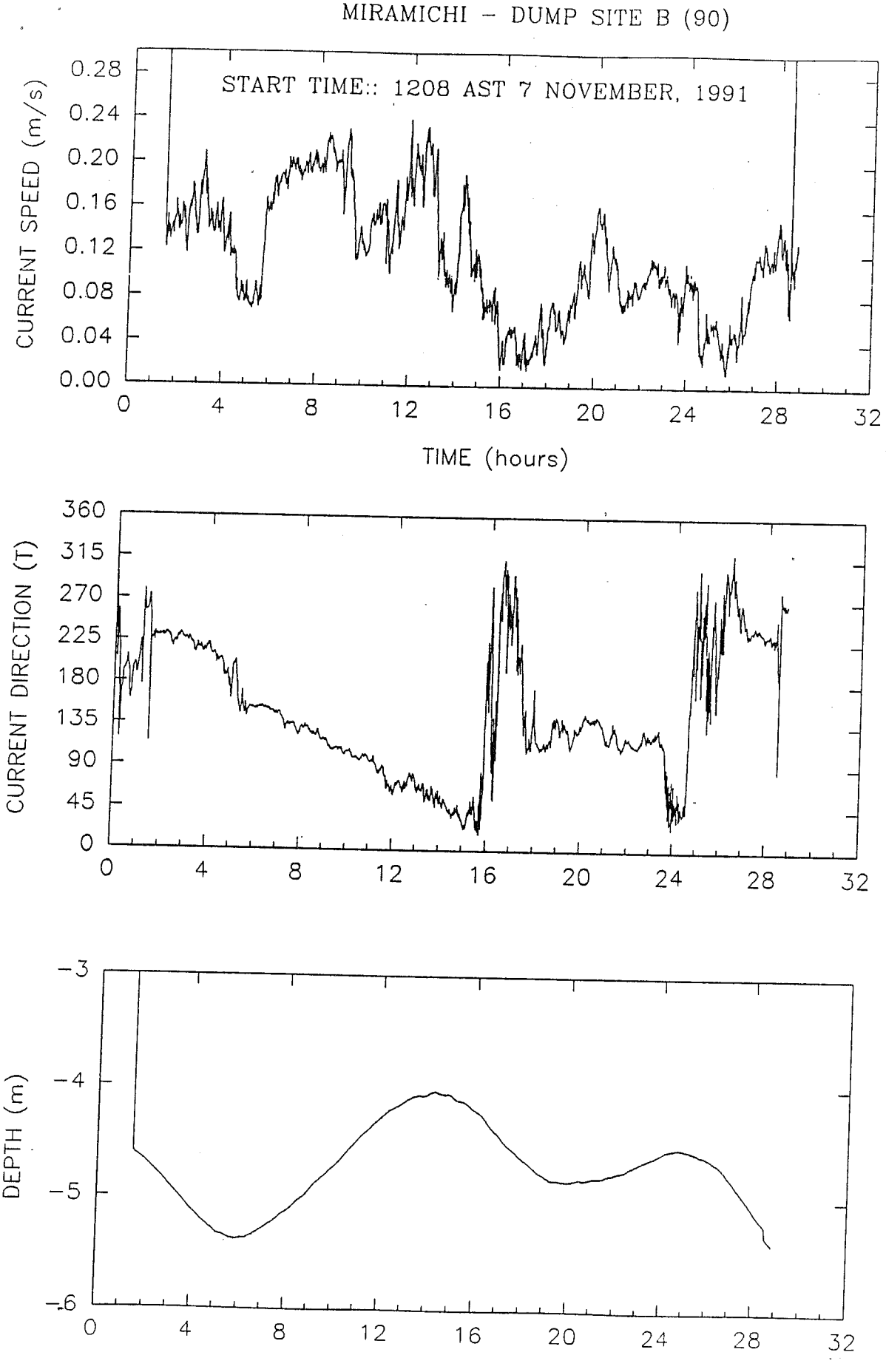
MIRAMICHI – DUMP SITE B (90)
START TIME:: 1208 AST 7 NOVEMBER, 1991
CURRENT SPEED (m/s)
0.28
0.24
0.20
0.16
0.12
0.08
0.04
0.00
0
4
8
12
16
20
24
28
32
TIME (hours)
CURRENT DIRECTION (T)
360
315
270
225
180
135
90
45
0
DEPTH (m)
-3
-4
-5
-6

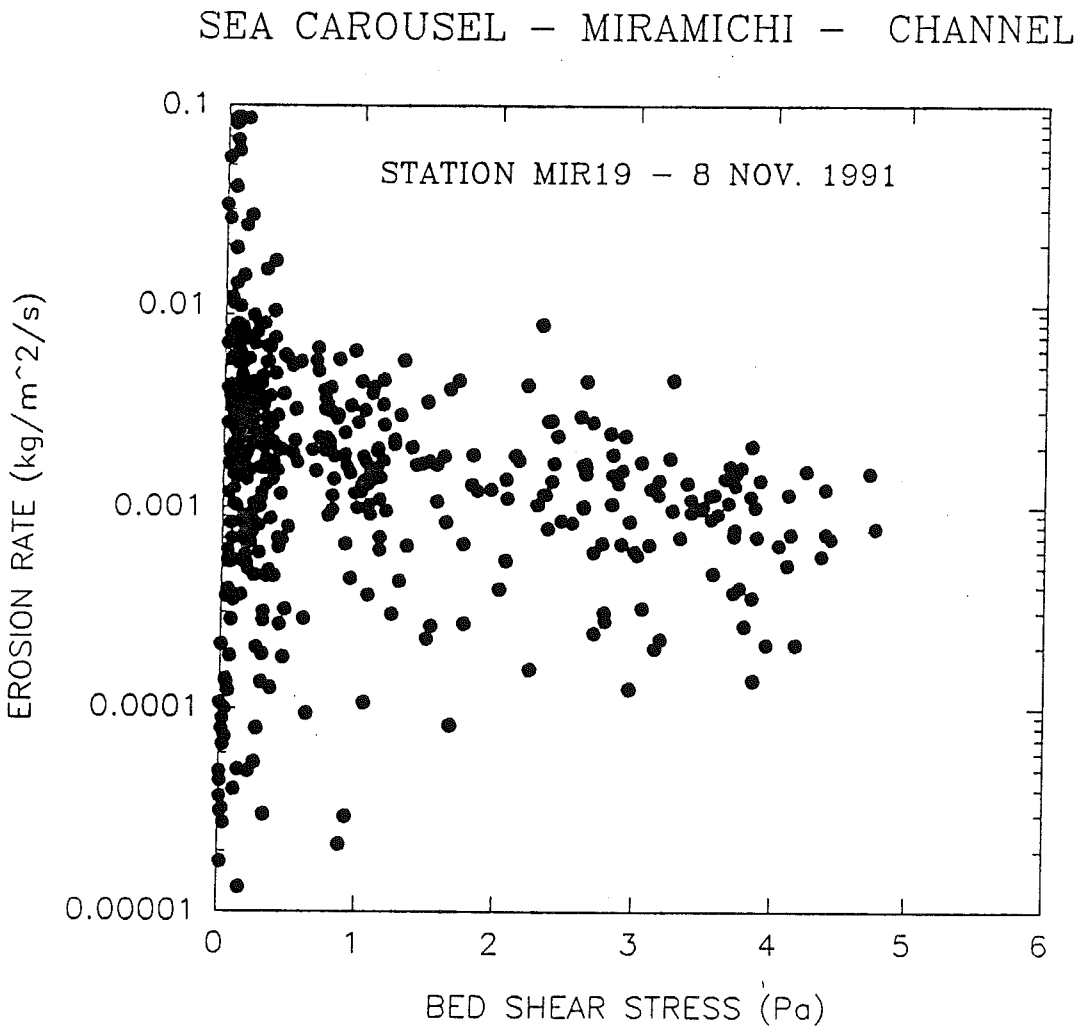
SEA CAROUSEL – MIRAMICHI – CHANNEL
STATION MIR19 – 8 NOV. 1991
EROSION RATE (kg/m^2/s)
0.1
0.01
0.001
0.0001
0.00001
0
1
2
3
4
5
6
BED SHEAR STRESS (Pa)

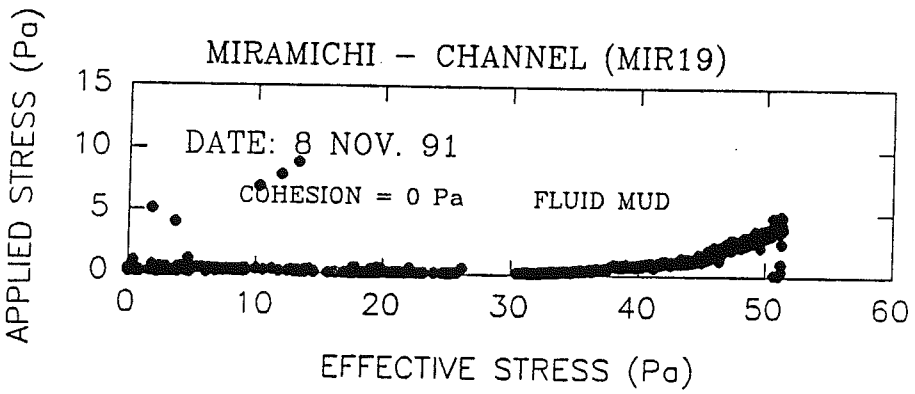
MIRAMICHI – CHANNEL (MIR19)
DATE: 8 NOV. 91
COHESION = 0 Pa
FLUID MUD
APPLIED STRESS (Pa)
EFFECTIVE STRESS (Pa)
0
5
10
15
0
10
20
30
40
50
60

SEA CAROUSEL – MIRAMICHI NAVIGATION CHANNEL

STATION MIR19 – 8 Nov. 1991

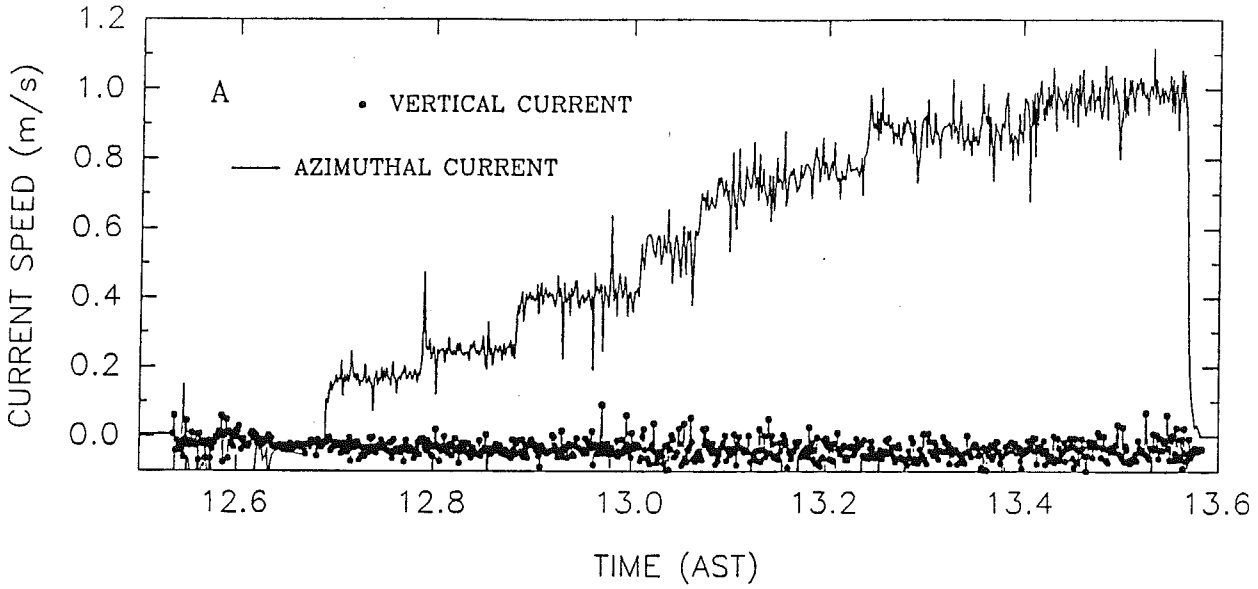

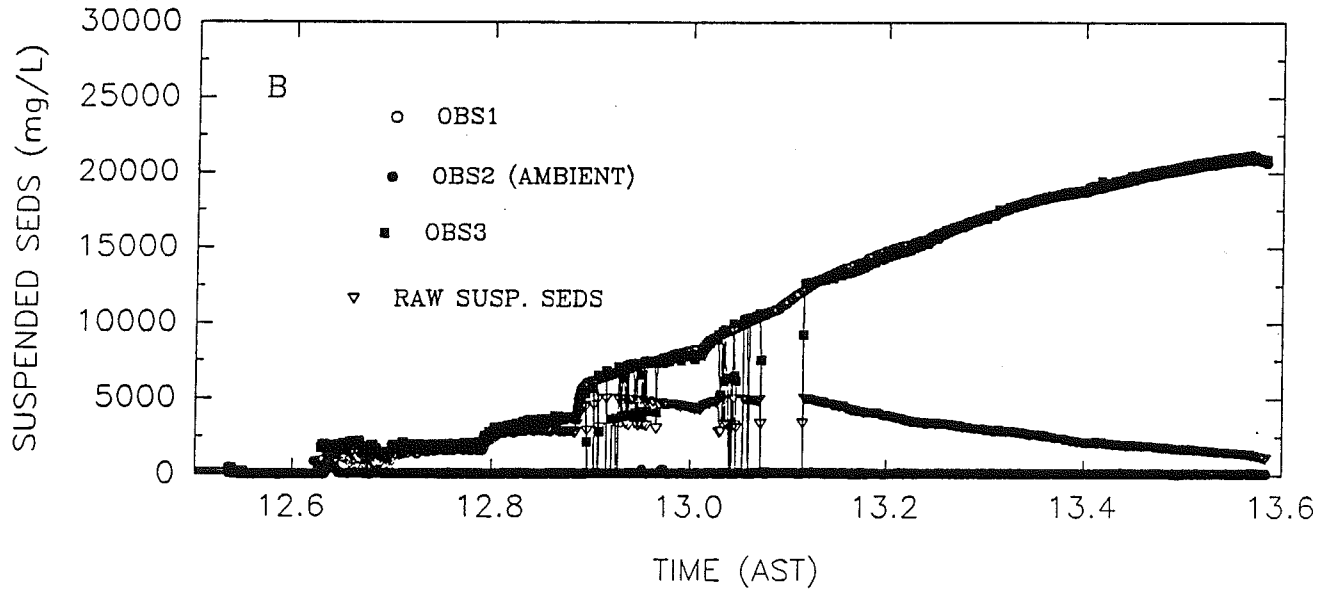

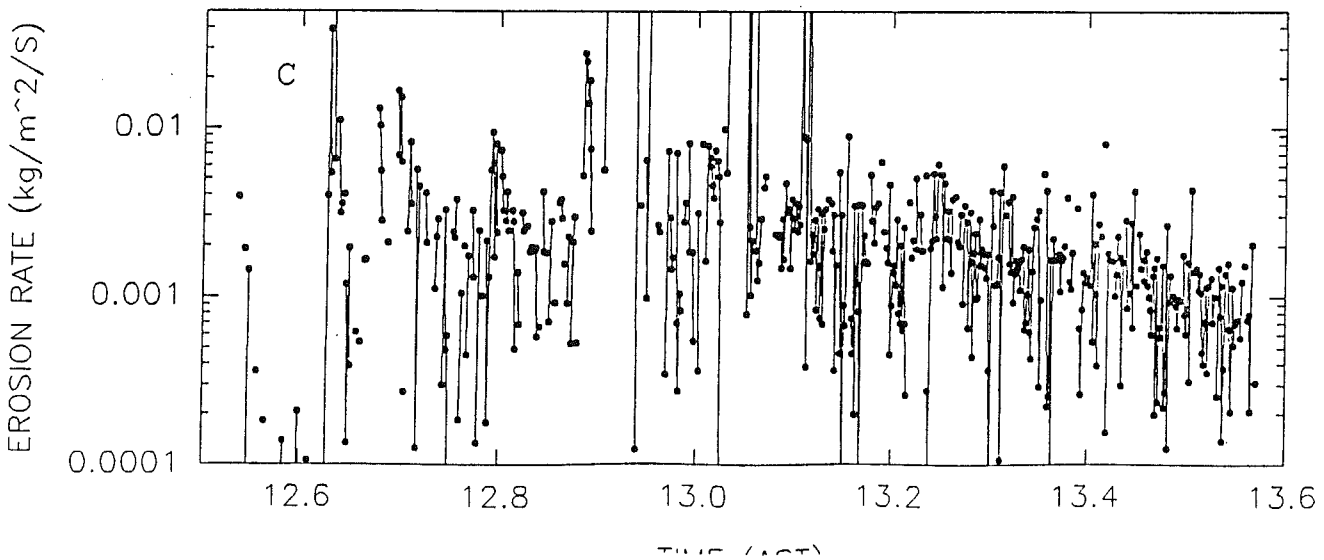

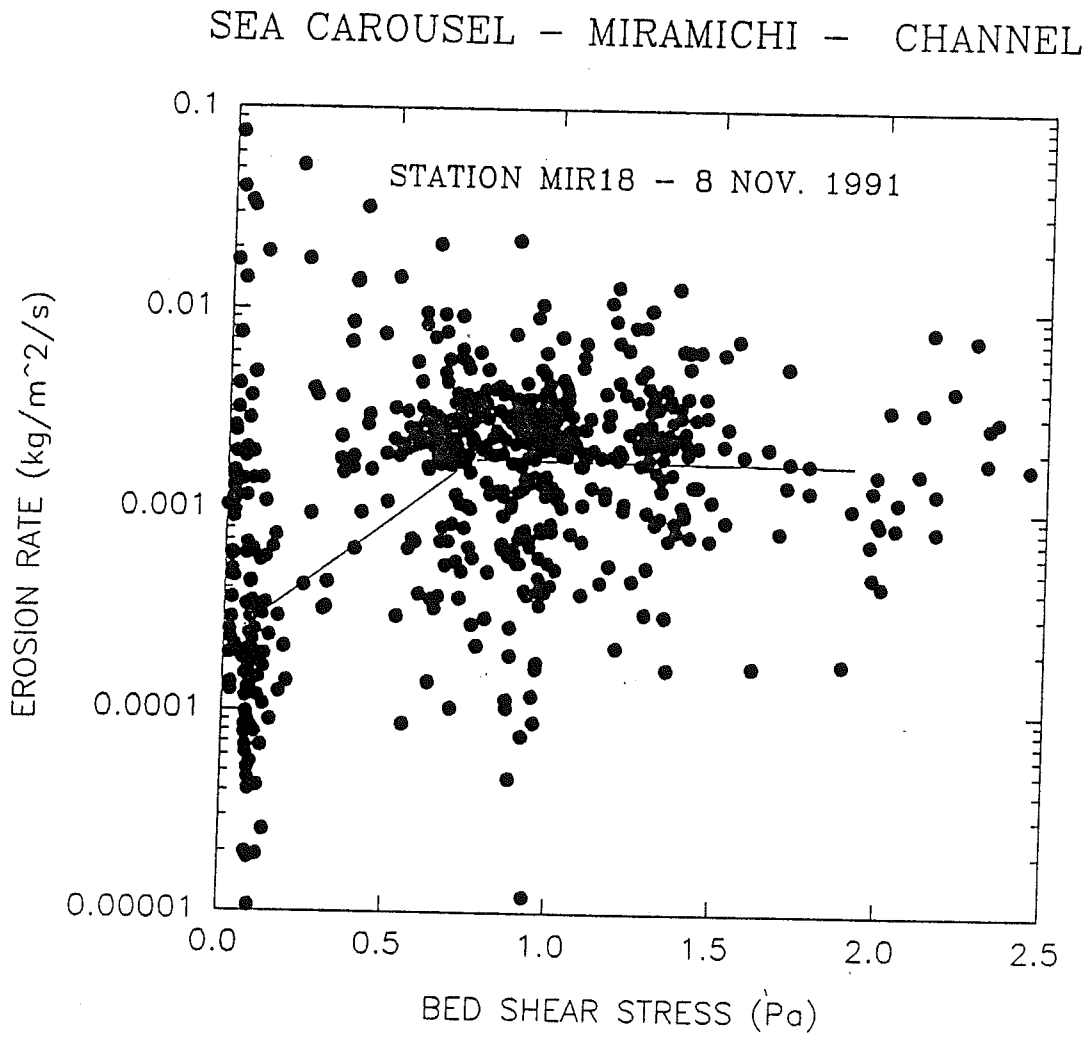
SEA CAROUSEL – MIRAMICHI – CHANNEL
STATION MIR18 – 8 NOV. 1991
EROSION RATE (kg/m^2/s)
0.1
0.01
0.001
0.0001
0.00001
0.0
0.5
1.0
1.5
2.0
2.5
BED SHEAR STRESS (Pa)

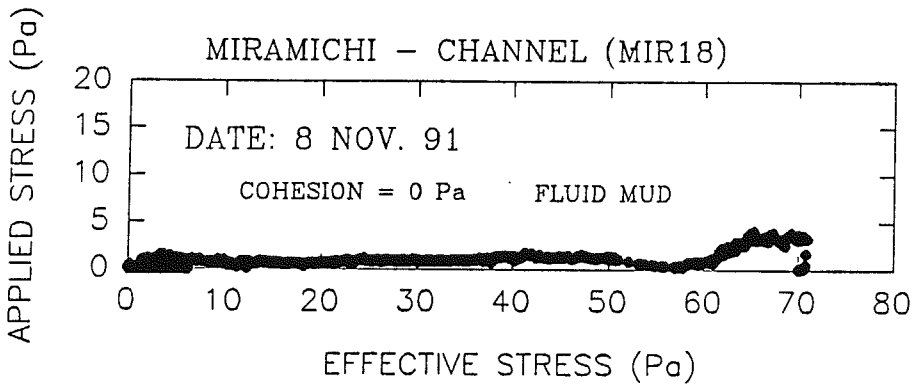
MIRAMICHI – CHANNEL (MIR18)
DATE: 8 NOV. 91
COHESION = 0 Pa
FLUID MUD
APPLIED STRESS (Pa)
EFFECTIVE STRESS (Pa)
0
5
10
15
20
0
10
20
30
40
50
60
70
80

SEA CAROUSEL – MIRAMICHI NAVIGATION CHANNEL

STATION MIR18 – 8 Nov. 1991

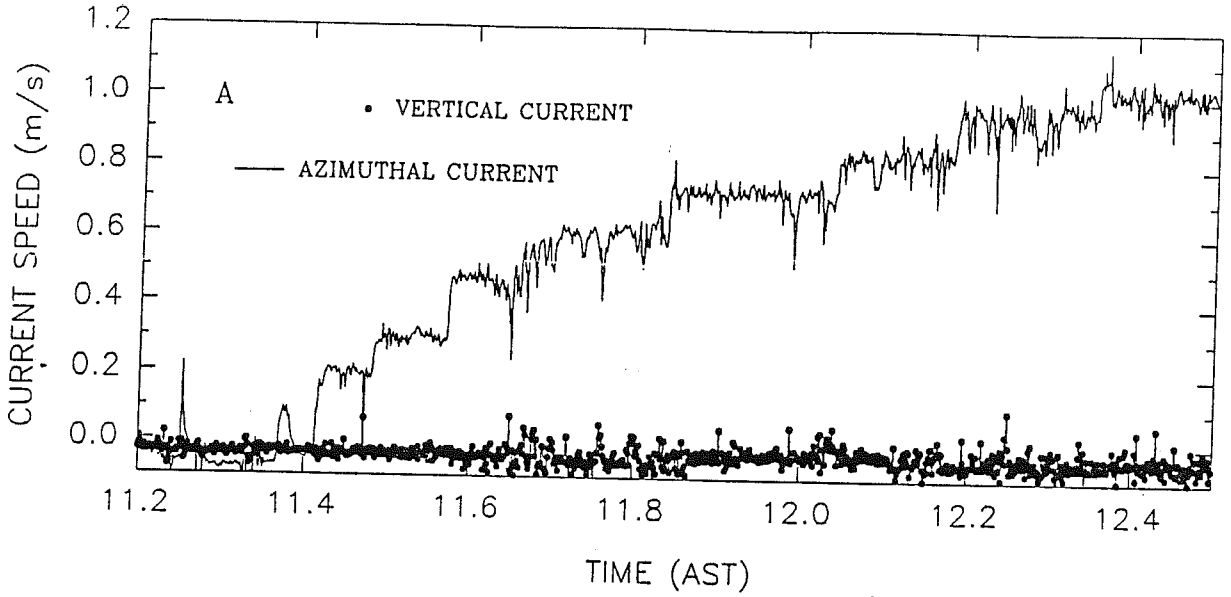

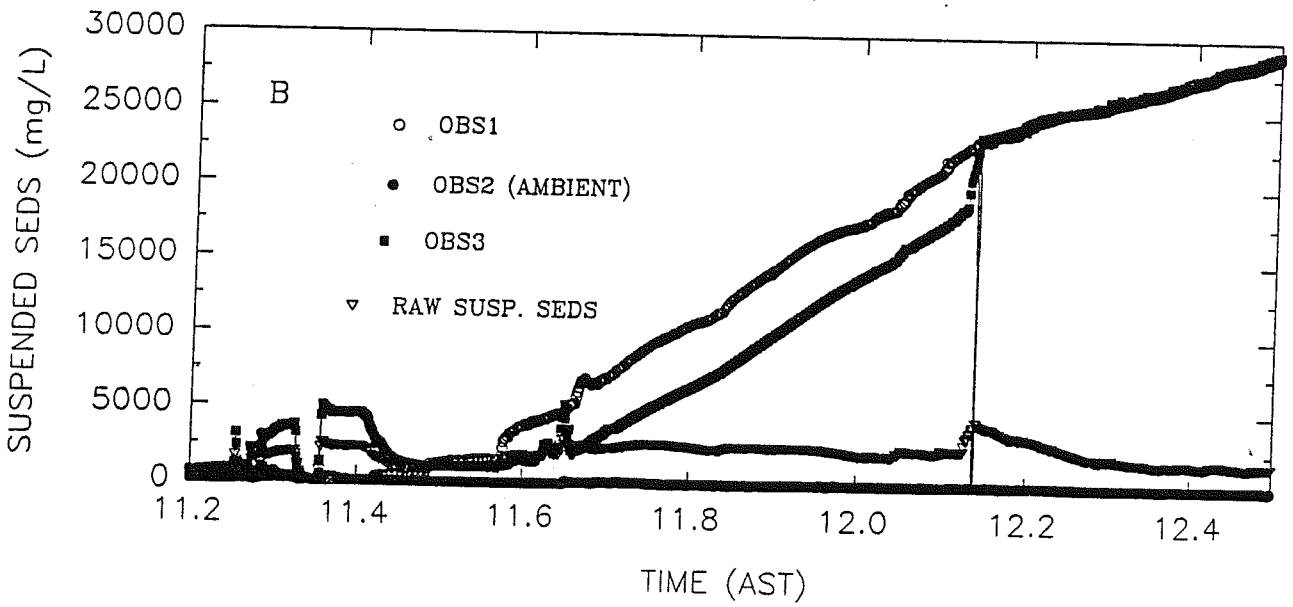

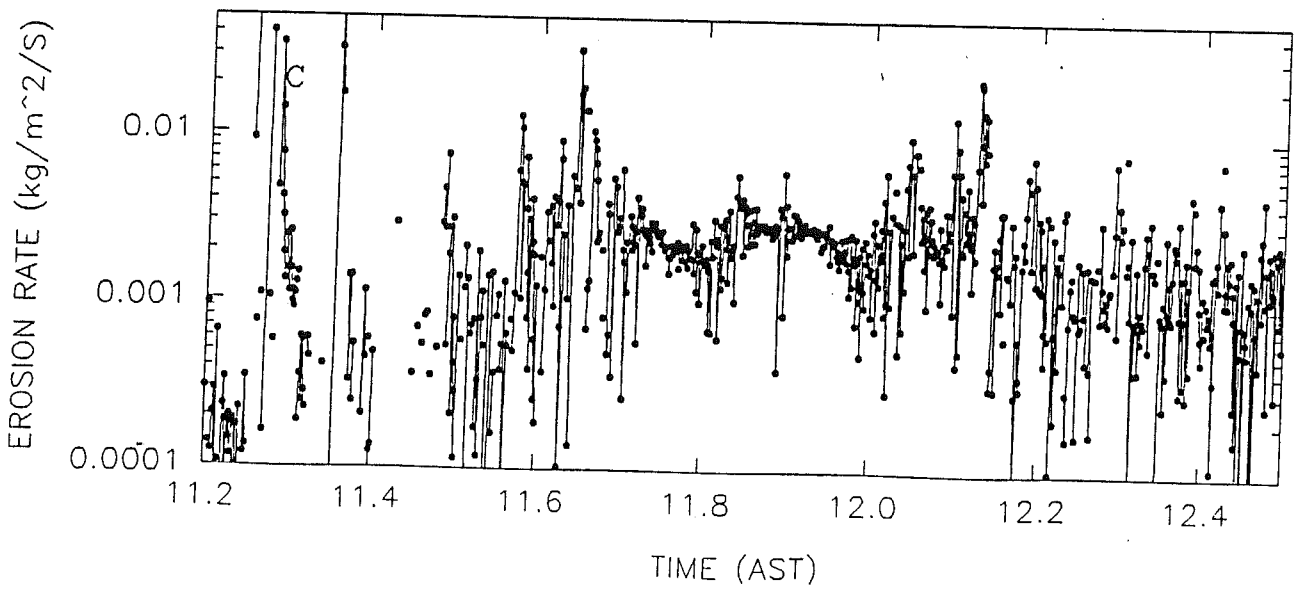

SEA CAROUSEL – MIRAMICHI – CONTROL SITE

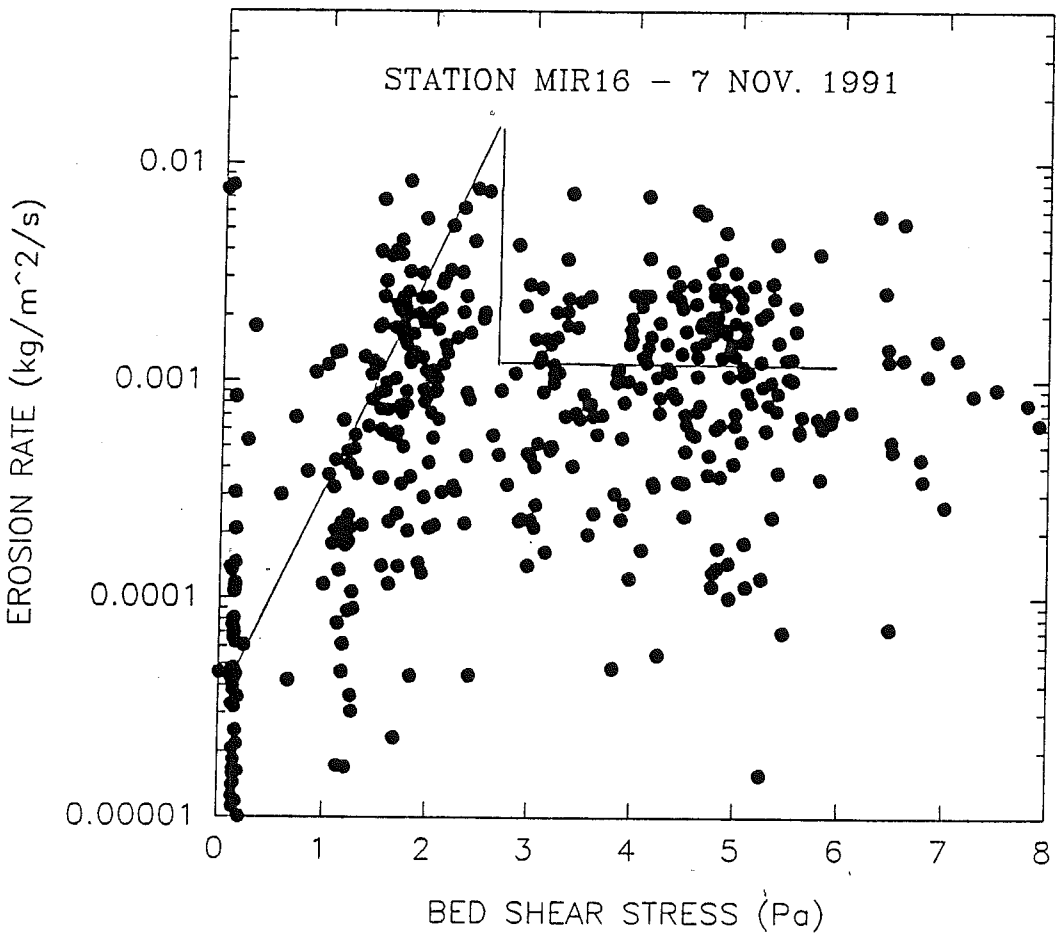

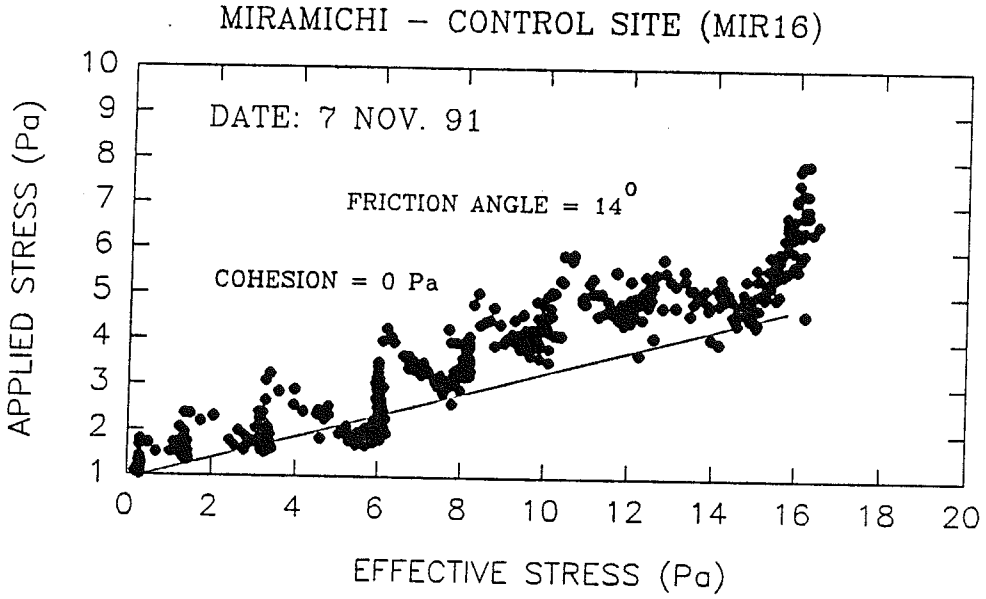
MIRAMICHI – CONTROL SITE (MIR16)
DATE: 7 NOV. 91
FRICTION ANGLE = 14°
COHESION = 0 Pa
APPLIED STRESS (Pa)
EFFECTIVE STRESS (Pa)
0
2
4
6
8
10
12
14
16
18
20
1
2
3
4
5
6
7
8
9
10

SEA CAROUSEL – MIRAMICHI CONTROL SITE

STATION MIR16 – 7 Nov. 1991

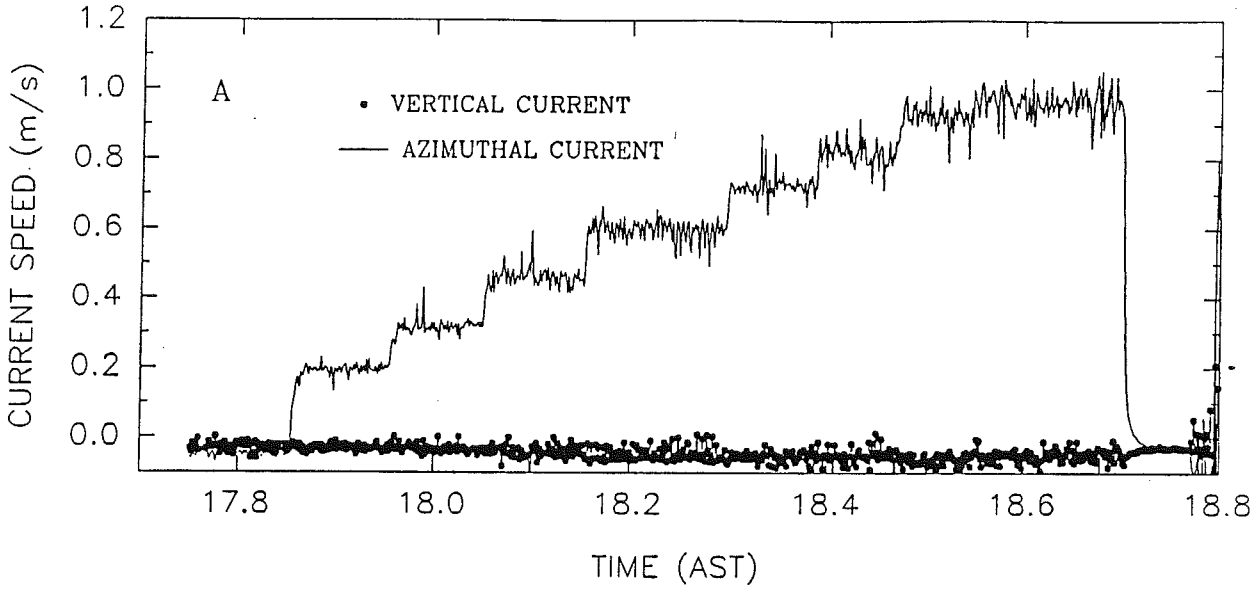

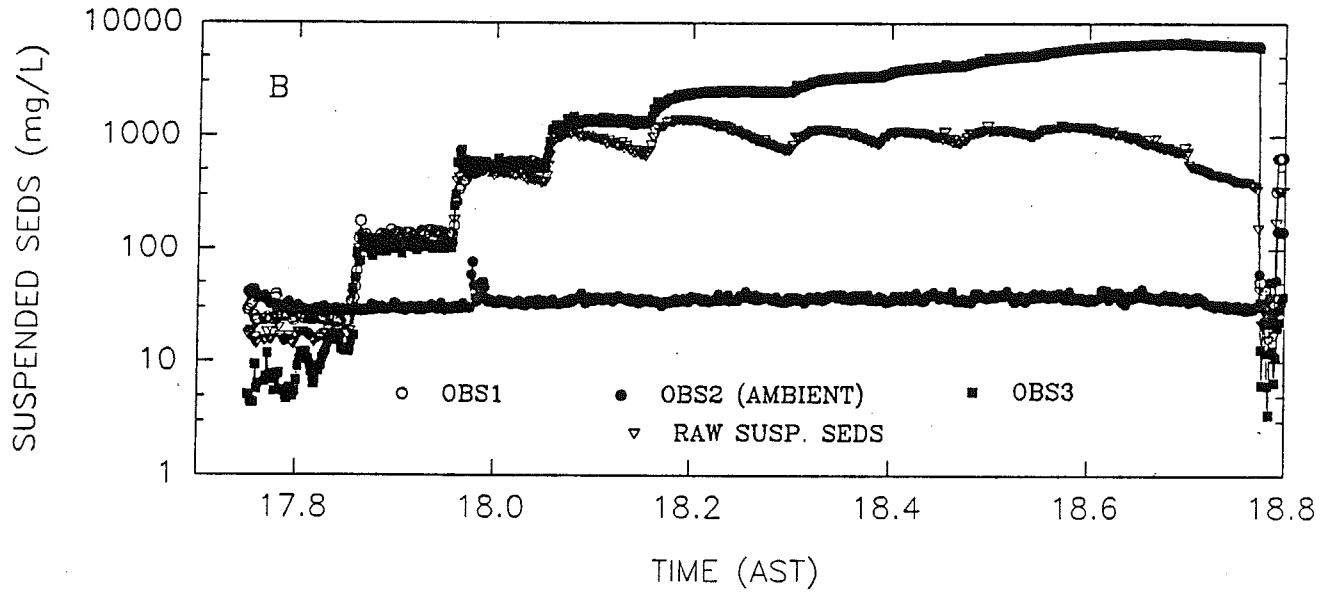

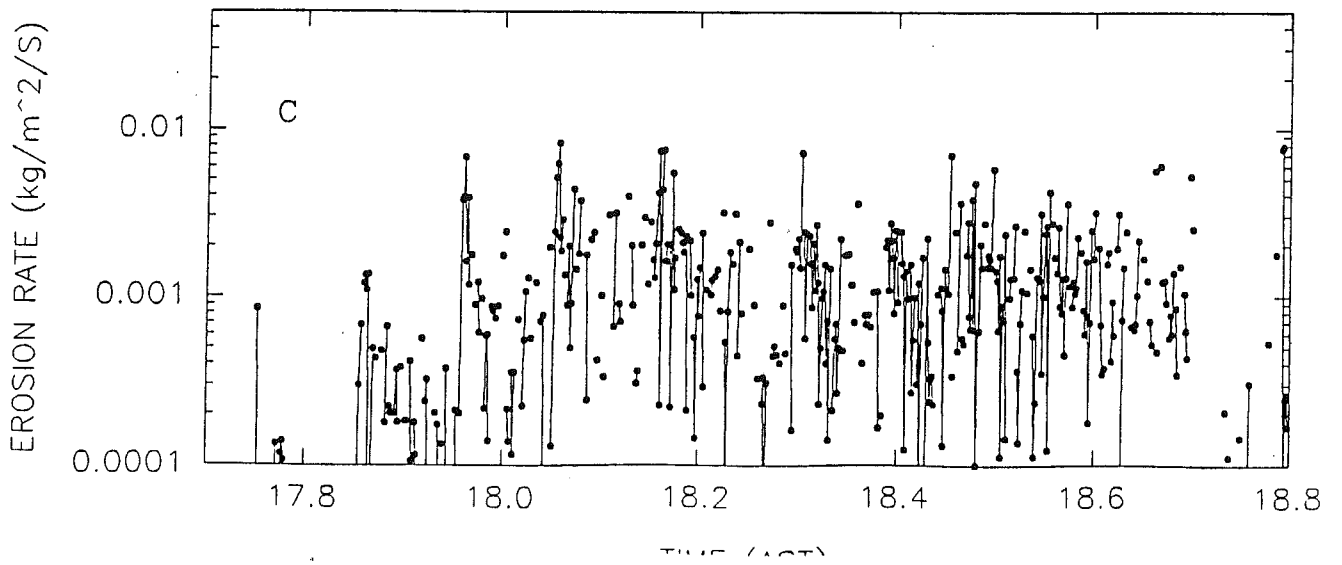

SEA CAROUSEL – MIRAMICHI – CONTROL SITE

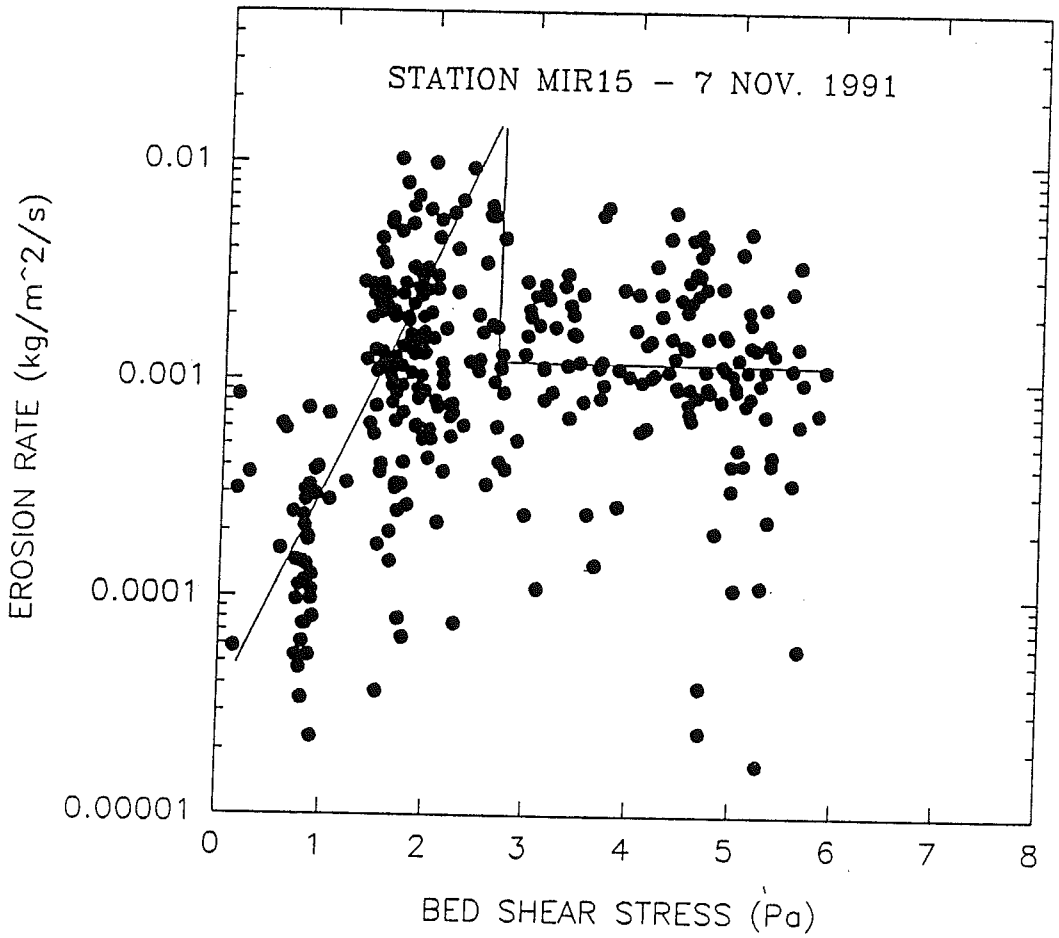

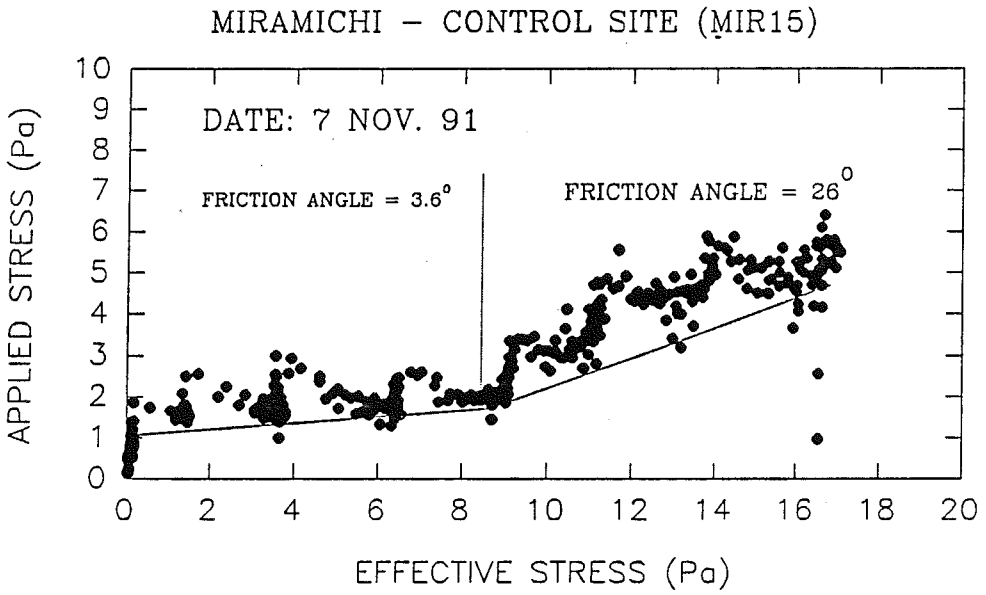
MIRAMICHI – CONTROL SITE (MIR15)
DATE: 7 NOV. 91
FRICTION ANGLE = 3.6°
FRICTION ANGLE = 26°
APPLIED STRESS (Pa)
EFFECTIVE STRESS (Pa)
0
1
2
3
4
5
6
7
8
9
10
0
2
4
6
8
10
12
14
16
18
20

SEA CAROUSEL – MIRAMICHI CONTROL SITE

STATION MIR15 – 7 Nov. 1991

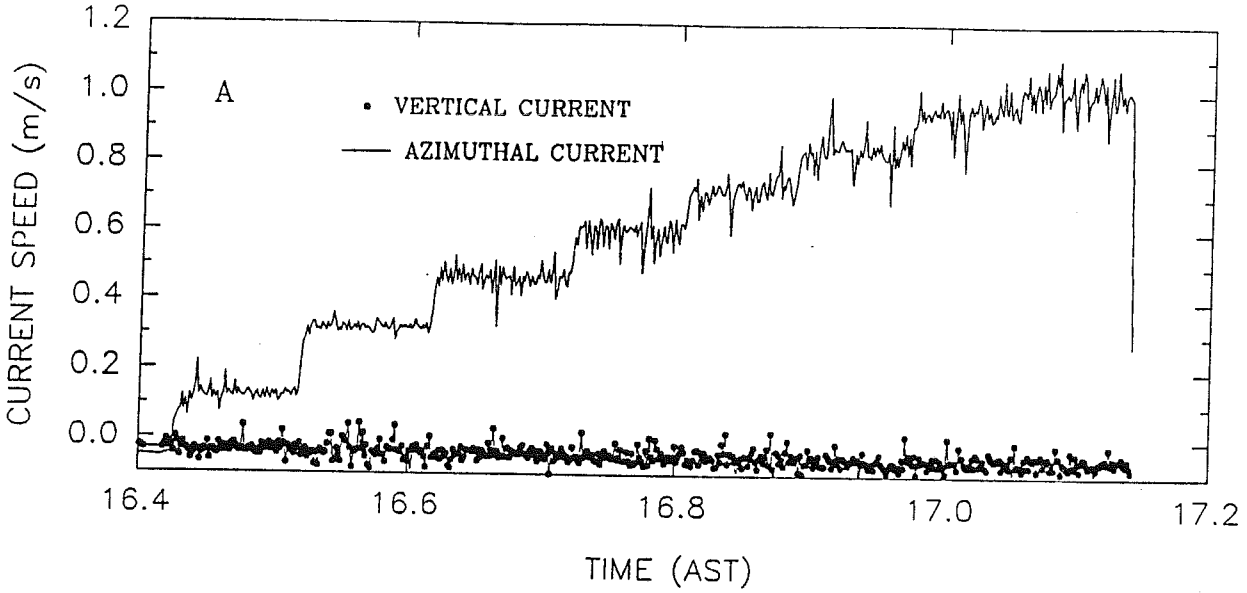

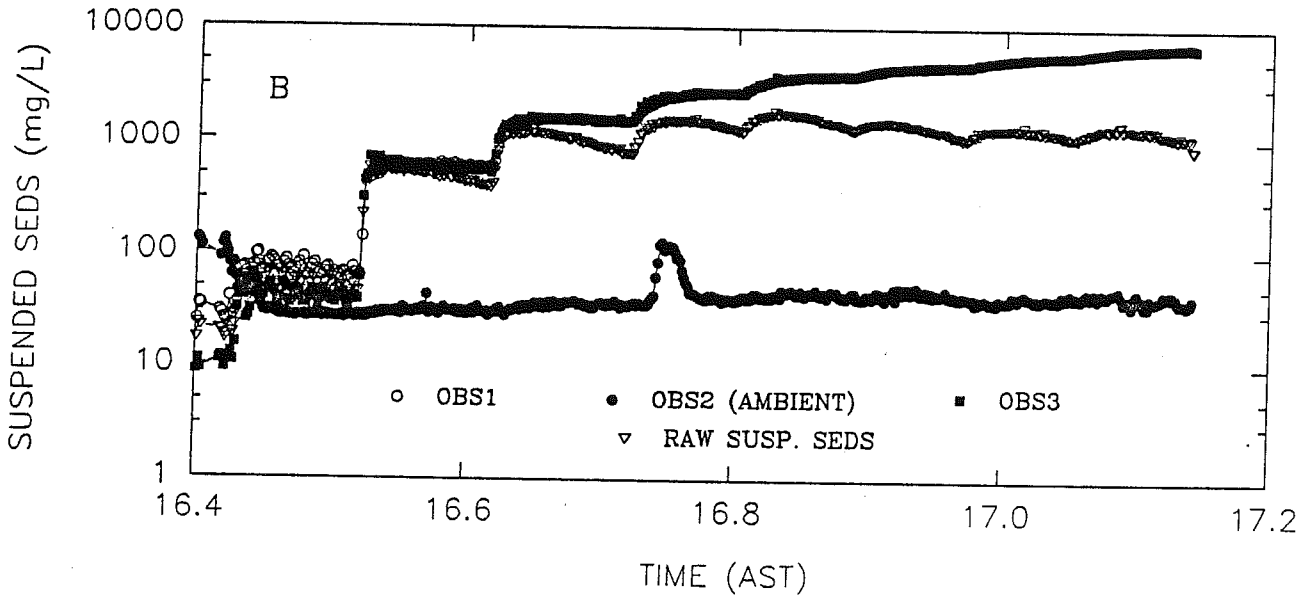

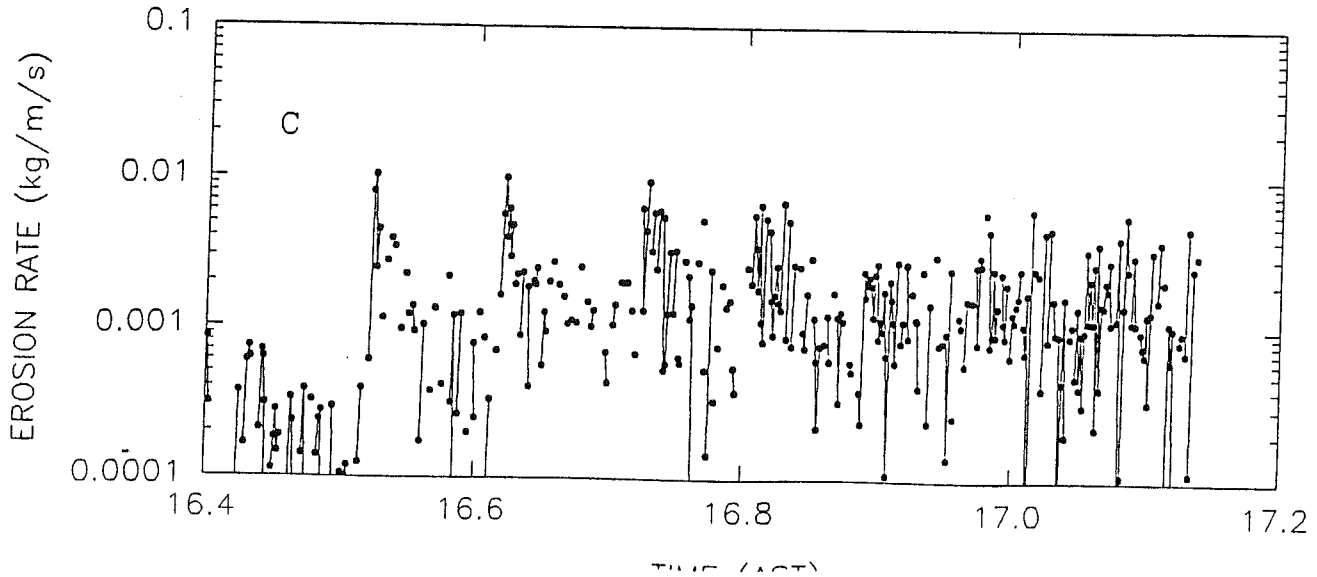

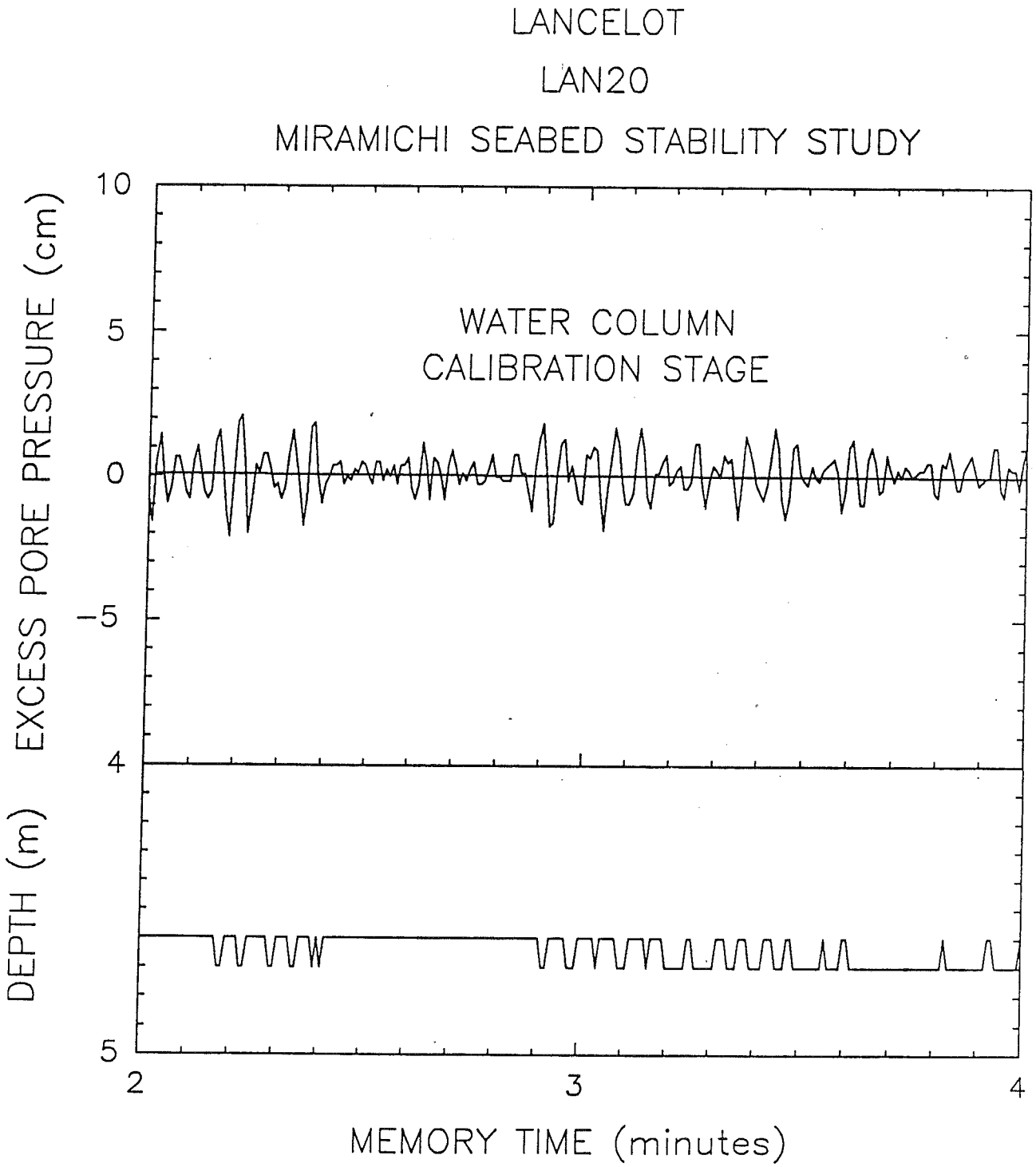
LANCELOT
LAN20
MIRAMICHI SEABED STABILITY STUDY
WATER COLUMN
CALIBRATION STAGE
10
5
0
−5
4
5
2
3
4
DEPTH (m) EXCESS PORE PRESSURE (cm)
MEMORY TIME (minutes)

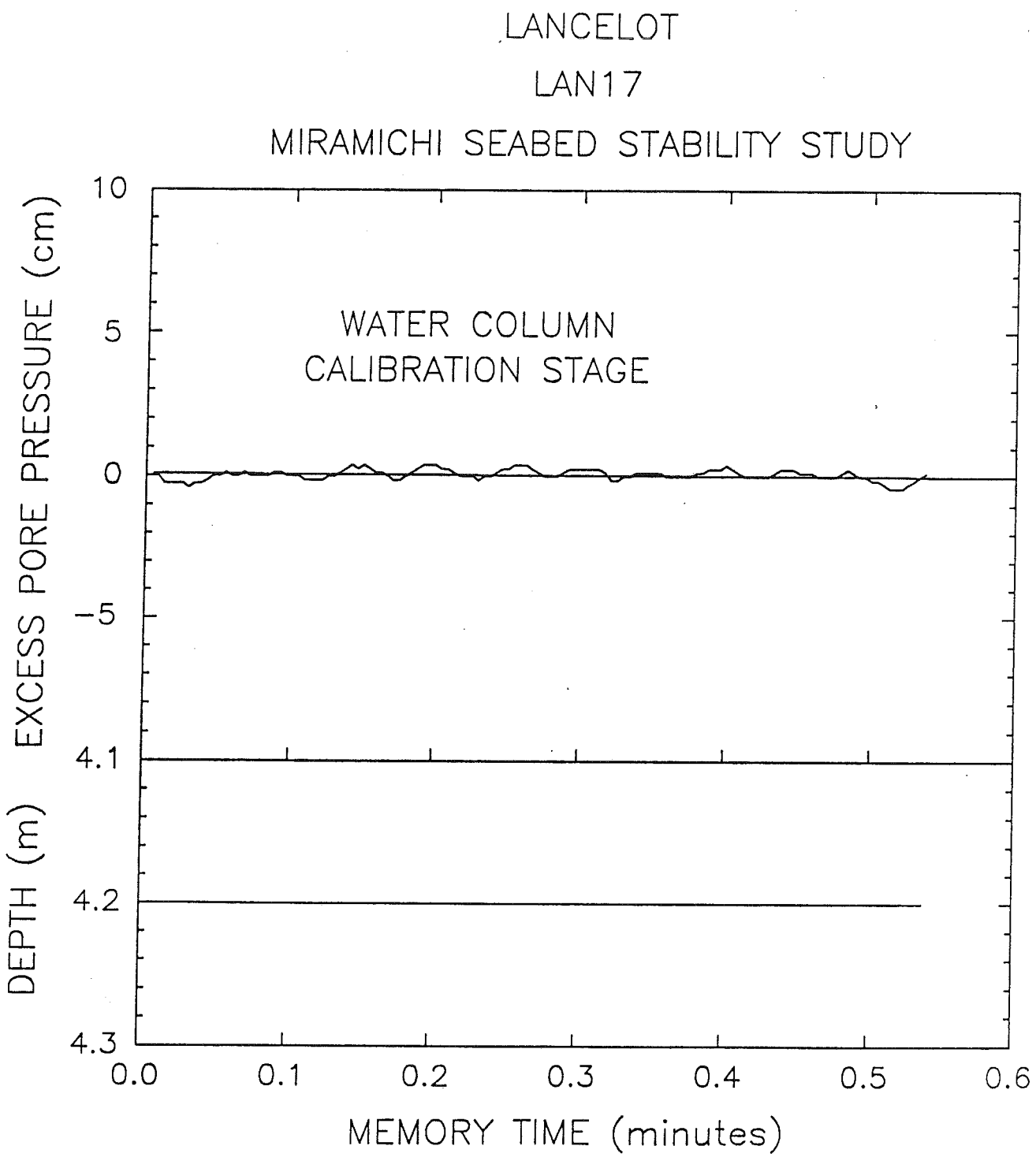
LANCELOT
LAN17
MIRAMICHI SEABED STABILITY STUDY
WATER COLUMN
CALIBRATION STAGE
EXCESS PORE PRESSURE (cm)
10
5
0
-5
DEPTH (m)
4.1
4.2
4.3
0.0
0.1
0.2
0.3
0.4
0.5
0.6
MEMORY TIME (minutes)

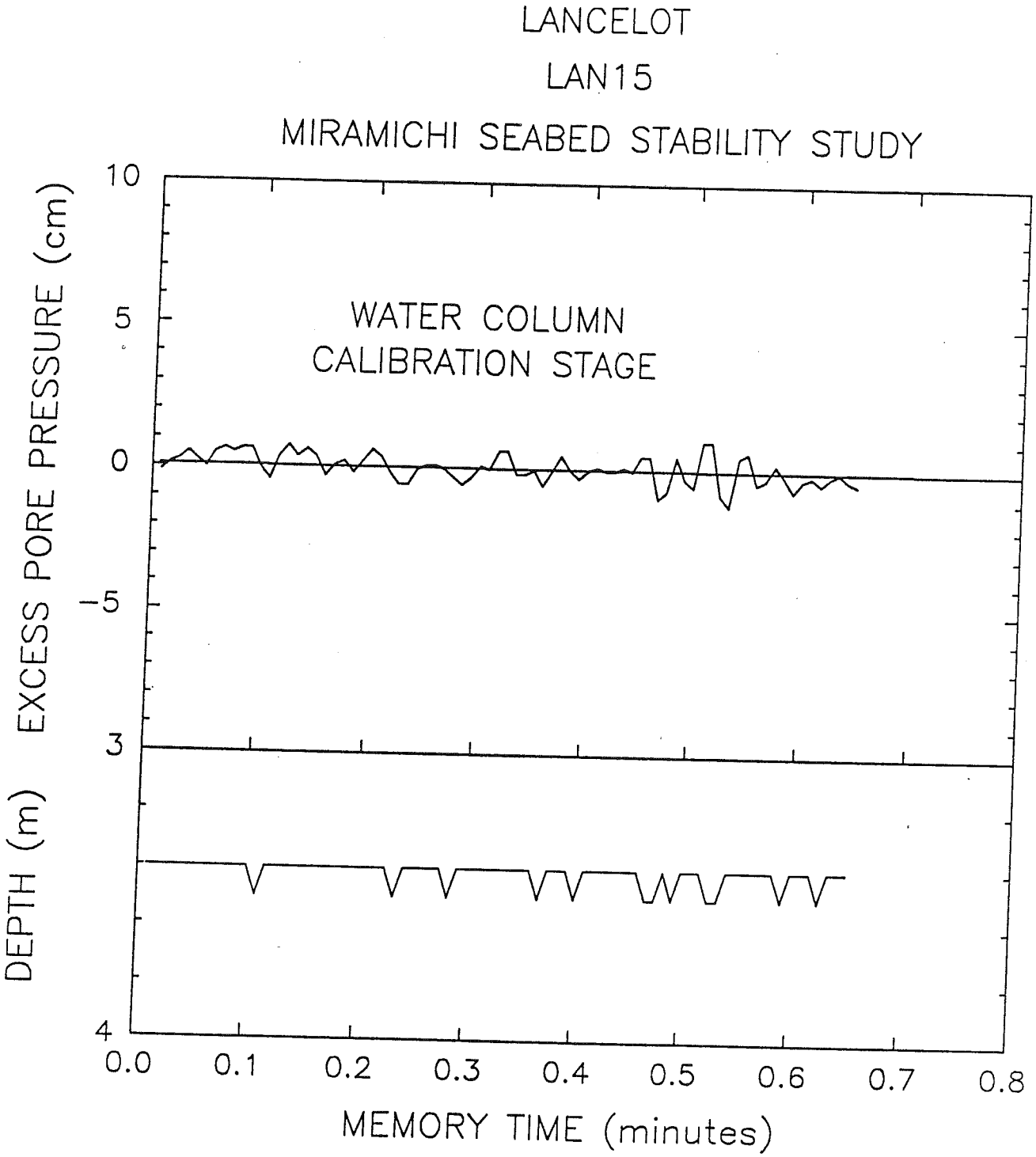
LANCELOT
LAN15
MIRAMICHI SEABED STABILITY STUDY
WATER COLUMN
CALIBRATION STAGE
EXCESS PORE PRESSURE (cm)
DEPTH (m)
10
5
0
−5
3
4
0.0
0.1
0.2
0.3
0.4
0.5
0.6
0.7
0.8
MEMORY TIME (minutes)

LANCELOT

LAN17

MIRAMICHI SEABED STABILITY STUDY

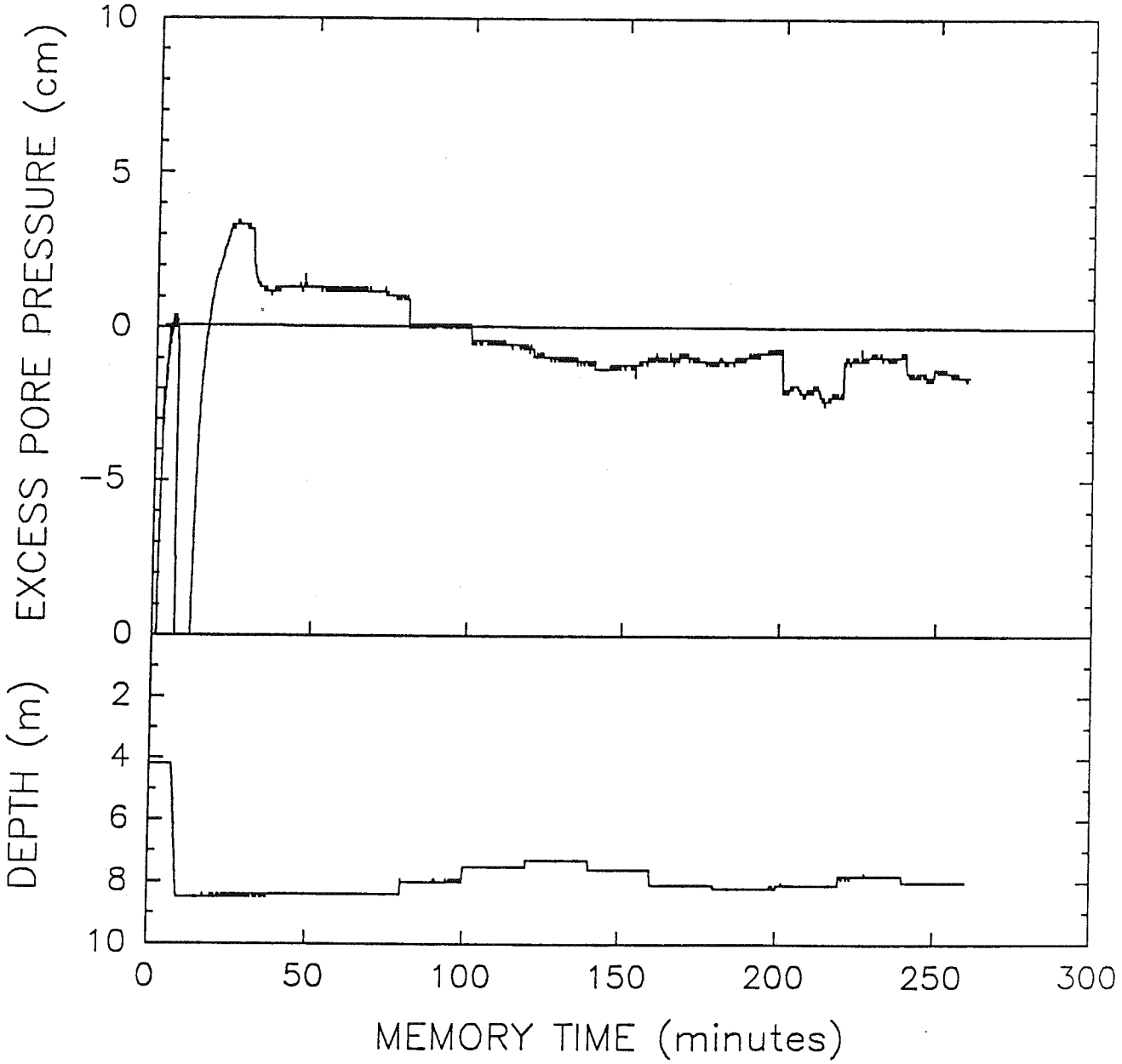

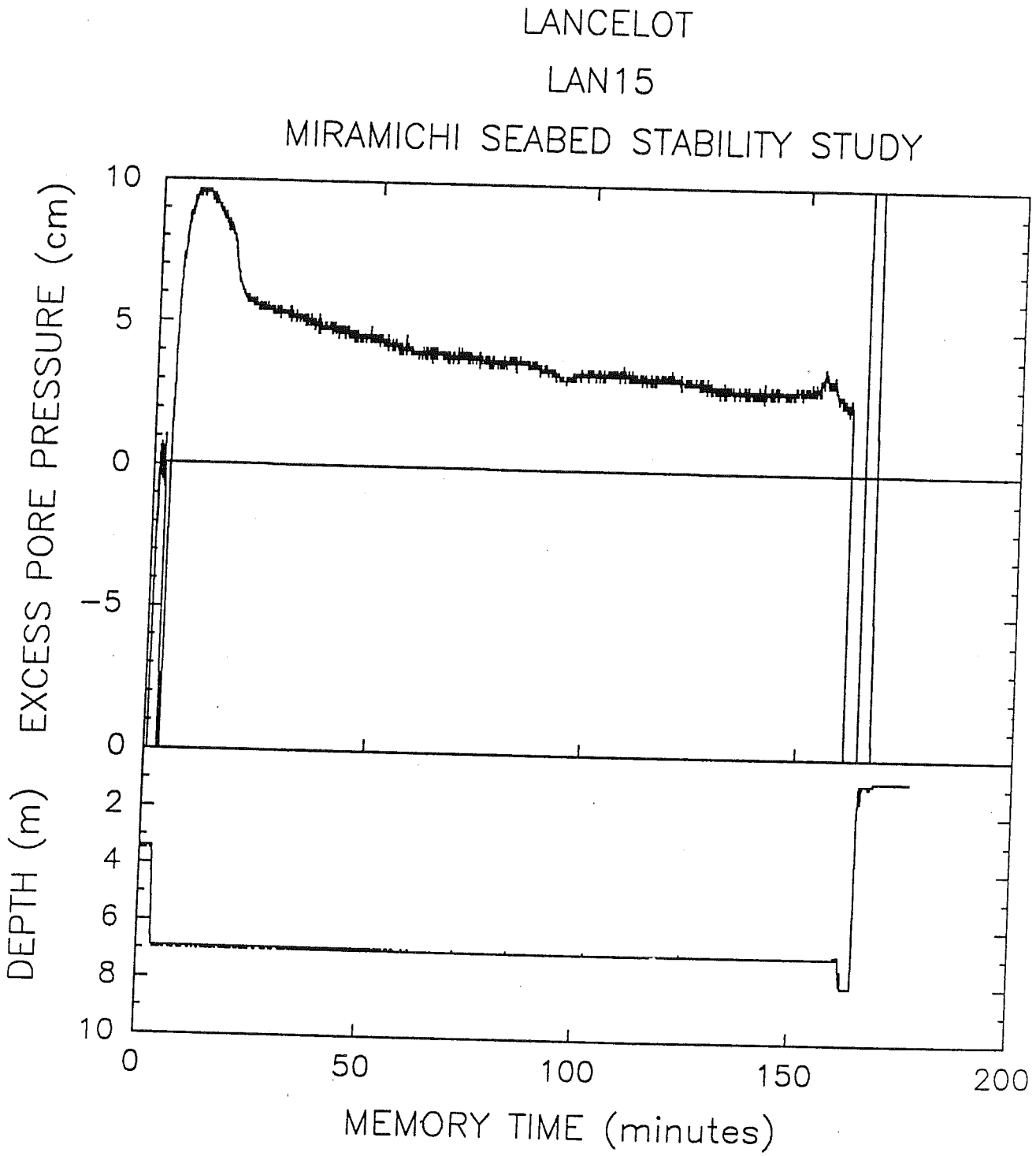
LANCELOT
LAN15
MIRAMICHI SEABED STABILITY STUDY
EXCESS PORE PRESSURE (cm)
10
5
0
−5
0
DEPTH (m)
2
4
6
8
10
0
50
100
150
200
MEMORY TIME (minutes)